NSF Grant ATM-9612519

National Science Foundation

MICROPHYSICAL CHARACTERISTICS OF ICE CRYSTALS AND SNOWFLAKES AS REVEALED BY POLARIMETRIC RADAR MEASUREMENTS

by Christine M. Reese Butler and Steven A. Rutledge

Colorado State University

DEPARTMENT OF ATMOSPHERIC SCIENCE

PAPER NO. 667

MICROPHYSICAL CHARACTERISTICS OF ICE CRYSTALS AND SNOWFLAKES AS REVEALED BY POLARIMETRIC RADAR MEASUREMENTS

by

Christine Musick Reese Butler

and

Steven A. Rutledge

Department of Atmospheric Science

Colorado State University

Fort Collins, CO 80523

Research Supported by

National Science Foundation

under Grant ATM-9612519

Summer 1998

Atmospheric Science Paper No. 667

ABSTRACT

MICROPHYSICAL CHARACTERISTICS OF ICE CRYSTALS AND SNOWFLAKES AS REVEALED BY POLARIMETRIC RADAR MEASUREMENTS

This research encompassed both observational and theoretical aspects of co-polar and differential reflectivity in the less explored, yet important, winter season precipitation. The observational portion was conducted with the multiparameter, CSU-CHILL radar and supplemented by observers at the Fort Collins Weather Station on the Campus of Colorado State University (FCL) who recorded microphysical features of the snowfall such as snow type, composition, size, and degree of riming. Additionally, a 2-D video disdrometer, located at FCL, made particle size distribution measurements. In order to compare the appropriate radar data with the ground observations, the approximate trajectory of the snow was computed from the height it was interrogated by the radar to the surface. The trajectory, applied in reverse from FCL, identified the source region of the observed snow in the 0.5° and 1° elevation scans of the radar.

The results of the observational analyses suggest that nearly homogeneous populations of aggregates can be distinguished from platelike crystals (i.e. dendrites, stellar crystals, and plates) using a combination of co-polar and differential reflectivity (Z and Z_{DR}) radar observations. Furthermore, it appears possible to discern whether or not the platelike crystals are intensely rimed. Additionally, the

results challenge the validity of the common assumption that aggregates always produce a Z_{DR} value of 0 dB.

Scattering model studies based on T-matrix theory and the Mueller matrix method were conducted to demonstrate the consistency of the observed radar variables with theoretical values and to test our speculations on which hydrometeor microphysical characteristics were responsible for the observed variations in those variables. Our modeling results suggest several conclusions. First, the aggregate shapes are more relevant and have more impact on Z_{DR} than generally expected; therefore, the modeling assumption that all aggregates are nearly spherical can produce erroneously low Z_{DR} values. Secondly, the size-dependent density formulas for aggregates which predict that bulk densities decrease with size may not always be applicable. Next, the canting of hydrometeors can overcome the influence of microphysical characteristics on Z_{DR}; thus, in a model, it is important to include canting for turbulent situations when it likely occurred and to exclude it for calmer situations where it was not likely to have occurred. Lastly, the model results validated the idea that intensely rimed platelike crystals could be distinguished from other platelike crystals and highlighted the problems that can be encountered if modelers depend upon size-dependent axis ratio formulas without considering the effects of riming.

ACKNOWLEDGEMENTS

We would like to express our appreciation to committee members, Dr. T. McKee and Dr. V. Chandrasekar for their input and guidance. Another essential contributor to these research efforts was Larry Carey, who spent months editing the code used in the modeling portion of this work. Furthermore, Larry, Paul Hein, Dr. Walt Petersen, and Tom Saxen served as inexhaustible sources of information on topics ranging from computers and their quirks, to radar theory and cloud physics.

Appreciation is expressed to Bob Bowie, Dave Brunkow, Pat Kennedy, and Ken Pattison (the CSU-CHILL staff) who operated the radar during this field project. Pat also provided guidance in establishing the observational procedures. Additionally, Dave and Pat supplied invaluable insight and advice on processing the radar data. The disdrometer data was collected by Dr. Bringi and his staff, and was reformatted by Ibrahim Amin Ibrahim.

This research was sponsored by the National Science Foundation, under grant number ATM-9612519

TABLE OF CONTENTS

LIST OF TABLES

Table Caption **Page**

LIST OF FIGURES

Figure Caption **Page**

Chapter 3:

Chapter 4:

CHAPTER 1

INTRODUCTION

1.1 Purpose

A great deal of work has been done to examine and interpret dual polarization radar observations in warm season convective storms while, in comparison, the interpretation of data in winter snowstorms remains relatively unexplored. Indeed, polarimetric radar was originally developed to identify hail and map heavy precipitation, promoting many studies of warm season convection. However, the impacts of snowfall are far-reaching, and any avenues that could potentially provide further insights should be pursued.

The primary objective of this thesis was to perform a preliminary examination of the microphysical information that could be acquired from the polarimetric radar data collected during winter precipitation events. In addition, scattering model studies were conducted to compare theoretical values of the multiparameter variables with observations and to test our speculations on which hydrometeor microphysical characteristics were responsible for the observed variations in those variables. A better understanding of the degree to which microphysical properties can be inferred from the

polarimetric radar data could be useful in a variety of applications. These applications include: improving Z-S relationships used to diagnose snowfall amounts, identifying hydrometeor types which is important for distinguishing between snow and dangerous freezing rain, remotely sensing ice water contents, and forecasting snow-induced visibility degradation.

1.2 Background Information

Numerous polarimetric variables are available from multiparameter radars such as the CSU-CHILL radar used in this study. However, in this particular study, we only considered the horizontally polarized equivalent reflectivity (Z_{he}) (henceforth referred to as reflectivity, Z, unless clarification is needed to avoid confusion), and the differential reflectivity variable (Z_{DR}). Differential reflectivity is based on the ratio of the radar reflectivity factor at horizontal polarization (Z_H) to that at vertical polarization (Z_V); thus, in essence, it measures the reflectivity-weighted mean axis ratio of the hydrometeors in the pulse volume. The axis ratio in this thesis is defined as the ratio of the minor axis to the major axis of the particle. Z_{DR} in decibels (dB) is defined mathematically as:

$$Z_{DR} = 10\log_{10}(Z_H/Z_V) \tag{1.1}$$

Although Z_{DR} is a strong function of the particle's geometric axis ratio, other factors affect the value of Z_{DR} including dielectric constant (another form of refractive index), density, axis ratio, drop size distribution, and fall mode.

The role of the dielectric constant is very significant, though not immediately apparent. The standard equation used to compute the back-scattering cross sections,

$$\sigma_{H,V} = (\pi^5/\lambda^4)|K|^2 D^6_{H,V} \tag{1.2}$$

would make it appear that in the ratio of σ_H to σ_V, the dielectric factor, $|K|^2$, would cancel, and thereby have no effect on Z_{DR}. However, equation (1.2) is based on the assumption of Rayleigh conditions which includes only spherical hydrometeors. Gans' theory, as described by Atlas et al. (1953), extends the Rayleigh condition equations to include ellipsoids. Atlas' equations (1)-(5) clearly illustrate that the magnitude of the dielectric constant, m^2, controls the extent to which the shape of the hydrometeor influences the backscatter power, and it does so in such a way that there is no cancellation in a ratio of horizontal to vertical reflectivity. Therefore, since the dielectric constant of water, for example, is much larger than the dielectric constant of ice (80 vs. 3), the Z_{DR} of a liquid hydrometeor will be much larger than the Z_{DR} for an ice hydrometeor with the same axis ratio. Within the ice phase the magnitude of the dielectric constant decreases as the bulk density decreases. Therefore, the greater the density of a snowflake or ice crystal, the more its shape contributes to the differential reflectivity.

The particle size distribution is important to differential reflectivity in a number of ways. Since Z_{DR} is reflectivity-weighted, and since the reflectivity factor goes as the sixth power of the particle diameter, Z_{DR} will be heavily weighted by the largest hydrometeors in the pulse volume. With this in mind, if the axis ratios of the hydrometeors are size-dependent, the particle size distribution becomes even more key.

Finally, the fall mode of the hydrometeor plays a role in Z_{DR}. In simple terms, the more the major axis cants around the horizontal in a wobbling fashion, the more the Z_H and Z_V of the hydrometeor population become alike, thus lowering Z_{DR}.

Up to this point, Z_{DR} values have been discussed qualitatively, and it has become apparent that in a relative sense, Z_{DR} values are higher for highly oblate particles and

considerably lower for hydrometeors that are nearly spherical. To illustrate the range of theoretical Z_{DR} values that can be expected for a variety of ice bulk densities and axis ratios, a simple model based on Gans' theory was exercised (L. Carey, personal communication). This model computes Z_{DR} for a single hydrometeor assuming the major axis is oriented in the horizontal. The results are depicted in Figure 1.1 for a range of ice particle types and densities. The trends are unmistakable as Z_{DR}, at a given density, decreases with increasing axis ratio (defined as the minor axis/major axis) and, for a given axis ratio, decreases with decreasing density. It also becomes evident that unless an aggregate has one of the higher densities and lower axis ratios, the resultant Z_{DR} will generally be ≤ 1 dB. Moreover, more solid, flat crystals will tend to have Z_{DR} values exceeding 1 dB.

1.3 Review of Previous Modeling Research

Despite the fact that our research is focused on Z_{DR} and Z alone, this section reviews research that involved any of the polarimetric variables in winter precipitation in order to adequately represent the context surrounding our work. Evans and Vivekanandan (1990) modeled the electromagnetic scattering properties of ice crystals using the discrete dipole approximation and the parameters and assumptions specified in Table 1.1. They calculated Z, Z_{DR}, linear depolarization ratio (LDR), and differential propagation phase shift (K_{DP}). LDR is the ratio of the vertically polarized return power to the horizontally polarized return power for horizontal transmit polarization, expressed in dB. K_{DP} is the difference between the phase shift in a forward traveling horizontally polarized wave and that in a forward traveling vertically polarized wave, and it is

Table 1.1 Summary of modeling researchers' assumptions

	Crystal Types	Sizes (mm)	Axis Ratios	Density (g/cm^3)	DSD	Fall Mode
Evans and Vivekanandan (1990)	plates, needles, columns	.06-2	size-dep. Formulas (0.2-0.02)	.92 and .23	$N=AD^{-3}$ A determined by total mass=.1g/m^3	Horiz. orient.
Vivekanandan et al. (1993)	plates	0-5	.2	.9	single particle	Horiz. orient.
	dry conical graupel	0-5		.5	single particles	apex upward
	aggregates	2-20	.8	.2 .5 and .8	single particle	Horiz. orient.
	MIX: crystal portion	.1-5	.2	.9	10dBZ: exp; D_0=1mm N_0=124.54 $mm^{-1}m^{-3}$	Horiz. orient.
	MIX: aggreg. portion	2-20	.8	.2	varied	tumbling
Matrosov et al. (1996)	plates, dendrites, needles, columns, bullets		size-dep. Formulas	size-dep formulas.	1st order Gamma: D_0=.1,.2,.5, and 1mm	stnd dev of cant from horiz 3-30°
	aggregates		.8 and .3	size-dep formula	1st order Gamma: D_0=.5, 1.5mm	" "
Ryzhkov et al. (1998)	same as both Matrosov lists	< 4	size-dep formulas	size-dep formulas	Exponential	Horiz. orient.

Table 1.2 Summary of Z_{DR} modeling results from previous researchers

Z_{DR} Results	Density g/cm^3	Plates	Needles	Columns	Conical Graupel	Aggregates
Evans and Vivekanandan (1990)	rho=.92	9 dB	4.2 dB	3.5 dB		
	rho=.23	2.2 dB	.8 dB	.7 dB		
Vivekanandan et al. (1993)	rho=.9	6.3 dB				
	rho=.8					.9-1.4 dB
	rho=.5				1dB	.6-.9 dB
	rho=.2					.2-.4 dB

expressed in degrees of phase shift/km. Note that K_{DP} is the range derivative of φ_{DP}, the differential phase (degrees). Evans and Vivekanandan (1990) not only explored the values of the polarimetric parameters for different crystal types, they also examined the variation as a function of elevation angle. Their results at K-band (0.8 cm) are shown in Figures 1.2-1.4. The information pertinent to our study is the order of highest to lowest Z_{DR} values which go from plates (smallest axis ratios) to needles to columns, and the magnitude of those Z_{DR} values from the 0° elevation scan which are summarized in Table 1.2. It is readily apparent from these results that axis ratio affects Z_{DR} even in ice; however, it is also apparent, when the results from the two different densities are compared, that the difference in Z_{DR} as the axis ratio changes is diminished at lower densities. Evans and Vivekanandan (1990) concluded that the particle shapes played an important role, and particle bulk density was a significant, contributing factor to the values of the polarimetric variables. They felt that with further work it would be possible to use the polarimetric radar data to distinguish between plates and prolate particles such as needles and columns. Furthermore, they argued that once assumptions are made about particle orientation and shape, the bulk density and total number concentration could be inferred from Z_{DR} and K_{DP} respectively.

Vivekanandan et al. (1993) conducted a rigorous modeling study with calculations based on the Mueller matrix formulation. This model allowed polarimetric radar variables to be computed for hydrometeor mixtures with various orientations, size distributions, shapes, and densities/dielectric constants. First, Vivekanandan et al. (1993) computed the polarimetric radar variables for single particles of each type. They followed this with a modeling study of various particle mixtures. Results that are

relevant to our work are shown in Table 1.2. Again, the influence of both the axis ratio and density are evident. Plates have a higher density and a lower axis ratio which corresponds to the higher 6.3 dB, Z_{DR} value. Aggregates have lower Z_{DR} values as a result of larger axis ratios (more nearly spherical in shape), and those values decrease markedly with density decreases. Figure 1.5 shows the model output produced for the mixture of individual platelike crystals and aggregates. For this computation, the reflectivity of the crystals was held to 10 dBZ, and the aggregate population was allowed to increase from -5 to 25 dBZ. Clearly the Z_{DR} is much higher at 6.2 dB when the crystal population is dominating and lowers as the aggregates increase in number, until it reaches approximately 0.4 dB when the reflectivity from aggregates reaches 25 dBZ.

Vivekanandan et al. (1994) built upon the results of Vivekanandan et al. (1993) by carrying out additional ice phase model computations of Z_{DR} for axis ratios from 0.1 to 0.95 with densities ranging from 0.01 to 0.92 g/cm^3. Oblate spheroid particles were modeled with the major axis assumed to be horizontally oriented. In each particle size distribution, they also assumed that all particles had the same density and axis ratio. Vivekanandan et al. (1994) acknowledge that these are overly restrictive assumptions, but believe they produce an initial starting place for a complicated situation. Vivekanandan et al. (1994) applied a two-dimensional curve fit to arrive at the following equations:

$$Z_{DR} = -11\rho^{0.95}\log(r) \qquad \text{for } Z_{DR} \leq 5\text{dB} \tag{1.3a}$$

$$Z_{DR} = -9.8\rho^{0.98}\log(r) \qquad \text{for } 5 < Z_{DR} \geq 9\text{dB} \tag{1.3b}$$

These equations illustrate the relation between Z_{DR}, density (ρ), and axis ratio (r). They state that since the Z_{DR} dependence upon axis ratio is logarithmic and density is almost linear, it may be possible to use Z_{DR} to retrieve the mean bulk density of the scatterers in a

radar pulse volume. In order to do so, however, an assumption must be made about the mean shape of the hydrometeors. In a similar fashion, Vivekanandan et al. (1994) also arrived at an equation for K_{DP} that relates it to ρ, r, wavelength of the radar (λ), and ice water content (IWC). K_{DP} was shown to only be a function of $\rho^{-.033}$; thus it primarily depends upon r and IWC, to the latter of which it is linearly related. As a result Vivekanandan et al. (1994) proposed that if, once again, an assumption was made about the mean shape (r), IWC could be retrieved from K_{DP}. This retrieval could be a significant improvement upon Z-IWC relations since the Z dependence upon IWC varies according to the shape of the drop size distribution. However, a difficulty is encountered when nearly spherical particles make up a portion of the hydrometeor population because K_{DP} is only sensitive to oblate and oriented particles. Thus, Vivekanandan et al. (1994) suggested that a model combining information from all three variables is needed such as the one for rain and hail mixtures described by Balakrishnan and Zrnic (1990). In addition, Vivekanandan et al. (1994) recommended the implementation of an ad hoc relationship between density and axis ratio:

$$\rho * r = .092 \tag{1.4}$$

They derived this equation from the estimation that a pristine plate with a density of $0.92 g/cm^3$ has an axis ratio of 0.1, while an aggregate has a bulk density of $0.1 g/cm^3$ and an axis ratio of 0.92. With this relationship, it would be possible to rewrite Equation (1.3) so that Z_{DR} only depended upon one parameter. Vivekanandan et al. (1994) concluded that quantifying winter precipitation is difficult, but it appears that the information available in the Z_{DR} and K_{DP} variables can be very useful in its remote sensing applications.

A rather different approach was taken by Matrosov et al. (1996). They utilized elliptically polarized waves for a K_a-band radar, and examined signatures in the elevation angle dependence of the depolarization ratio (similar to LDR described above, but for an elliptical rather than linear polarization) to differentiate between particle types. The authors explained that the advantage to a circular polarization over a linear one is that the circular depolarization ratio (CDR) only depends on the reflectivity-weighted mean particle aspect ratio as projected on the incident wave polarization plane. LDR, on the other hand, depends on the particle orientation in addition to the above. The elliptical depolarization ratio (DR) has an added advantage in that it can be useful for weaker echoes than either CDR or LDR due to a better signal-to-noise ratio. However, the price for the improved signal-to-noise ratio is that the distinction between different particle shapes is reduced. Given the parameters as established in Table 1.1, Matrosov et al. (1996) found that dendrites and plates exhibited a DR change of more than 5 dB between the 0° scan and the 90° scan. The columns, needles, bullets, and aggregates produced DR changes of less than 1 dB. However, some distinction within those groups was still possible using the magnitude of the DR values. For example, the DR value of the elongated crystals generally remained in the -8 to -11 dB range; whereas, the aggregates and blockier columns tended to be less than -12 dB. The authors conclude that this approach showed merit for distinguishing between some particle shapes and crudely estimating axis ratios, but uncertainties would stem from errors in the measurements, assumptions made for bulk densities, and any lack of spatial homogeneity over the relatively broad area interrogated in the 0° to 90° scans.

Ryzhkov et al. (1998) had a similar goal to Vivekanandan et al. (1994), establishing an equation for IWC. They began with different assumptions for particle shape and density as outlined in Table 1.1 (e.g. Ryzhkov et al. (1998) completely based shape on the hydrometeor size via published formulas, whereas Vivekanandan et al. (1994) had made no assumption of shape based on size); consequently, according to Ryzhkov et al. (1998), they arrived at a different conclusion. While Vivekanandan et al. (1994) reasoned that K_{DP} was almost linearly related to IWC, Ryzhkov et al. (1998) found that a linear relationship with IWC was more complicated. They derived the following equation:

$$IWC = [K_{DP}(\lambda/30\pi)C_1]/(1-Z_{DR}^{-1}) \quad (1.5)$$

where the value of C_1 depends upon the assumptions made for the dependence of density on the equivolumetric diameter and assumptions made about the types of crystals present. The authors asserted that this equation is not affected by radar calibration errors since it does not include the absolute value of the radar reflectivity factor; however, Z_{DR} calibration issues that were encountered in our study suggest otherwise and will be discussed in the next chapter. It is also important to note that this equation is only valid for particles with L, the major axis size parameter, in the range between 0 and 4 mm. Furthermore, once aggregates become involved, the applicability of Equation (1.5) begins to deteriorate, just as Vivekanandan et al. (1994) encountered with their IWC equation.

Ryzhkov et al. (1998) took data from winter storms and computed average K_{DP} and Z_{DR} values over 48 and 24 gates, respectively, as well as the applicable standard errors. They discovered that for typical K_{DP} and Z_{DR} values of .2°km^{-1} and 1 dB in what they classified as 'cold storms', the standard errors in the measurements caused a standard

error in the IWC estimation of 40-45%. We feel that this finding highlights an issue of great importance for winter precipitation research with a polarimetric radar—the measurements have a finite accuracy that plays an extremely important role when attempting to detect and capitalize upon small changes in the various polarimetric variables for the purpose of inferring microphysical processes. Ryzhkov et al. (1998) also analyzed the applicability of their IWC equation in the context of a dataset that included in situ measurements from a T-28 aircraft. According to their evaluation, the correlation coefficient between the aircraft collected IWC and the Z_{DR}-K_{DP} calculation method was approximately 0.69 compared to the 0.52 of a Z-IWC calculated value. The rms difference improved from 0.5 g/m^3 to 0.4 g/m^3. Ryzhkov et al. (1998) concluded that though more work with in situ data was needed, their results suggested that estimations of IWC with their method should be possible for ice water contents greater than 0.1 g/m^3, except in heavily aggregated snow.

1.4 Review of Previous Observational Research

Bader et al. (1987) conducted a data collection project in southern England using the Chilbolton dual polarization radar and in situ aircraft. The aircraft were primarily used to collect ice particle images from a 2-D cloud probe and 2-D precipitation probe. The probes had 0.8 mm and 6.4 mm detector arrays, respectively.

Table 1.3 Precipitation characteristics from Bader et al. (1987) for four aircraft passes

Run	Aircraft Height	Air Temp.	Crystal types manually classified from the collected images
a	3.7 km	-11.5°C	Lightly rimed single crystals, areas of numerous capped columns
b	3.1 km	-8.0°C	Mixed single crystals
c	2.5 km	-4.0°C	Needles and aggregates of needles, mixed single crystals
d	1.9 km	-2.0°C	Aggregates and heavily rimed single crystals

The analysis focused primarily on four passes made by the aircraft, and their characteristics as reported by Bader et al. (1987) are listed in Table 1.3. Since the cloud probe provided the bulk of the data for the manual classification of particle types, classification of particles larger than about 1.5 mm was not possible. The resolution of the precipitation probe was deemed too coarse for their work. The authors did not attempt to classify particles smaller than 0.5 mm since 95% of the reflectivity was associated with particles larger than 0.5 mm. Figures 1.6 and 1.7 show the size and type distributions from Bader et al. (1987) for each aircraft pass listed in Table 1.3. They admit that the noisiness in the data is likely a result of errors in the particle identification and the small size of the samples used. The Z_{DR} and Z measurements corresponding to Figures 1.6 and 1.7 are shown in Figure 1.8. The data includes all measurements within 1.5 beamwidths of the aircraft location. The beamwidth of the Chilbolton radar is 0.25°.

Bader et al. (1987) highlighted several points of interest. The first came from a pass not listed in Table 1.3. This pass was in a different region than the others, at a height of 3 km, with a temperature of -7°C. The Z_{DR} values were generally greater than 3dB, the reflectivity was relatively low, and the particle observations indicate dominance by planar and dendritic crystals up to 2 mm in diameter. These observations are consistent with the theory discussed in the previous sections. The second region of interest is depicted in the upper panel of Figure 1.8. This pass was at a temperature of -11°C. We focus at a range of 50 km where the peak Z_{DR} was approximately 1.2 dB. From Figure 1.7, it is clear that this was a region of high plate and dendrite concentrations. The third observation made by Bader et al. (1987) was that at the -2°C and -4°C levels, the Z_{DR} rarely exceeded 1 dB; additionally, some of the lowest Z_{DR} observations were located at the -2°C level near 37

km where, according to Figure 1.6, the greatest concentration of large particles was also located, presumably aggregates. We believe that in each of the regions described above, it is important to take note of not only the extreme Z_{DR} values as highlighted by the authors, but also the variation in Z_{DR} values which, at a given range, differ by only one or two tenths dB up to 1.5 dB. The final point of discussion by Bader et al. (1987) is also important. They examine two regions on the 3.1 km (-8°C) pass at the 34 km and 40 km ranges. The 34 km range region exhibits Z_{DR} values around 1.9 dB, while the 40 km range region exhibits Z_{DR} values around 0.8 dB. They compared the types of single crystals present in each region and found them to be rather similar, though none of the crystals were absolutely pristine. As they searched for an explanation of the Z_{DR} difference, they looked at the concentration of smaller particles, less than 1.5 mm, and larger particles, greater than 1.5 mm, at each range. The area of lower Z_{DR} had 2500 smaller hydrometeors and 300 larger ones per cubic meter, while the area of higher Z_{DR} had 850 smaller hydrometeors and only 80 larger ones per cubic meter. Bader et al. (1987) speculated that the larger hydrometeors have a higher axis ratio and lower bulk density. Despite the fact that the larger particles exist in relatively low numbers, their contribution toward lowering Z_{DR} becomes notable since Z_{DR} is a reflectivity-weighted variable. Bader et al. (1987) made a few calculations using Gans' Theory to substantiate the validity of their theory. This concept was later demonstrated further in the modeling already discussed by Vivekanandan et al. (1993) as shown in Figure 1.5. Bader et al. (1987) concluded that Z and Z_{DR} strongly reflected the hydrometeor size distribution in that low Z and high Z_{DR} was indicative of light precipitation and vice-versa. However,

they felt that Z_{DR} alone could not improve Z-S relations except to possibly indicate effective ice bulk density.

Vivekanandan et al. (1994) also analyzed data collected by aircraft and compared it to their C-band dual-polarization radar observations. Figure 1.9 shows a scattergram of Z vs. Z_{DR} from 200 m above and below the aircraft in two different regions, both at 2.4 km above the ground. The figure also depicts the particle classification results derived by manual inspection of the particle images. A general summary of the diagrams would conclude that the Z_{DR} for the dendritic population was higher, and the Z was lower. On the other hand, the more aggregated and rimed population had a lower Z_{DR} and higher Z. However, again, we feel it is important to notice the range of values in each scattergram. The dendritic Z_{DR} values ranged from 0 to 5 dB, while the aggregates and rimed crystals had Z_{DR} values up to 1.5 dB. Even though only a few points were at the extreme ends of those ranges, there was a relatively substantial region of overlap between the two populations near Z_{DR} values of 1 dB. They concluded that it appeared feasible to separate aggregate and dendrite populations using Z and Z_{DR}.

Ryzhkov and Zrnic (1997) examined six Oklahoma snowstorms with the intent of establishing some identifying characteristics in the polarimetric radar variables for snow that could be compared to those established for rain. In addition, they wanted to characterize the melting layer in the vertical and the horizontal rain/snow transition line. They used the 10 cm wavelength Cimarron radar and considered K_{DP}, Z_{DR}, and the cross-correlation coefficient, ρ_{hv}. The six storms were classified according to their surface temperature; thus, events with surface temperatures below -5°C were categorized as 'cold' storms, and those with surface temperatures near 0°C were categorized as 'warm'

storms. The authors stated that no large aggregates were observed during the cold storms, but in contrast the warm storms were associated with prolific aggregation. Figure 1.10 shows typical mean profiles for 'warm' and 'cold' storms. The values were averaged over 5° azimuth and 10 km in range. In general, the warm storms exhibited higher values of Z and lower values of Z_{DR} which, in theory, would be due to the higher aggregation efficiency in warmer temperatures. Both exhibited increases in Z and decreases in both Z_{DR} and K_{DP} as height decreased; these observations are consistent with increasing aggregation efficiency with increasing temperature. In order to get a sense of the range of values that would be found within each type of storm, Ryzhkov and Zrnic (1997) plotted Z_{DR} and K_{DP} versus Z from points within the 0.5° elevation scan. Figure 1.11 shows their results. Figure 1.12 is a plot of Z_{DR} and K_{DP} versus Z from the warm storms for the rain and snow portions of the event. From these two figures the authors concluded that average values of Z_{DR} do not exceed 0.6 dB in pure snow if Z is less than 35 dBZ. Furthermore, they found that neither K_{DP} nor Z_{DR} displayed a systematic dependence on Z. Additionally, they concluded that in a warm snow event, precipitation could be quantified as snow (versus rain) when the Z_{DR} values were less than 0.2 dB and Z was less than 35 dBZ; moreover, through further investigation, they identified a pronounced Z_{DR} maximum and ρ_{hv} minimum signature that appeared to more reliably indicate a rain to snow transition than the classical bright band identification.

The analysis and modeling presented in this thesis will support some of the results and conclusions supplied by the researchers described above, but it will also be contradictory in some aspects. The organization of this thesis will continue as follows: Chapter 2 presents the methods used to collect and analyze the data, while Chapter 3 and

Chapter 4 discuss the results from the radar observations and the modeling efforts, respectively. Chapter 5 will finish with conclusions and recommendations for further study.

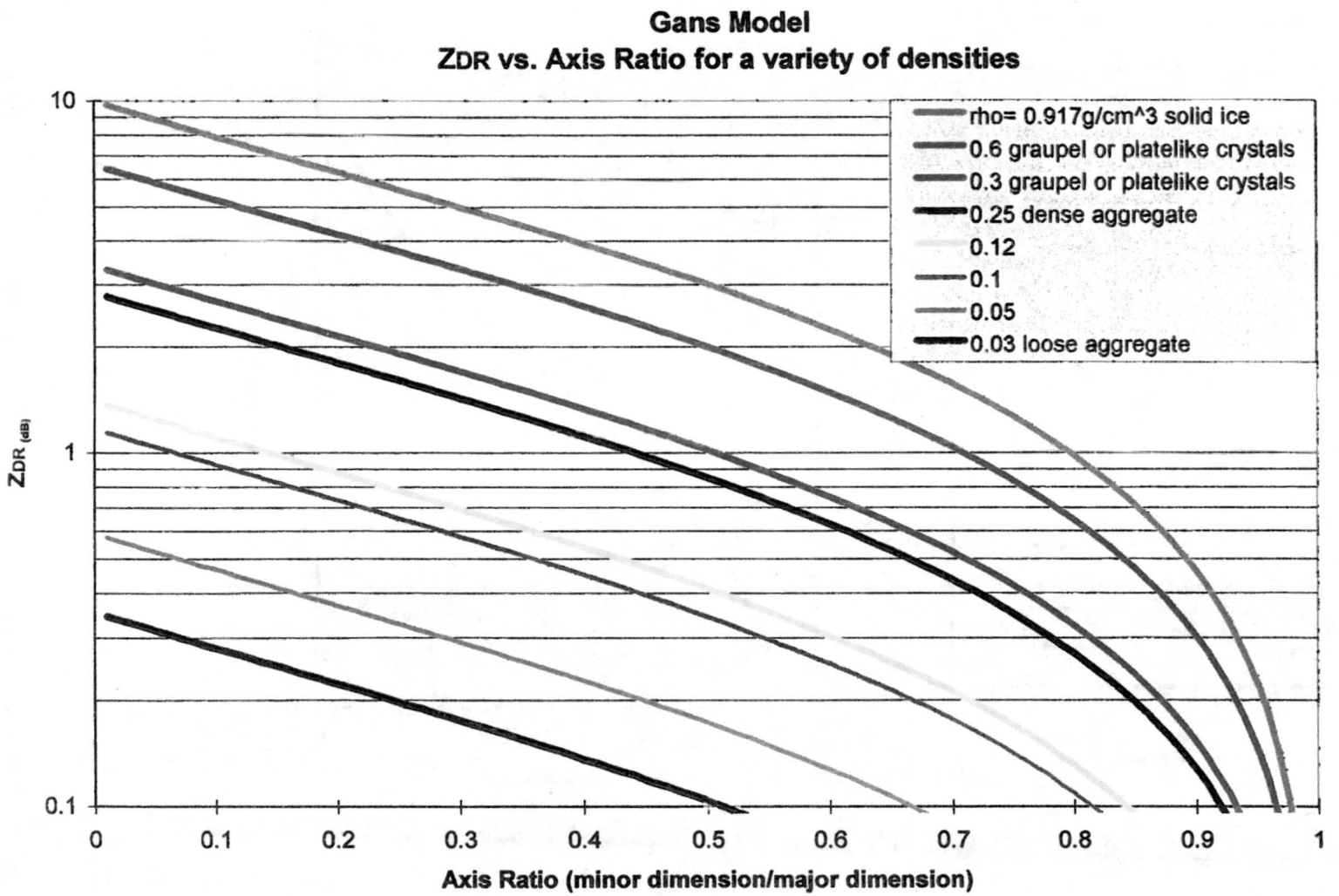

Figure 1.1: Z_{DR} as a function of axis ratio and density according to Gans' Theory.

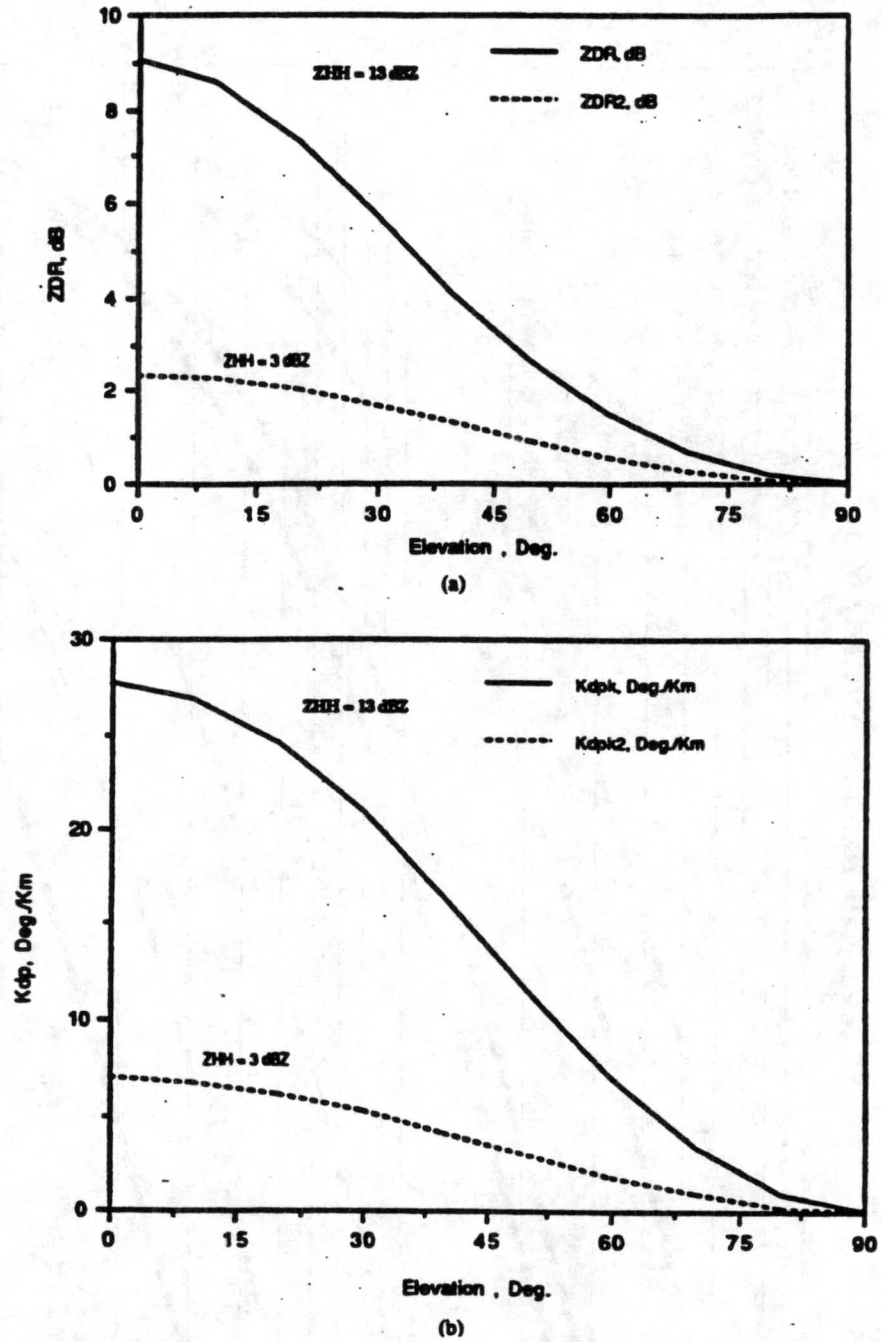

Figure 1.2: Modeled Z_{DR} and K_{DP} at K-band as a function of elevation angle for plates. (0.92 g/cm^3 density, solid line; 0.23 g/cm^3 density, dashed line; from Evans and Vivekanandan 1990)

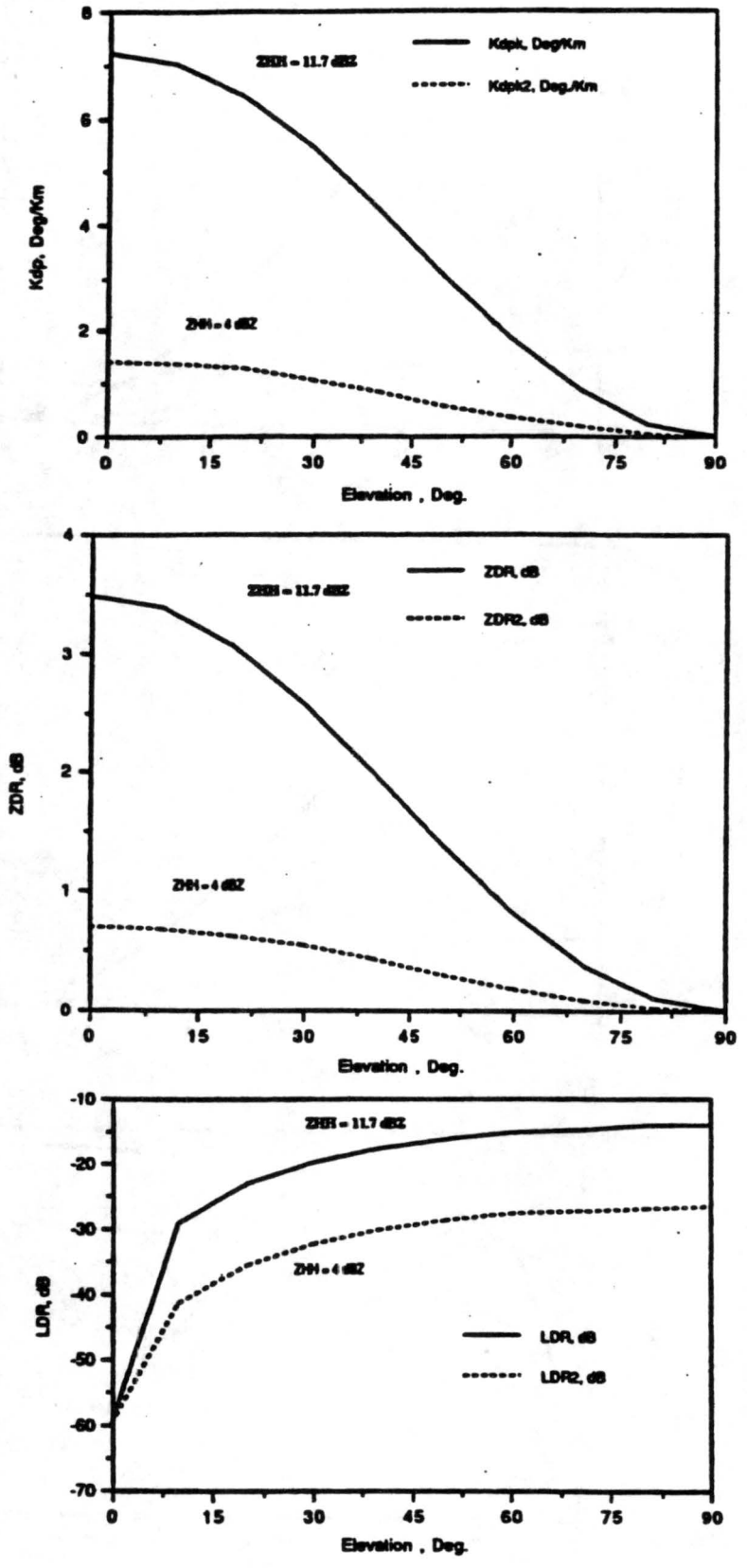

Figure 1.3: Same as Figure 1.2 except includes LDR and is for columns. (From Evans and Vivekanandan 1990)

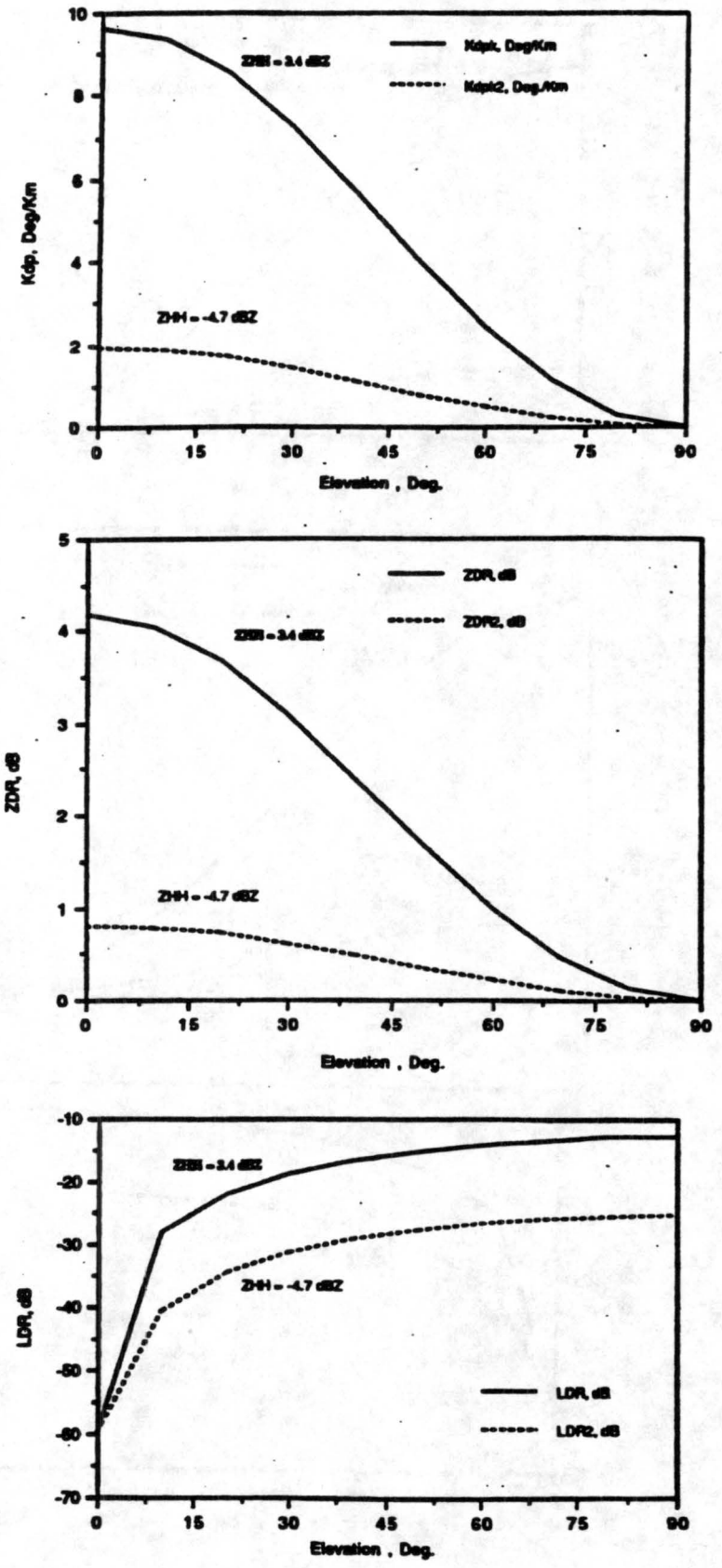

Figure 1.4: Same as Figure 1.3 except for needles. (From Evans and Vivekanandan 1990)

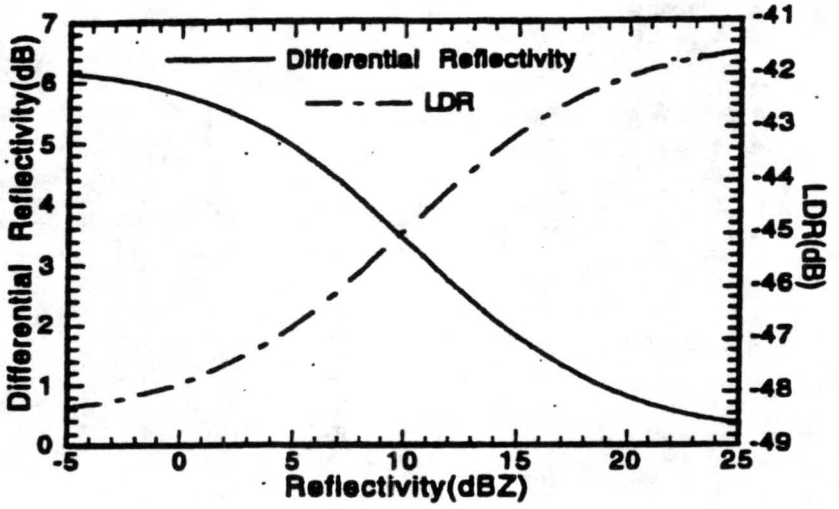

Figure 1.5: Modeled Z_{DR} and LDR of precipitation mixture of aggregates and 10 dBZ of plates versus aggregate reflectivity. (From Vivekanandan et al. 1993)

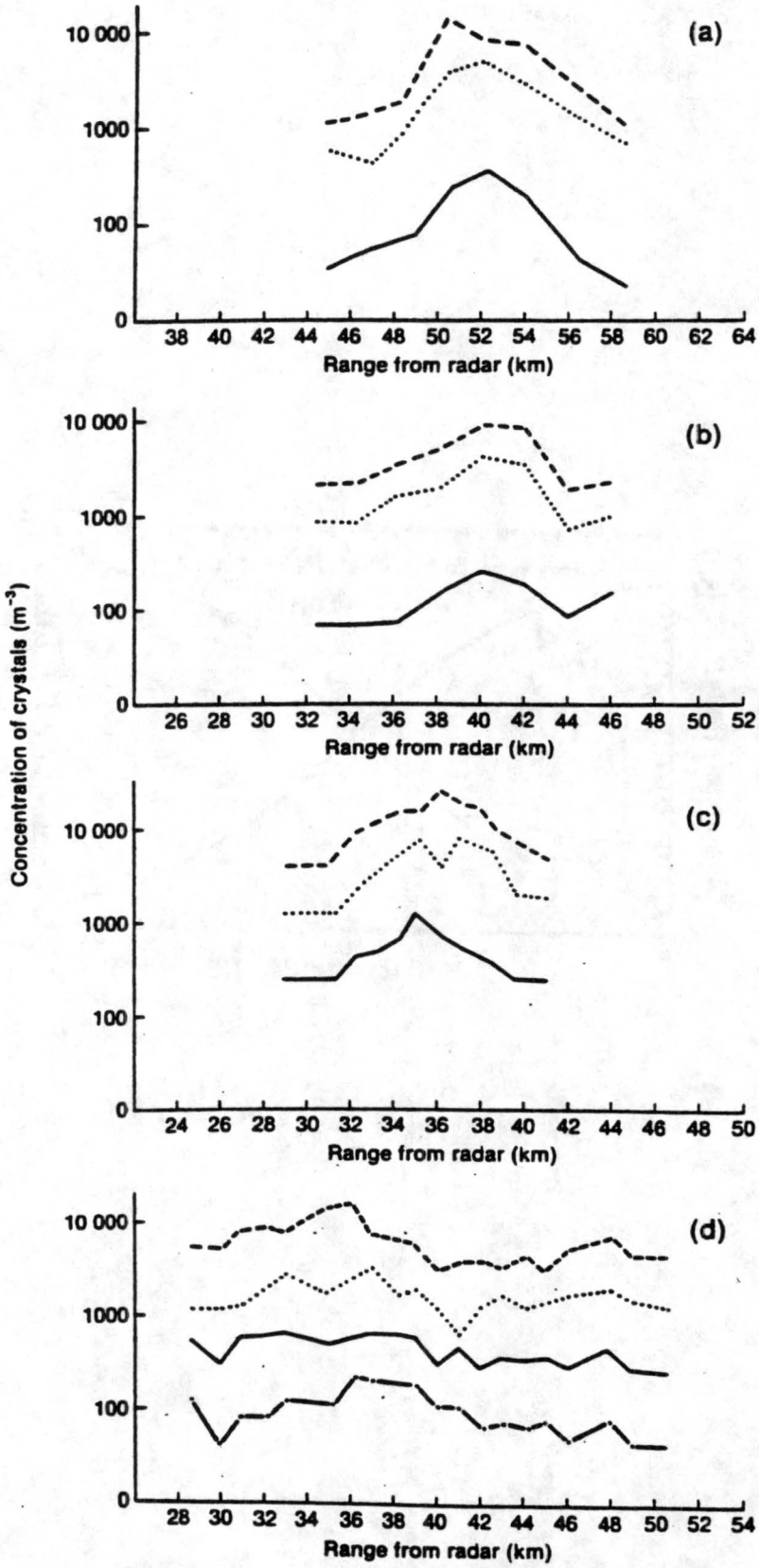

Figure 1.6: Particle size distributions for four aircraft runs described in Table 1.3. (diameters in mm: 0.2-0.5, dashed line; 0.5-1.5, dotted line; 1.5-2.5, solid line; >2.5, dash-dot line; from Bader et al. 1987)

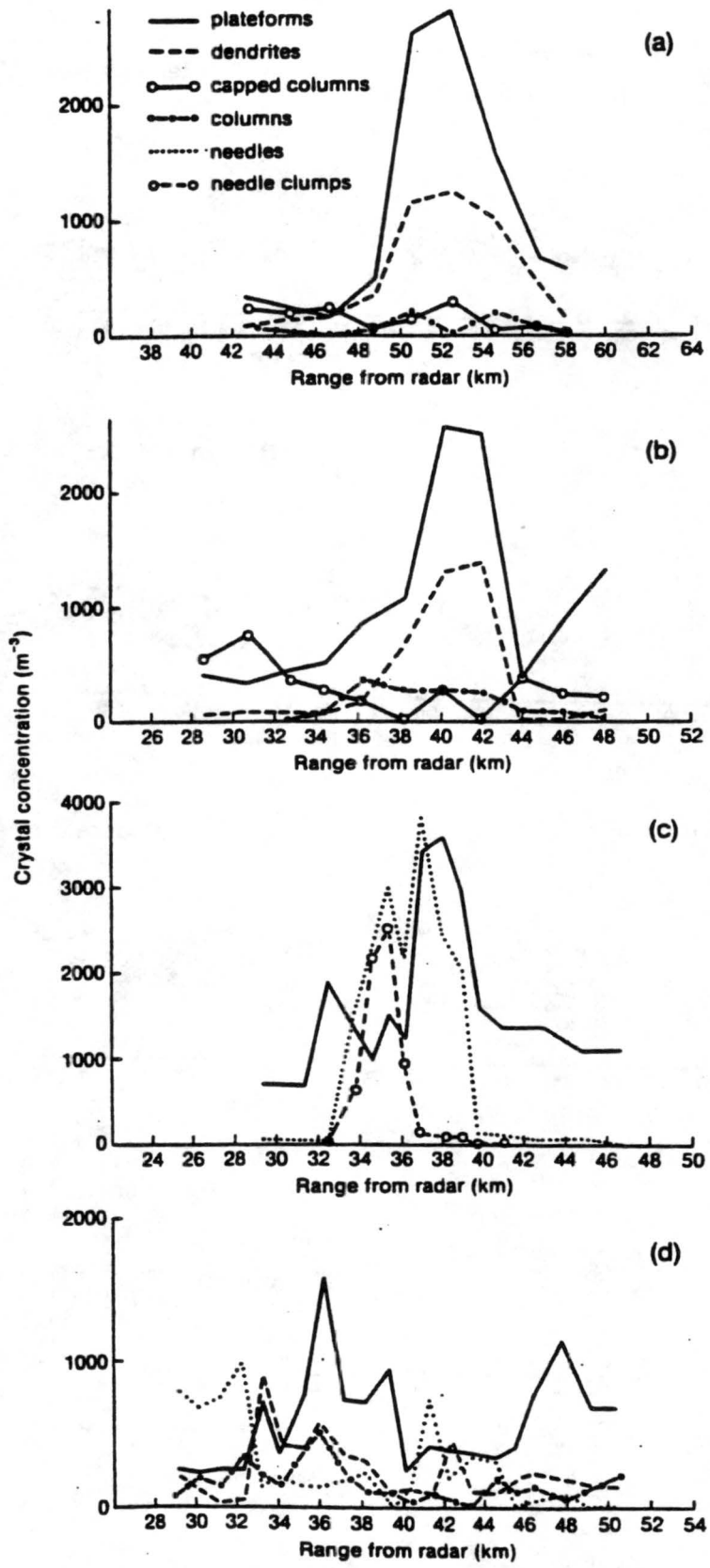

Figure 1.7: Concentrations of particle types for four aircraft runs described in Table 1.3. (From Bader et al. 1987)

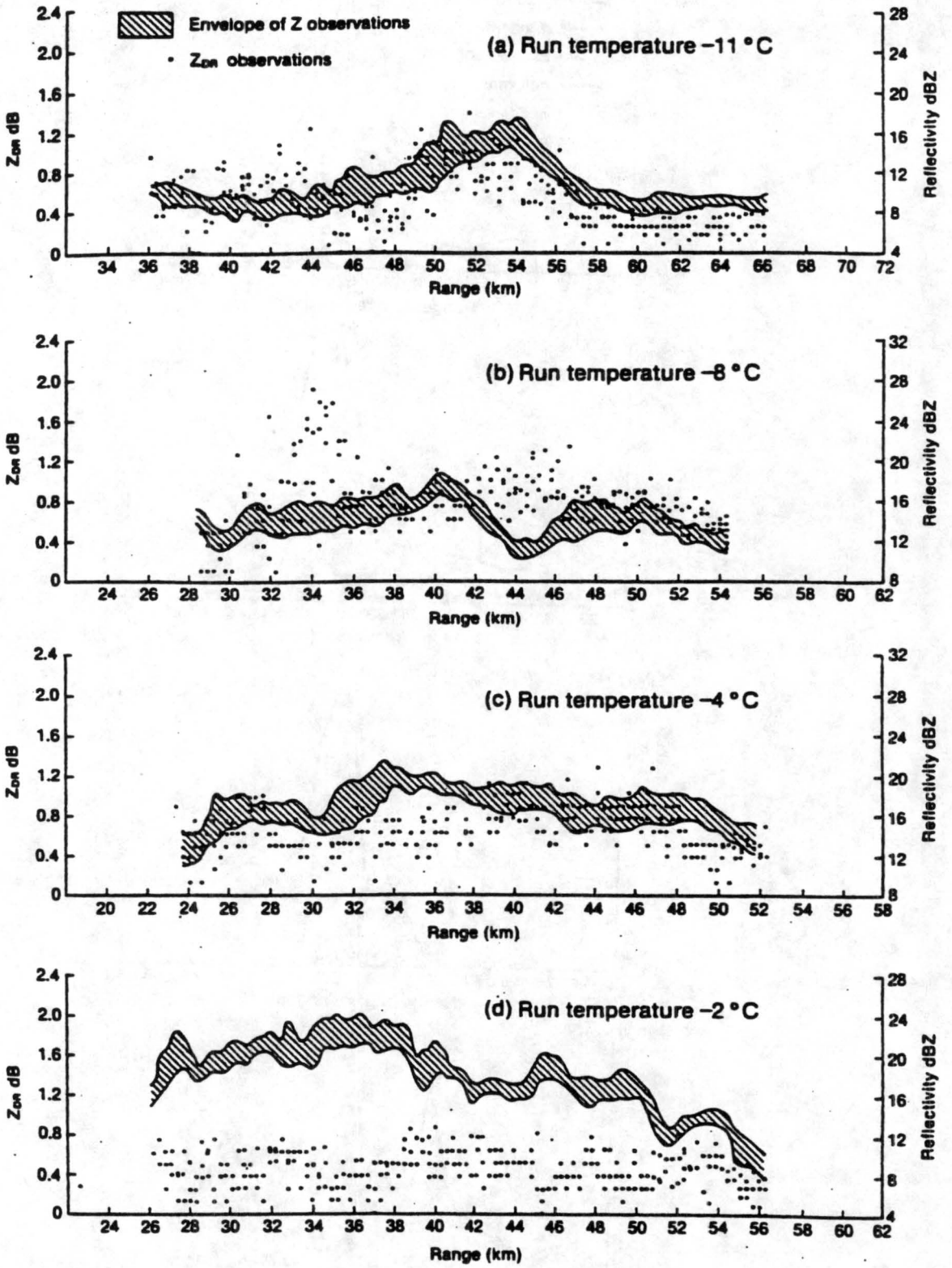

Figure 1.8: Z and Z_{DR} radar observations corresponding to four aircraft runs described in Table 1.3. (From Bader et al. 1987)

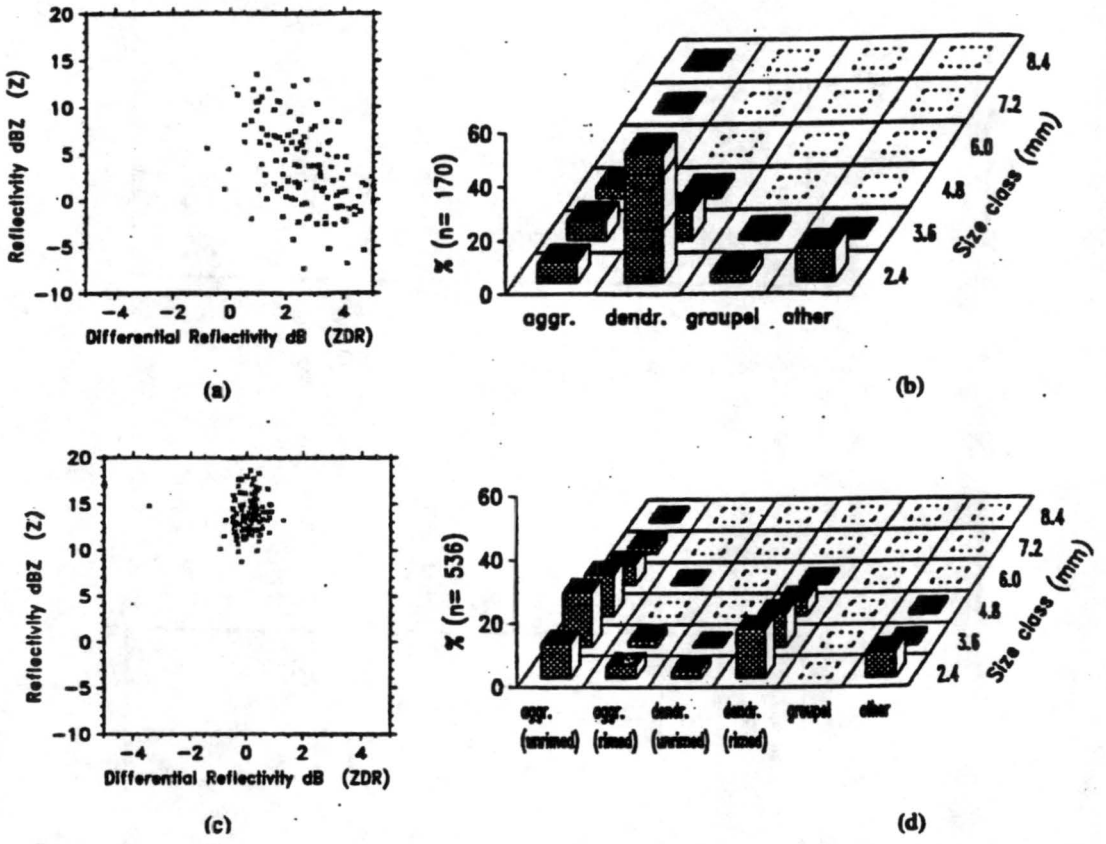

Figure 1.9: Scatter plots of Z vs. Z_{DR} and corresponding concentrations of particle types collected by aircraft. (From Vivekanandan et al. 1994, with changes.)

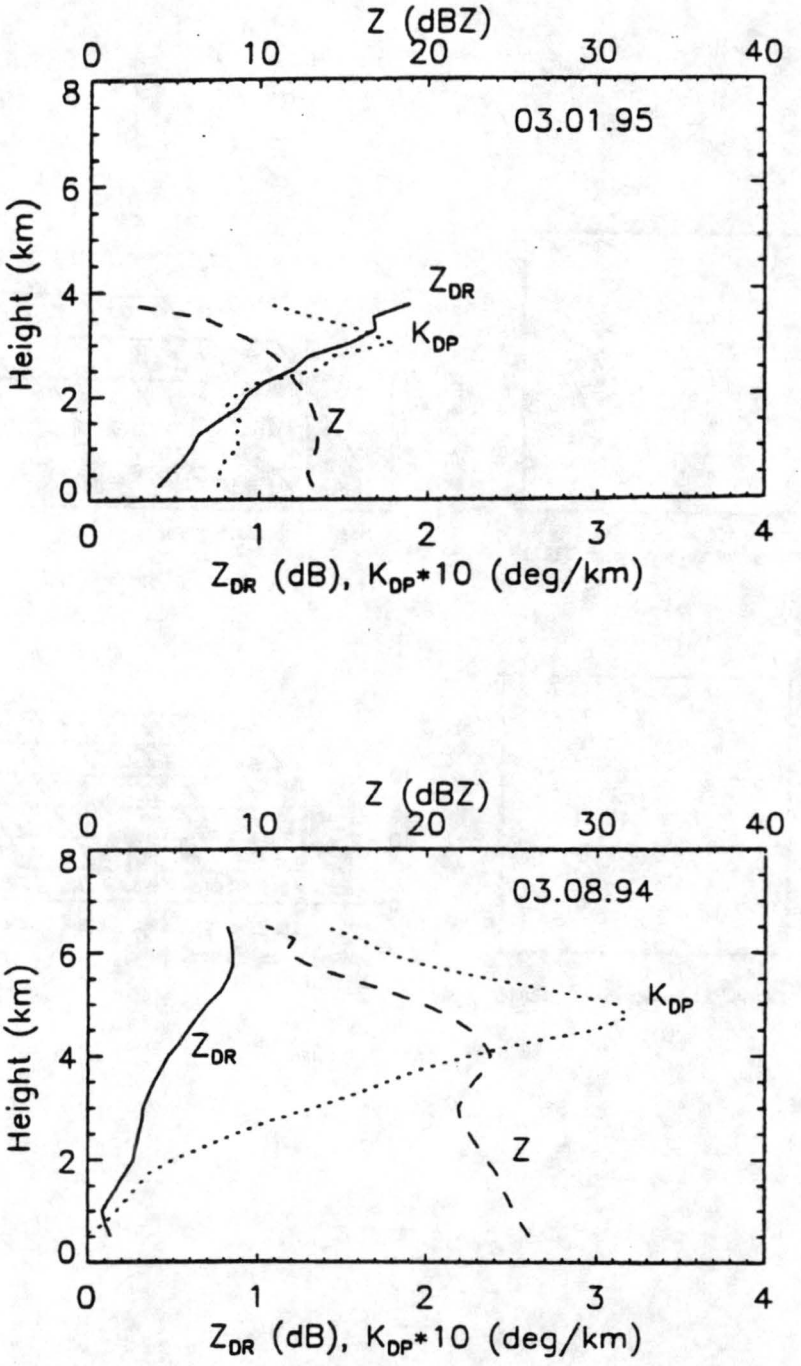

Figure 1.10: Vertical profiles of Z, Z_{DR}, and K_{DP} for 'cold' storms (top) and 'warm' storms (bottom). (From Ryzhkov and Zrnic, in press)

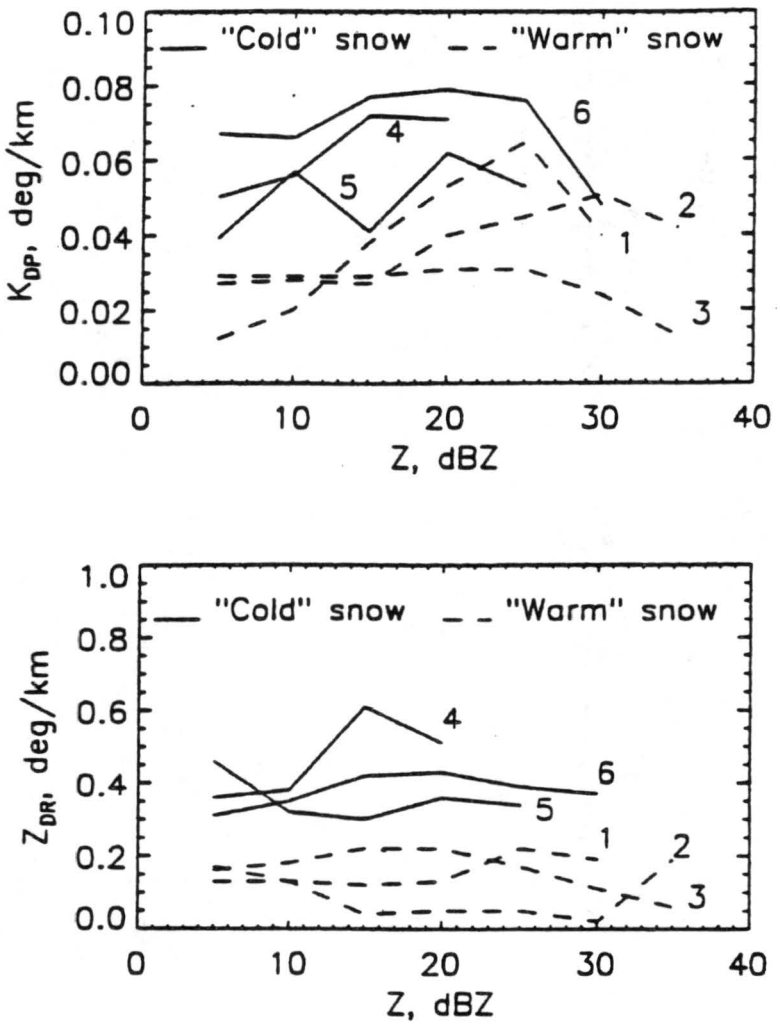

Figure 1.11: K_{DP} vs. Z (top) and Z_{DR} vs. Z (bottom) for snow near surface in six storms. (1 - 8 Mar 1994; 2 - 5 Jan 95; 3 - 18 Dec 95; 4 - 1 Mar 95; 5 - 2 Mar 95; 6 - 1 Feb 96; from Ryzhkov and Zrnic, in press)

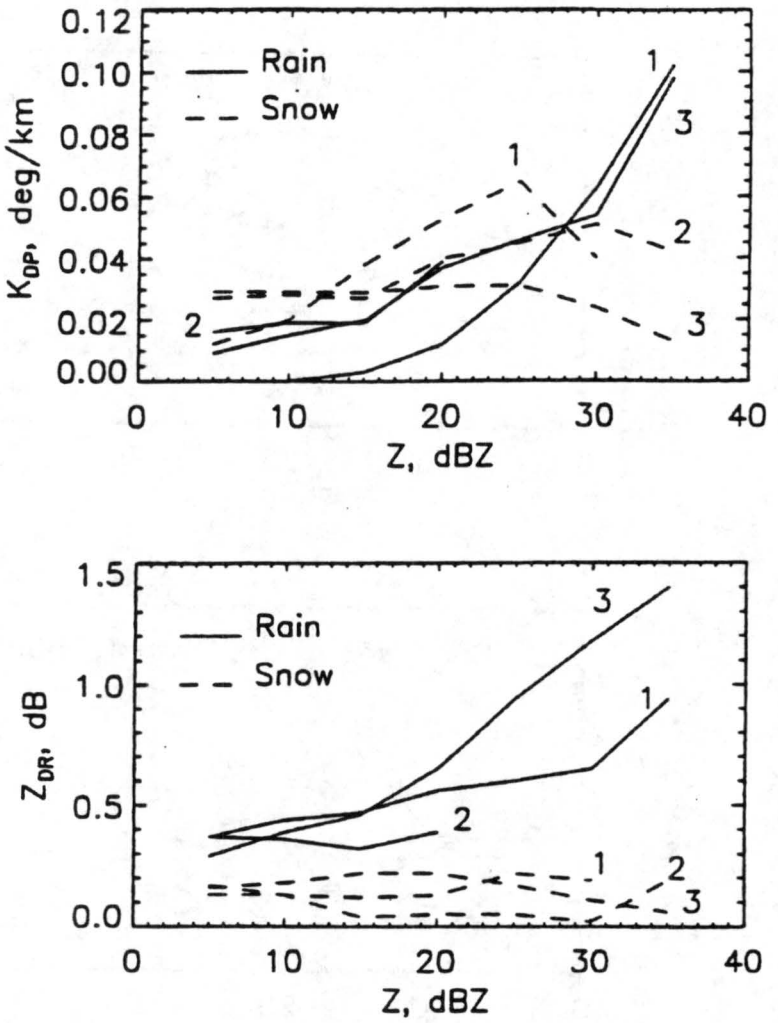

Figure 1.12: Same as Figure 1.11 except for 'warm' snow compared to rain. (From Ryzhkov and Zrnic, in press)

CHAPTER 2

DATA COLLECTION AND ANALYSIS METHODS

2.1 Data Collection

The CSU-CHILL National Radar Facility (located near Greeley, CO) was the primary instrument utilized in our study. CHILL is an S-band, dual-polarized, Doppler radar that employs two separate transmitters to transmit horizontally and vertically polarized. It also has two separate receivers which allow it to concurrently receive horizontally and vertically polarized returns. The specific operational characteristics of the radar during the 1997 winter precipitation season are shown below in Table 2.1.

Table 2.1 CSU-CHILL radar characteristics

CSU-CHILL Radar Characteristic	Value
Wavelength (cm)	11
Antenna diameter (m)	8.5
3 dB beamwidth (°)	1.0
Peak power (kW)	800
Pulse length/2 (m)	150
Pulse repetition frequency (Hz)	1000
Number of Samples	128
Receiver noise power (dBm)	-115
Maximum range	150

The scanning strategy varied during the 1997 data collection season and combined plan-position indicator (PPI) scans with range-height indicator scans (RHI), but several important characteristics remained relatively consistent. Generally in the PPI scans, the first two sweeps were at elevation angles near 0.5° and 1.0°. The radar data examined in this study were almost exclusively comprised of those two lowest sweeps. Every 30 minutes one particular PPI scan was run which was coordinated for a dual Doppler analysis with the National Center for Atmospheric Research (NCAR) S-pol radar, an S-band, polarimetric, Doppler radar. S-pol was operated near Erie, CO for our field experiment (PROWS; Polarimetric Radar Observations of Winter Storms). The S-pol was operating during two of the four events examined in this study, so velocity and reflectivity data were also used from the National Weather Service's NEXRAD WSR-88D Doppler radar in Cheyenne, WY for the purpose of performing dual Doppler analyses with the CHILL radar. Those analyses are described later in this chapter.

A field observer was located approximately 40 km to the west northwest of the CHILL radar at the Ft. Collins Weather Station on the Campus of Colorado State University (FCL). This observer was responsible for recording the visibility and snow depth. More importantly, the observer also maintained field notes documenting chronological (approximately every 10 minutes), subjective evaluations of snowfall intensity and changes in intensity, snowfall composition such as proportions of various snow types and sizes in the population, and degree of riming. These field notes provided valuable ground truth information that became the primary tool for subdividing radar data according to snow type and identifying microphysical characteristics of the hydrometeors during the analysis phase of our research. In addition to the visual observations, the

observer collected samples of snowflakes on slides coated with a solution of formvar and ethylene dichloride. Unfortunately, many of the slides collected during the events considered here did not turn out well due to a variety of problems.

Since FCL is an established observing site, standard meteorological information was automatically recorded such as temperature, wind speed and direction at 10 m, and wind speed only at 20 m. These records served as useful sources of information. Additional instrumentation was also set up specifically for the winter research project including an automated, Belfort, weighing bucket snow gauge from NCAR that was installed at FCL with an Alter wind shield around it. A 2D video disdrometer leased from Joanneum Research, Graz, Austria (Schonhuber et al., 1995) was mounted in a van and parked at the FCL site. The data from the snow gauge were not used in this particular paper, but will be important for future work. The disdrometer data did not become available until near the end of the analyses presented here due to software problems, so it is only referred to briefly.

2.2 Data Analysis

The first step in the processing of the radar data was, of course, the removal of corrupted data. There were several different sources of contamination including ground clutter from the foothills of the Rocky Mountains located a few miles west of FCL. At a few azimuths, beam blockage was present due to buildings and large trees near the radar site. These problems were handled simply by deleting the areas and beams specifically affected. Ground clutter and other bad data points were removed by applying a correlation coefficient (ρ_{hv}) threshold of 0.6; consequently, any gates with ρ_{hv} values below the threshold were deleted from all of the data fields. A more complicated

corruption of Z_{DR} measurements was encountered in regions of high reflectivity gradients, most notably adjacent to the blocked beams, due to a mismatch in the antenna beam patterns at horizontal and vertical polarizations as discussed by Herzegh and Carbone (1984). Several algorithms were applied to try to automate the removal of the bad data, but the limited success led to an effective, but brute force method of visual inspection and beam deletion. Additionally, gates with Z_{DR} values less than -1 dB were deleted from the Z_{DR} field only. All of the above editing was performed using the Research Data Support System (RDSS) software that was written at NCAR (Oye and Carbone, 1981).

The final adjustment to the data also involved Z_{DR}. The seemingly high number of gates with negative Z_{DR} values on the Universal Format (UF) tapes that were unrelated to high reflectivity gradients triggered a rather extensive investigation of the CHILL radar's Z_{DR} calibration. The calibration is comprised of two corrections; the first correction (the field correction) is applied before the data are recorded, and the second, more subjective correction is applied in the analysis phase at the radar site before the UF tapes are produced. The purpose of the field correction is to assure that Z_{DR} values from approximately –3.0 to +9.0 dB are recorded, and it is based on power readings from the two transmitters. This part of the calibration is not reevaluated daily, yet drift in the transmitter trigger delay can cause variations in Z_{DR} from day to day which is why the second correction mentioned above is applied. Originally, this second correction was being determined by the radar technicians by examining the radar images for any indications of obviously skewed values. Through the course of our investigation, we discovered that such a method was not accurate enough, and it is being modified. As a result, it was necessary to find a way to further adjust the tapes of the events that had

already been recorded using the original calibration method. The best known method available to inspect the Z_{DR} values for a lingering bias above and beyond the calibration was to examine data from a vertically pointing scan that had been conducted during the event. Theoretically, in any precipitation event, the Z_{DR} values in a vertically pointing scan should be centered on zero with a certain amount of symmetrical scatter expected. Hydrometeors whose lower faces present a nearly circular cross section to the radar would naturally produce a Z_{DR} value of 0 dB (small raindrops are obviously the best targets for this technique), but statistically even the asymmetrical particles would be randomly oriented in the horizontal so as to also produce a Z_{DR} value around 0 dB.

The vertical scans had not been included in every event of the winter and spring of 1997, but three out of the four cases examined in detail in this thesis did have vertically pointing data. The fourth event occurred on a day that a new calibration analysis had been performed at the radar. Hence, for that case, the Z_{DR} values were assumed to be correct without additional adjustment. Z_{DR} bins 0.1 dB in width were created, and the number of gates from the vertically pointing scans with Z_{DR} values that fell within each bin were tabulated and plotted in a histogram. These histograms are shown in Figures 2.1 to 2.3. The spike on the low end is deceptive because that bin actually includes the tabulation of all the gates with Z_{DR} values less than or equal to the value indicated by that bin. A solution to this problem was not pursued because the trimmed means that were calculated always fell within the same bin as the median. The similarity between the median and trimmed mean indicated that the shape of the distribution was relatively symmetrical, and it was not necessary to determine the exact shape of the lower end of the curve in order to infer the bias. The correction needed to adjust the median value to

zero for each event's vertically pointing data histogram was applied to all of the respective Z_{DR} scans from that event. Figures 2.1 to 2.3 indicate that the corrections ranged from adding 0.55 to 1.05 dB which influenced the results tremendously. Our experience highlights the importance of frequent radar calibrations and the inclusion of vertical scans in each event, especially for winter situations where one attempts to relate Z_{DR} changes on the order of several tenths of a dB to changes in storm microphysics. Additionally, any researcher working with Z_{DR} data should not assume the values were insensitive to calibration issues just because Z_{DR} is based on a ratio of reflectivity factors. This issue is probably more significant for radars such as the CHILL that operate with separate transmitters and separate receivers for the respective horizontally and vertically polarized waves. In conclusion, from the results of the Z_{DR} bias investigation, it appears that the Z_{DR} values, with all of the corrections included, have an uncertainty on the order of 0.2 dB.

Once the radar data were edited and corrected, further analysis could commence. Since one of the primary goals of this study was to compare the polarimetric variables from the 0.5° and 1.0° elevation scans to the ground-based observations at FCL, adjustments needed to be made for the time and distance that the hydrometeors traveled from their location when viewed by the radar to the surface where the ground-based observations were made. In other words, the source region in the radar scan from which the snow at FCL originated needed to be identified. In order to designate the source region, a back trajectory was calculated for numerous times throughout each event. The time intervals between calculations were selected by examining the 10 m and 20 m tower wind data for homogeneity. Whenever there was a significant change in the 10 m wind

direction (20° or more) or 20 m mean speed (more than 3-4 m/s increase or decrease in the time average), a new back trajectory was calculated and used for all the subsequent radar volumes until another similar wind change was encountered. The method used to calculate the back trajectories themselves was rather rigorous. For each designated time interval, the wind fields were computed using dual-Doppler techniques with simultaneous CHILL and S-pol or WSR-88D wind velocity data. First, the radar data had to be translated to a Cartesian grid using REORDER, a software package developed by NCAR. The gridding was done with horizontal and vertical resolutions of 0.5 km and 0.35 km, respectively, using a Cressman weighting scheme (Cressman, 1959). The radius of influence was set at 1.2° in the azimuthal direction and 1° in elevation. Once the gridding was done, the dual-Doppler analysis was accomplished using the CEDRIC software, also developed by NCAR. Hydrometeor fallspeeds were calculated using a stratiform reflectivity-fall speed relationship. Furthermore an assumption was made that vertical air motions were small relative to particle fallspeeds; hence, the vertical air motion contribution was neglected.

The resultant wind streamlines were always inspected for signs of convergence that could have lead to more than one source region, but that was never a problem. The back trajectory was computed in layers; since the first available level of dual-Doppler derived wind data was 350 m, the 10 m wind direction readings and the 20 m tower wind speeds were used in the lowest layer to calculate the trajectory to the source region at 350 m. In each successive layer the dual-Doppler derived wind vectors from the location established at the top of the previous layer were used to continue back tracking the snow path upward to the top of the next layer. The intersection of the trajectory with the radar

beam was generally near 350 m for the 0.5° elevation scan and in the vicinity of 700 m for the 1° elevation scan, but it was manually calculated for each trajectory depending on the range of the source region. The radar beam heights changed with range from the radar due to the simple triangular geometry of the non-zero elevation angle, the curvature of the earth, and changes in the index. The latter two effects were calculated using the method described by Doviak and Zrnic (1993). Additionally, in order to align the radar observation times with that of the field notes, the average descent time for the snow was added to the radar scan times. Therefore, within the limitations of the calculations and assumptions, the radar measurements were of the same population of hydrometeors that ultimately ended up on the ground at FCL.

The source region was defined to include all of the gates within a radius of approximately one kilometer from the point calculated in the back trajectory. A time series of polarimetric data was created for each event by averaging the values from all of the gates in the source region for each PPI scan recorded. The source region was kept small enough to resolve variations of snow type, intensity, and character that can occur over very short distances (Lo and Passarelli, 1982; Thomason et al., 1995; Bader et al., 1987), but large enough to allow for smoothing of the radar measurements (Ryzhkov et al., 1998; Ryzhkov and Zrnic, 1997).

Information recorded in the field notes enabled us to partition each case according to the characteristics of the snow observed on the ground at FCL. Time intervals were singled out when the majority of the snow falling was either aggregated or comprised of individual platelike crystals (i.e. dendrites, stellar crystals, and plates). Further distinctions within these two broad categories was possible at times. Scatter plots were

then created of reflectivity versus Z_{DR} values from time intervals designated as approximately homogeneous, thereby yielding a comparison of radar parameters between different snow types.

The analysis methods described in this chapter are by no means perfect, and some of the most important sources of error are discussed here. First and foremost, comparing observations of a population of hydrometeors at the ground by an observer to those by a radar at 350 and/or 700 m can be a problem. Not only are the sampling volumes quite different, but the judgment by the observer concerning when the snow was nearly homogeneous was highly subjective. An eye can be drawn to the larger particles and be more aware of the volumetric dominance than the actual numerical dominance of one snow type over the other. Fortunately, that is similar to the way the radar views the population (recall the sixth power of diameter weighting for reflectivity). Furthermore, any changes in the characteristics of the hydrometeor population between the time it was viewed by radar and the time it was viewed at the ground (approximately 6 minutes from the 0.5° scan and 12 minutes from the 1° scan) are completely unknown. Additional errors may have been introduced in the trajectory calculations such as variations in the wind field on scales smaller than resolved by the radars, or deviations of the actual fallspeeds from those predicted by the reflectivity-fallspeed relationship.

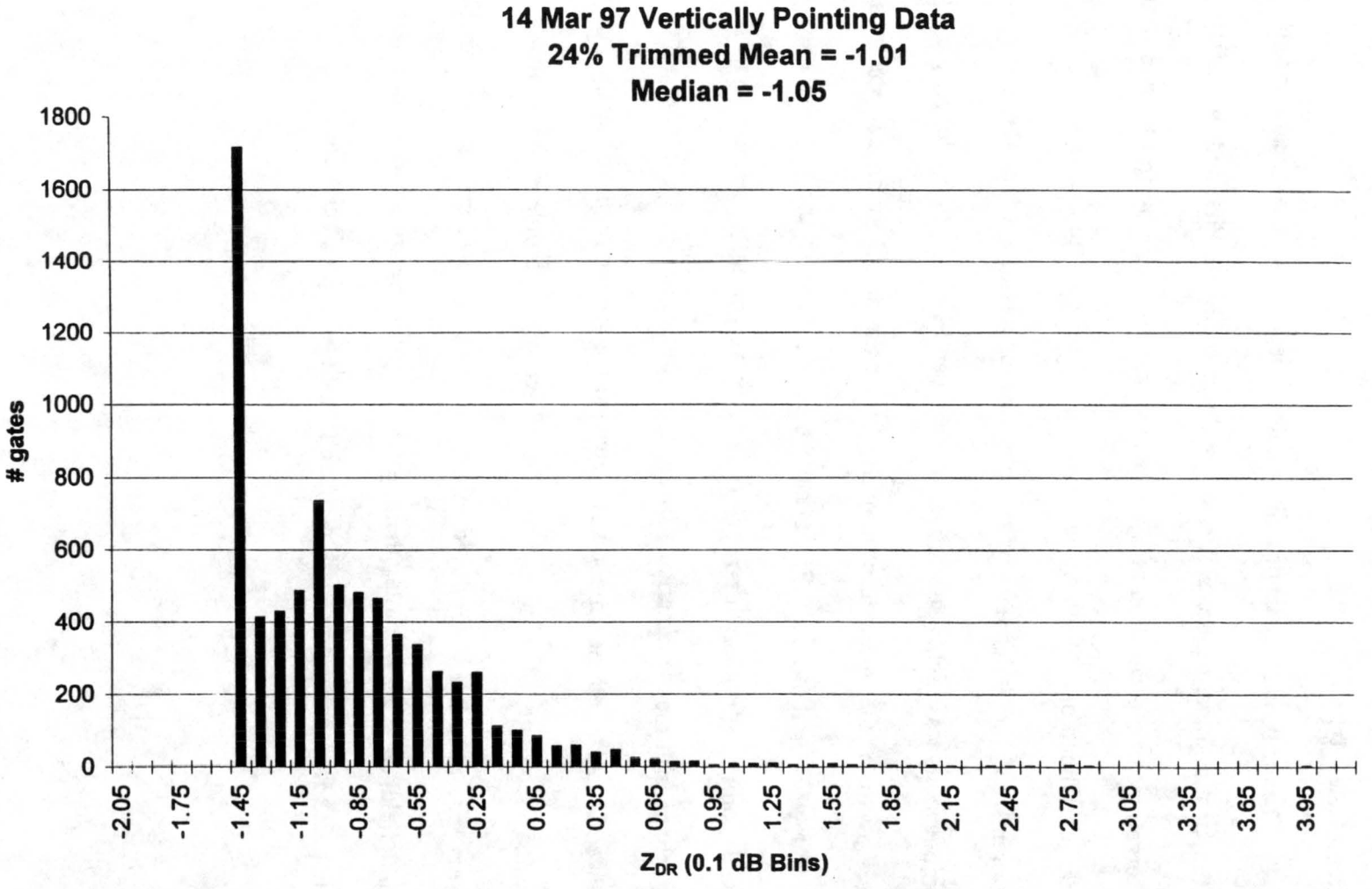

Figure 2.1: Histogram of vertically pointing Z_{DR} data for 14 March 1997. (First bin includes gates from all smaller bins.)

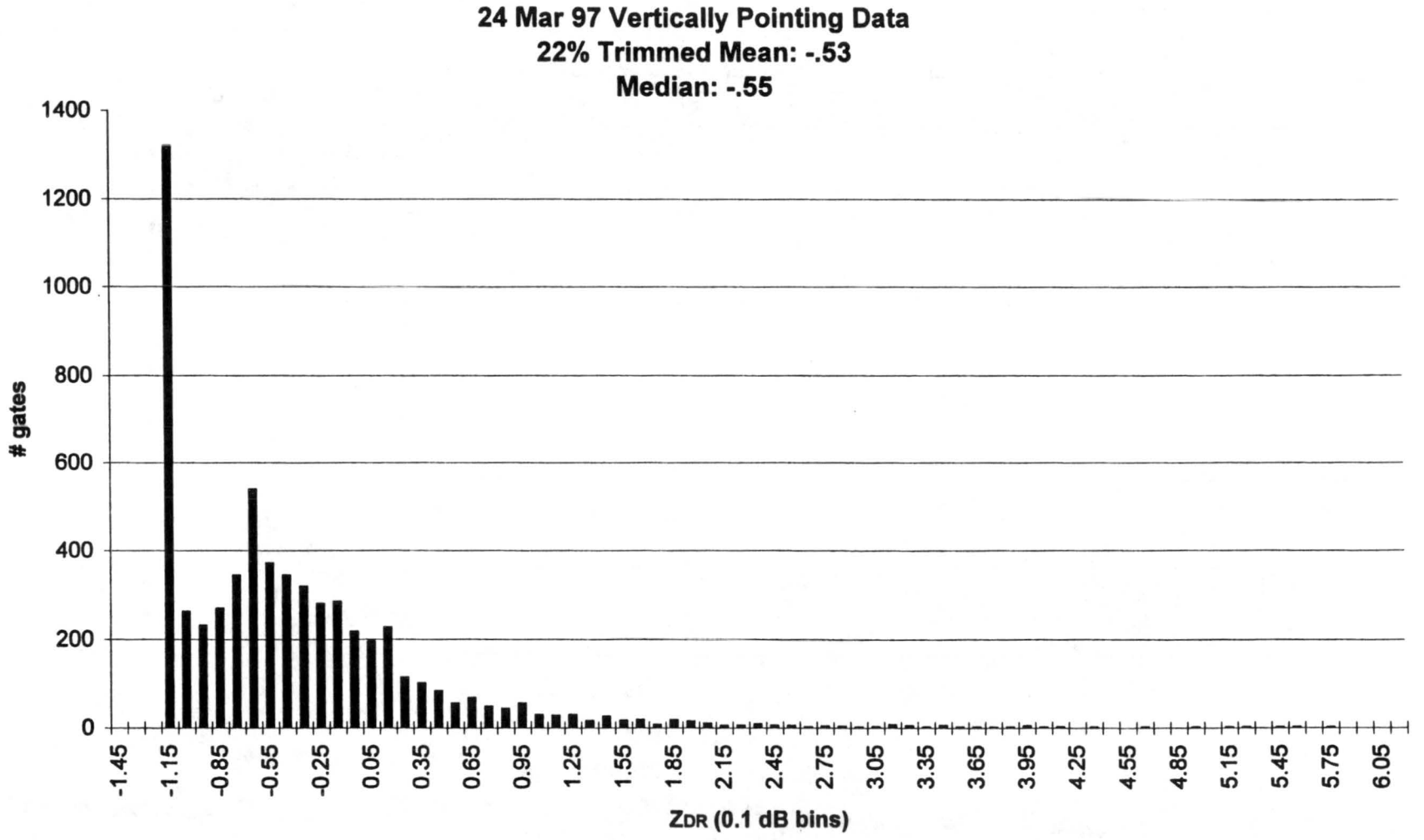

Figure 2.2: Histogram of vertically pointing Z_{DR} data for 24 March 1997. (First bin includes gates from all smaller bins.)

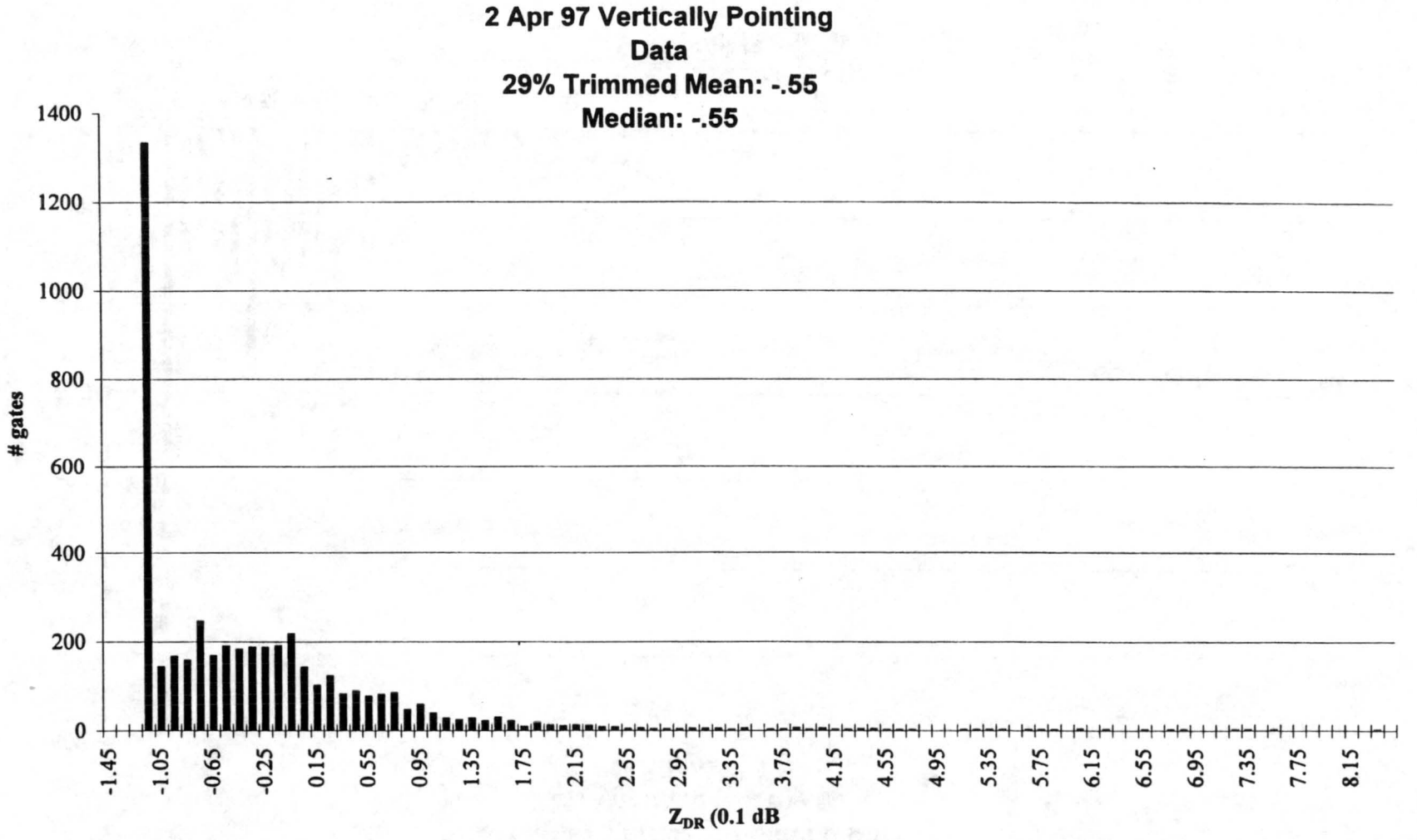

Figure 2.3: Histogram of vertically pointing Z_{DR} data for 2 April 1997. (First bin includes gates from all smaller bins.)

CHAPTER 3

RADAR DATA RESULTS

3.1 Case Descriptions

Four cases (dates in Greenwich Mean Time) were selected for in-depth analysis: 13-14 March 1997, 24 March 1997, 2 April 1997, and 4-5 April 1997. Brief synoptic summaries derived from upper air charts and the Nested Grid Model (NGM) analyses are shown below in Table 3.1. Other distinguishing features for each event are shown in Table 3.2.

Table 3.1 Synoptic nature of events

Synoptic Influences at FCL	**13-14Mar97**	**24Mar97**	**2Apr97**	**4-5Apr97**
Cold Front	strong	moderate	moderate	strong
Upslope	strong, shallow	strong, shallow	moderate strength and depth	moderate strength and depth
Upper Level Trough Passage	brushed FCL	yes, at 700mb	no, but closed lows to west	yes, at 700, 500, and 300mb
Positive Vorticity Advection	weak	weak	--	unknown
Vertical Velocity	weak	moderate	moderate	moderate
Jet Stream	overhead	--	--	--

Table 3.2 Event features

	13-14Mar97	24Mar97	2Apr97	4-5Apr97
Duration of Observations	2345Z 13Mar to 0840Z 14Mar	1720Z to 2240Z	0605Z to 2030Z	rain: 2245-0425Z snow: 0425Z-0520Z
Total snow depth accumulated during observation	2.7"	.7" + initial melt	2.5" + initial and final melt	all melted
Surface air temperature range	steady decrease -4.5° to -9.3°C	3.1° to -1°C	2.4° to -1.4°C	1.9° to .8°C
Approximate Sfc-700m ΔT using DIA soundings	4.0 to 6.8°C	6.3°C	4°C	4.1°C
Wind speed (20m tower time averages)	3-4m/s	8-10m/s til 22Z; 6m/s after	6m/s 06-07Z 2-3m/s after	6-7m/s
Minimum visibility	5/16 mile	3/16 mile	~ 1/2 mile	> 1/2 mile
Snow wetness	relatively dry	wet	wet	very wet
Rain/Snow transition?	No	drizzle turned to snow	No	Yes

The most important features to note from Table 3.2 are the temperatures and the winds. The temperatures in the 13-14 March case were considerably lower than the others, at the surface and at 700 m. (The 700 m level approximately corresponds to the height of the 1° elevation scan from CHILL.) The winds during the 13-14 March and 2 April events were significantly lighter than the other two. Initially it was thought that the extensive amount of blockage affecting data near the FCL site would prevent the 0.5° elevation scans from being useful in the analyses. However, the trajectories in the two light wind cases identified source regions outside, though sometimes very near, the blocked beams. As a result, the 13-14 March and 2 April cases have two levels of polarimetric data, the 0.5° and 1° elevation scans, while the 24 March and 4-5 April cases only have data from the 1° elevation scan. The horizontal distances from the trajectory-identified source regions to the FCL site are shown in Table 3.3. As stated previously, each case may have had more than one source region.

Table 3.3 Distance from FCL to source regions

	13-14 March 97	24 March 97	2 April 97	4-5 April 97
0.5° elevation scan	0.8 to 1.4 km	3.8 to 5.1 km	1 to 1.8 km	5.4 km
1° elevation scan	1.2 to 2.9 km	10 to 13.7 km	2.4 to 4.4 km	12.6 km

The lateral displacements were obviously significant for some of the events.

3.2 Timelines

Figures 3.1 to 3.6 are the Z and Z_{DR} timelines for each event. Each point represents the source region average from one PPI scan, and the line is a six point moving average. Detailed interpretation of these particular charts is not possible without the field notes; however, the overall patterns and range of values are apparent. As observed and modeled by previous researchers (e.g. Bader et al., 1987; Vivekanandan et al., 1994), portions of the timelines exhibit the tendency for Z_{DR} to decrease as Z increases, and vice-versa. This trend is especially apparent at the start and end of events where there was frequently a transition between platelike crystals and aggregates. Examples include the beginning and end of the 13-14 March event at both elevations angles (Figures 3.1 and 3.2), 2040-2110Z on 24 March (Figure 3.3), and 2310 to 0110Z on 4-5 April (Figure 3.6). Other times during those events were often periods of little change in either parameter. The 2 April case was more variable, but in Figure 3.4 the trend can still be detected during most of the observational period: 0810-0930Z, 1210-1410Z, 1410-1610Z, and 1650-1730Z. That trend does not prevail for all times in all cases, though. For example, at the end of the 2 April event, both Z and Z_{DR} decreased because nearly spherical snow pellets became dominant (lower Z_{DR}), and the snowfall rate decreased (lower reflectivity).

Generally the reflectivity ranged from -5 to 25 dBZ during the 13-14 March event, with a few lower values. The Z_{DR} values were typically between 0 and 3 dB, but a few instances of values as high as 4 and 8 dB were also observed. These values are consistent with the range of observations found by Vivekanandan et al. (1994), and relatively consistent, though slightly larger, than the range found by Bader et al. (1987). Our Z_{DR} values were also well within the modeled ranges outlined in Table 1.2. However, our results indicate that extreme caution should be taken with the conclusion made by Ryzhkov and Zrnic (1997) that snow only produces Z_{DR} values less than 0.6 dB. Table 3.4 is a statistical summary of the Z_{DR} values (the FCL source region average) from every scan recorded during snowfall. The data is organized first by event, and then according to scan level and storm type as defined by Ryzhkov and Zrnic (1997) ('warm': T_{sfc} near 0°C; 'cold': T_{sfc} < -5°C). Our results are, in fact, completely contradictory to their conclusions; the majority of the scans had Z_{DR} values exceeding 0.6 dB.

Table 3.4 Statistical summary of observations in every event and scan

Scan	'cold' or 'warm'	Rain/snow transition?	Date	# scans with Z_{DR}>.2 to # total scans	# scans with Z_{DR}> .6 to # total scans
0.5°	cold	no	13-14 Mar97	92/92	92/92
0.5°	warm	no	2 Apr97	121/128	75/128
1.0°	cold	no	13-14 Mar97	86/86	86/86
1.0°	warm	sprinkles to snow	24 Mar97	57/57	47/57
1.0°	warm	no	2 Apr97	106/106	97/106
1.0°	warm	rain to snow	4-5 Apr97	51/65	20/65
All 0.5° events				96.8%	75.9%
All 1.0° events				95.5%	79.6%
0.5° warm event				94.5%	58.6%
All 1.0° warm events				93.9%	71.9%
Rain/Snow events (only 1.0° events available)				88.5%	54.9%

The best comparison is with the compilation of all 0.5° scan events (a 75.9% majority of scans with $Z_{DR} > 0.6$; see Table 3.4) since most of the cases in Ryzhkov and Zrnic (1997) used that scan. Additionally, Ryzhkov and Zrnic (1997) concluded that when distinguishing between rain and snow, precipitation could be quantified as snow when the Z_{DR} values were < 0.2 dB. (They acknowledged that drizzle alone would also produce Z_{DR} values near 0 dB, but in their cases, there were always enough non-spherical drops to generate larger Z_{DR} values). Our data, as shown in Table 3.4, suggest that such values ($Z_{DR} < 0.2$ dB) only comprise a very small subset of what Ryzhkov and Zrnic (1997) termed 'warm snow' (less than 12%), and the unstated, converse conclusion that precipitation could be quantified as rain if Z_{DR} values were greater than 0.2 dB would be false. It should be noted that our rain/snow event data were not directly comparable since they were only available from 1.0° scans, but at that level, less than 5% of the radar scans recorded during the snow portions of the events would have qualified to be quantified as snow by the 0.2 Z_{DR} threshold. The one 0.5° scan warm event we had is consistent with that evaluation. The only two explanations we can propose to explain the significantly different results of Ryzhkov and Zrnic (1997) would be calibration errors (which could be a very important factor) or incorrect snow type classifications. For example, it is possible that the hydrometeor populations in the cold snow events had more aggregates than they thought, similar to the example from Bader et al. (1987), and as a result, the Z_{DR} values were lower than expected for individual crystals.

3.3 Scatter Plots of Z vs. Z_{DR}

Figure 3.7 is basically a transformation of all the points on the 1° elevation scan timelines into one Z vs. Z_{DR} scatter plot. It illustrates again the general trend that Z_{DR}

decreases as Z increases; however, some of the 2 April points demonstrate that exceptions to such a trend certainly exist.

Figures 3.8 and 3.9 are also Z vs. Z_{DR} scatter plots for the 0.5° and 1° elevation scans, respectively, but the field notes were incorporated to provide further insight. Only periods of time throughout each event identified with relatively homogeneous snowfall were included. These periods were first categorized by the snow form, either aggregates or individual, platelike crystals. The aggregate time periods certainly had coexisting individual crystals, but the aggregates appeared to be numerous enough to dominate the population. Within the individual crystal category, periods of platelike crystals with intense riming were identified and plotted separately from other platelike crystals. The degree of riming that we refer to as 'intense' was one step above heavy riming and one step below graupel. The intense riming was easily characterized by an unmistakable three-dimensional appearance of the crystal. In these circumstances, the depth of rime on the face of the crystal was near 1 mm, yet its original form was not yet obscured like a snow pellet or graupel particle. The aggregates were only divided on the plot by date, but significant variations within the aggregate classification will be discussed in the context of specific comments from the field notes. It is essential that any interpretations or conclusions drawn from these snow type scatter plots be tempered with the understanding of the limitations that were inherent in the methods used for their creation. The field observations were recorded at the ground by observers. In contrast, the 0.5° and 1° elevation scan radar observations were taken approximately 350 m and 700 m above ground, giving the hydrometeor populations roughly 6 and 12 minutes of time, respectively, to alter their character as they drifted towards the surface. An adjustment

was made for the time offset itself between the radar and observer measurements, but the exact extent of the evolutionary effects on the population remains uncertain. (Although, a sense of those effects will be gleaned from comparisons made later between the available 0.5° scans and the corresponding 1° scans.) Furthermore, the observer was only capable of making subjective evaluations of the composition and nature of the snowfall.

The most prominent feature of Figures 3.8 and 3.9 is the rather well-defined separation between aggregates, platelike crystals, and intensely rimed platelike crystals. The aggregates consistently had lower differential reflectivities than the platelike crystals, with the exception of the intensely rimed platelike crystals. The intensely rimed platelike crystals had Z_{DR} values similar to the aggregates (also observed by Vivekanandan et al., 1994, as seen in Figure 1.9), but their reflectivity values were lower which provided distinction between the two categories. The rest of this section will be based on Figure 3.9 from the 1° elevation scan in order to include data from all four events, and it will focus will be on the relative differences between Z_{DR} values.

Within the aggregate category, there appears to be two distinct populations, one with higher Z_{DR} values than the other. As discussed in Chapter 1, Z_{DR} is influenced by dielectric constant, bulk density, axis ratio, particle size distribution, and fall mode. After examining the field notes corresponding to numerous samples from each of the two aggregate populations, as they were manifested in Figure 3.9, there seems to be a number of possible ways in which several of the above factors may have been responsible for the observed Z_{DR} separation among the aggregates. Table 3.5 outlines the aggregate characteristics as described in the field notes for four distinct periods and their respective radar data values from the 1° scan. First, compare the riming in examples two and three.

Example three had heavier riming than example two which would therefore produce a greater bulk density. The higher bulk density would, in turn, produce a larger Z_{DR} for a given axis ratio. Furthermore, in example three, the aggregates were observed to be elongated which would contribute to a higher Z_{DR}.

Table 3.5 Characteristics of four specific aggregate periods

	Date/ Time (GMT)	Riming	Particles in Aggregate Composition	Size Range (cm) & Shape	Z_{DR} (dB) 1°scan	Z (dBZ) 1°scan
1	0810-0820 2 Apr 97	not mentioned	snow pellets, dendrites/stellar	majority: 0.8-1 many: 1-1.5; noted 0.4 axis ratios	1.12	24.4
2	1410-1420 2 Apr 97	'appears to be less' than earlier	dendrites	majority: 0.5 some: 1	0.68	19.6
3	1600-1610 2 Apr 97	heavy	so rimed, hard to tell if was dendritic or stellar origins; some crystals fused together	majority: 0.7 some: 1-1.5; noted elongation	1.4	19.0
4	0050-0100 14 Mar 97	unknown intensity	most: 'small rimed bits' some: snow pellets, and dendrites	majority: 0.8-1 some: up to 1.8	1.2	23.9

Indeed, the Z_{DR} observed for example three was significantly higher than example two. Next compare the composition of examples one and four with that of example two. Conceivably the snow pellets of examples one and four, and the small bits of example four would individually have higher densities than the dendrites in example two, thereby producing a higher aggregate bulk density. The field notes for example one specifically described a typical axis ratio of 0.4 which indicated elongation and could explain, in conjunction with a higher bulk density, its higher observed Z_{DR} value. Shape (spherical, elongated, etc.) was not specifically identified during the time period of example four or most of the other time periods. However, from the times in the field notes that did record observations of shape, recollection by the observers, and additional moments of

observation during snowstorms in 1998, there seems to be a pattern of elongation for larger aggregates. Such a growth pattern could be explained by the swinging and spiraling motion observed in falling snowflakes by many researchers (e.g. Kajikawa, 1982; Sasyo, 1977; Zikmunda and Vali, 1972) which would enhance collection at the sides of the aggregate. Thus, it is reasonable to assume that during a period when aggregates were as large as 1.8 cm, such as example four, a fair amount of elongation was present. The inferred higher bulk density and relatively high observed Z_{DR} value provide further evidence that such an assumption is physically plausible. Similar assumptions will be applied later in the modeling chapter to examine the results.

Two additional factors need to be considered. The majority of the points in the lower Z_{DR} aggregate group in Figure 3.9 were from the 24 March and 4-5 April events. The characteristics listed in the field notes during the aggregate periods of those events included much of the same variety listed in the four examples of Table 3.5. However, the Z_{DR} values did not show the same variation, but remained nearly the same. The condition that was consistent for all of the 24 March and 4-5 April aggregate periods was the high wind speeds. Researchers have found that snow hydrometeors tend to fall with a nearly horizontal orientation when observed under conditions where the particles are protected from the wind (Kajikawa, 1976; Sasyo, 1977; Zikmunda and Vali, 1972). This observation is generally assumed to apply in real atmospheric conditions, but it is less applicable for turbulent conditions which cause the aggregates to cant over larger angles or tumble (Kajikawa, 1992; Sassen, 1980; Sasyo, 1977). Therefore, it is highly likely that the hydrometeors in the 24 March and 4-5 April events were canting, and their lower Z_{DR} values resulted from the influence of the aggregate fall mode more than any of the other

factors discussed above. The final possibility we can suggest to explain the separation of Z_{DR} values among the aggregates is related to the particle size distribution. It is quite possible that the size distribution of a hydrometeor population observed at the ground had evolved significantly since being interrogated by the radar at approximately 700 m. Two events could have similar, large aggregates at the ground, but if the most efficient phase of aggregation for one event was at or below the radar beam, the observed Z_{DR} values would be different than the observed Z_{DR} values for another event in which most of the aggregation had already occurred by the time the hydrometeors passed through the radar beam. This issue will be discussed in greater detail at the end of this chapter when the available 0.5° elevation scan data are compared to the 1° data.

The disparity within the platelike crystal category in Figure 3.9 is even more striking than the division among the aggregates. The field notes indicate that two primary factors were involved: riming and size of major dimension. Rime generally collects most significantly on the faces of platelike crystals (Pruppacher and Klett, 1997) which increases the axis ratio by increasing the minor dimension. The impact that a given depth of rime could have on the axis ratio of a crystal depends on the size of the major dimension. A larger crystal would need significantly more riming to achieve a particular, relatively large axis ratio compared to a smaller crystal, and, of course, the larger the axis ratio, the lower the Z_{DR}. This explains why some crystals had much larger Z_{DR} values than intensely rimed crystals of the same size. It was amazing how precisely the changes in riming or size chronicled in the field notes corresponded with the chronological changes evident in the radar data. For example, the platelike crystals observed from 0920Z through 0950Z on 2 April 1997 were documented as moderate to heavily rimed

sector plates and dendrites in the 2-3 mm size range, and the Z_{DR} values from the 5 scans in that period averaged 2.1 dB. The next notation in the field notes was made 10 minutes later at 1000Z, and it stated that the precipitation rate had decreased (consistent with the decrease in radar reflectivity at that time from around 12-15 dBZ to 5-8 dBZ). All of the individual crystals, mostly plates, were smaller, less than or equal to 1 mm in diameter, and they were heavily to intensely rimed. Concurrently, the Z_{DR} dropped from 2.1 dB (0948Z) to 1.1 dB. This Z_{DR} value persisted until 1032Z at which time it decreased to 0.9 dB. The field notes indicate that at that time the snowfall rate had increased again (consistent with the higher radar reflectivity values); the crystals were generally in the 1-2 mm size range, but they had become so intensely rimed that they were 'taking on more 3-D shapes'. The Z_{DR} values dramatically increased again at 1055Z to values around 2 dB. The 1050Z entry in the field notes stated that the dendrites were getting larger, up to 3 mm, and flatter, 'not as 3-D as they were before'. By 1100Z, the observer documented that the dendritic crystals were in the 2-4 mm size range and were only moderately rimed. All of these shifts in Z_{DR} and others were remarkably consistent with the riming, size of major dimension, and Z_{DR} relationship concepts discussed above. Not only were the Z_{DR} shifts consistent with the microphysical observations of the crystals, they were rather large in magnitude, on the order of 1 dB; our results emphasize the significant role riming can have on differential reflectivity. Moreover, our results should serve to caution modelers who would rely solely on diameter based formulas to prescribe axis ratios because significant deviations occur within a given size range due to riming, and those deviations generate large deviations in Z_{DR}.

3.4 Comparison of 0.5° and 1° Elevation Scan Data

To gain more insight on the microphysical evolution in the hydrometeor population during its descent from the level where it was viewed by the radar to the surface, we compared the 0.5° elevation scan data with the 1° elevation scan data for the two cases where the 0.5° elevation scan data were available, 13-14 March and 2 April. The first comparisons were in the form of the timeline, so entire events were included with all the different types and combinations of ice particles. Figures 3.10 and 3.12 show the Z_{DR} and Z timelines, respectively, for the 13-14 March event, and Figures 3.11 and 3.13 are the same for the 2 April event. For both events, there appears to be little difference in the reflectivities between the two scan levels. Figures 3.10 and 3.12, however, do have some interesting features. In Figure 3.10, the first half of the 13-14 March case tended to exhibit a small decrease in the Z_{DR} values on the order of 0.2-0.3 dB as the hydrometeors fell from around 700 m to 350 m. For times later than 0400Z, little if any change was observed in Z_{DR} with height.

Approximately half of the 2 April event, Figure 2.11, also had Z_{DR} values decrease on the order of 0.2-0.3 dB or less from the higher scan to the lower one. However, the other half of the event exhibited more significant decreases in Z_{DR} values, often 0.4-0.8 dB. These sharp decreases in Z_{DR} between levels occurred almost exclusively during periods of dominance by aggregates, but a notable exception occurred around 0900Z during a period of sector plates, stellar crystals, and dendrites. The field notes around 0900Z indicate that most of the crystals were around 2 mm in size, and some of them were rimed beyond recognition, though others had very little riming. With a warm surface temperature of -0.7°C at 0900Z at FCL and a temperature change of 4°C

from the surface to 700 m (Table 3.2), the cloud layer between scan levels likely contained most of the supercooled cloud drops that rimed the crystals (Pruppacher and Klett, 1997). Thus, it would be logical for the Z_{DR} to decrease from the higher scan to the lower one as the riming increased the axis ratio of many of the crystals. Another possible explanation would be that small aggregates formed between the scan levels. This may have been jointly or solely responsible for the Z_{DR} decrease. We performed a rough calculation to see how much growth by aggregation could be expected during the approximate six minute travel time between scan levels. We used an aggregate diameter growth equation from Rogers (1974), and the results indicated that it would be feasible for an aggregate to grow by 2 mm to 4 mm. As described in Chapter 1, Bader et al. (1987) observed an example where particle samples from two regions indicated that individual crystals (similar types) were the dominant snow type in both regions. However, the Z_{DR} value in one region was 0.8 dB lower than the other. Bader et al. (1987) determined that the difference was due to the fact that the sample with the lower Z_{DR} contained more aggregates than the other. Thus, it is conceivable that small aggregates formed between the scan levels and caused the Z_{DR} to decrease.

The periods during the two events that were dominated by aggregates also behaved differently. In a rough sense, that can be seen by looking at 0050-0100Z on Figure 3.10 and 1400-1610Z on Figure 3.11. The 13-14 March case showed small decreases in the aggregate Z_{DR} values from the higher scan to the lower one, while the 2 April case exhibited large decreases. The exact values were extracted from the data, and the average change in Z_{DR} from the 1° scan to the 0.5° scan during the aggregate periods of the 13-14 March event was -0.2 dB. The average change in Z_{DR} during the aggregate

periods of the 2 April event, however, was -0.8 dB. The 13-14 March period of dominance by aggregates was certainly shorter and had fewer PPI scans to average together, but only 2 of the 24 PPI scans in the 2 April aggregate period had Z_{DR} differences between the two scan levels that were smaller in magnitude than the largest one in the 13-14 March period. In fact, 15 of the 24 PPI scans had differences greater than 1.5 times the largest one in the 13-14 March case. Therefore, the conclusion that the Z_{DR} exhibited significantly greater changes between scans during the 2 April event than the 13-14 March event seems valid and not just an artifact of sample size.

The next question is why the different trends existed. Once again, the temperature profile outlined in Table 3.2 is key. Between 1400 and 1610Z on 2 April, the surface temperature reported at FCL was generally between 1.1°C and 1.7°C. The temperature difference between the surface and 700 m was approximately 4°C; therefore, the temperature at the 1° scan was around -2.6°C. This temperature is ideal for aggregation which is most efficient between 0 and -5°C (Pruppacher and Klett, 1997). Therefore aggregation, which would reduce the concentration of individual platelike crystals and at the same time produce larger aggregates, could account for the observed decrease in Z_{DR}. Such a shift in the hydrometeor population would result in a Z_{DR} decrease because the bulk densities of the aggregates would be lower, and the axis ratios would be higher. As described previously, the growth by aggregation calculation verified that the growth between levels could be significant.

The temperatures in the 13-14 March case only reached -5°C right at the surface, so those ice particles were not exposed to the most efficient temperature conditions for aggregation. The aggregation efficiency decreases with decreasing temperature; however,

a secondary maximum exists around -15°C (Pruppacher and Klett, 1997) which was above the 1° scan in the 13-14 March case. Thus, it is possible that most of the aggregation had already occurred by the time the hydrometeor population was interrogated by the radar in the 1° scan, and only minimal aggregation took place before it passed through the 0.5° scan. In such a scenario, little Z_{DR} change would be expected between levels, consistent with the small changes observed in this case. Furthermore, the Z_{DR} values from the 13-14 March aggregate period in the 0.5° scan (around 1 dB) were distinctly higher than those from the 2 April aggregate periods (generally < 0.75 dB; Figure 3.8), and we propose that this was due to a smaller population of aggregates during the former period. (A population with fewer aggregates would produce higher Z_{DR} values, as discussed previously in reference to the Bader et al. (1987) findings.) The temperature conditions were less conducive for aggregation, and the disdrometer data is consistent with this explanation (See Figures 3.14 and 4.1-4.3). In addition, the modeling results in Figure 1.5 (Vivekanandan et al., 1993) illustrate that a decrease in the aggregate reflectivity contribution of a few dBZ can change the Z_{DR} by an amount comparable to the differences observed between the 13-14 March and 2 April cases.

Given the above analysis of the comparisons between the 0.5° and 1° scans, it appears that the Z_{DR} values from the 0.5° scan are sometimes better qualified for direct comparison to the different categories of snow observed at the ground. However, the previous analyses and discussions in this chapter based on the 1° scan data in Figure 3.9 are still applicable despite this conclusion because they were focused on relative differences among and within the snow type categories, not on the actual magnitudes. Those relative differences are still apparent in the 0.5° scan data of Figure 3.8. Take for

example, the two distinct aggregate groups identified in Figure 3.9. Detailed data analysis revealed that points in the aggregate group with Z_{DR} values between 0.5 and 0.8 dB in the 1° scan generally ended up between 0.0 and 0.4 dB in the 0.5° scan (there are more 2 April points in the 0.5° scan's 0.0 to 0.4 dB range than between 0.5 to 0.8 in the 1° scan because more 0.5° PPI scans were available with good data, not because points shifted from one group in Figure 3.9 to another in Figure 3.8). The group of aggregate points in Figure 3.9 with Z_{DR} values between 0.8 and 1.7 maintained its distinction in the 0.5° scan with values in the range 0.4 to 0.9 dB. The two groups in Figure 3.8 have almost no distance between them, unlike Figure 3.9; however, they do exist on opposite ends of the range of observed aggregate values, and the microphysical reasons for the separation that were previously discussed are still valid. The relative difference between the intensely platelike crystals and the other platelike crystals was also maintained from one scan to the other.

The actual range of values in the 0.5° scan for each particular snow type observed at the ground were generally consistent with results from previous researchers such as Vivekanandan et al. (1994) and Bader et al. (1987). For example, Bader et al. (1987) observed that the Z_{DR} was generally less than 1 dB for areas with significant aggregation, and our observations are consistent. The bulk of the dendrite dominated observations by Vivekanandan et al. (1994) had Z_{DR} values between 1 and 4 dB, as did our less rimed platelike crystals. However, some minor differences also existed. Most of the Z_{DR} values observed by Bader et al. (1987) did not exceed 1.2 dB, with one instance of values up to 2 dB. In contrast, our platelike crystal observations had Z_{DR} values almost exclusively greater than 1.2 dB. The Z_{DR} values observed by Vivekanandan et al. (1994) for the

aggregate and rimed dendrite categories established a range that extended up to 1.5 dB, similar to our data, but the bulk of their readings were below 0.5 dB. In fact, it appears that almost half of their Z_{DR} values were less than 0 dB, and they concluded that the average was about 0 dB. Our aggregate data from the 0.5° scan are relatively few in number, but even when doubled in size by including the intensely rimed platelike crystals as Vivekanandan et al. (1994) did, our average Z_{DR} value was 0.62 dB (or 0.59 dB when the 13-14 March points, which were thought to contain fewer aggregates, are excluded). Perhaps calibration issues are to blame for the disagreement. However, we feel that we were as meticulous as possible with that issue; therefore, we present our data as evidence to dispute a pervasive perception that aggregates should display 0 dB Z_{DR} values. Even the model results in Figure 1.5 from Vivekanandan et al. (1993) only allow the Z_{DR} to drop to 0.4 dB when the aggregate contribution to the population is overwhelming at 25 dBZ, and the crystal contribution is only 10 dBZ. It is certainly true that aggregates tend to generate Z_{DR} values closer to 0 dB than most unrimed or light to moderately rimed individual crystals do. However, our work suggests that the assumption that aggregates will produce Z_{DR} values of 0 dB can be a poor one, depending upon the degree of Z_{DR} precision required.

In this chapter we have presented somewhat circumstantial evidence indicating that our observed variations of Z and Z_{DR} in time and space are consistent with inferred microphysical processes. Furthermore, our results suggest that radar measurements of Z and Z_{DR} can be used to distinguish between three classifications of snowfall. The first consists of intensely rimed platelike crystals. The second classification includes all other platelike crystals, and the third classification is composed of aggregates.

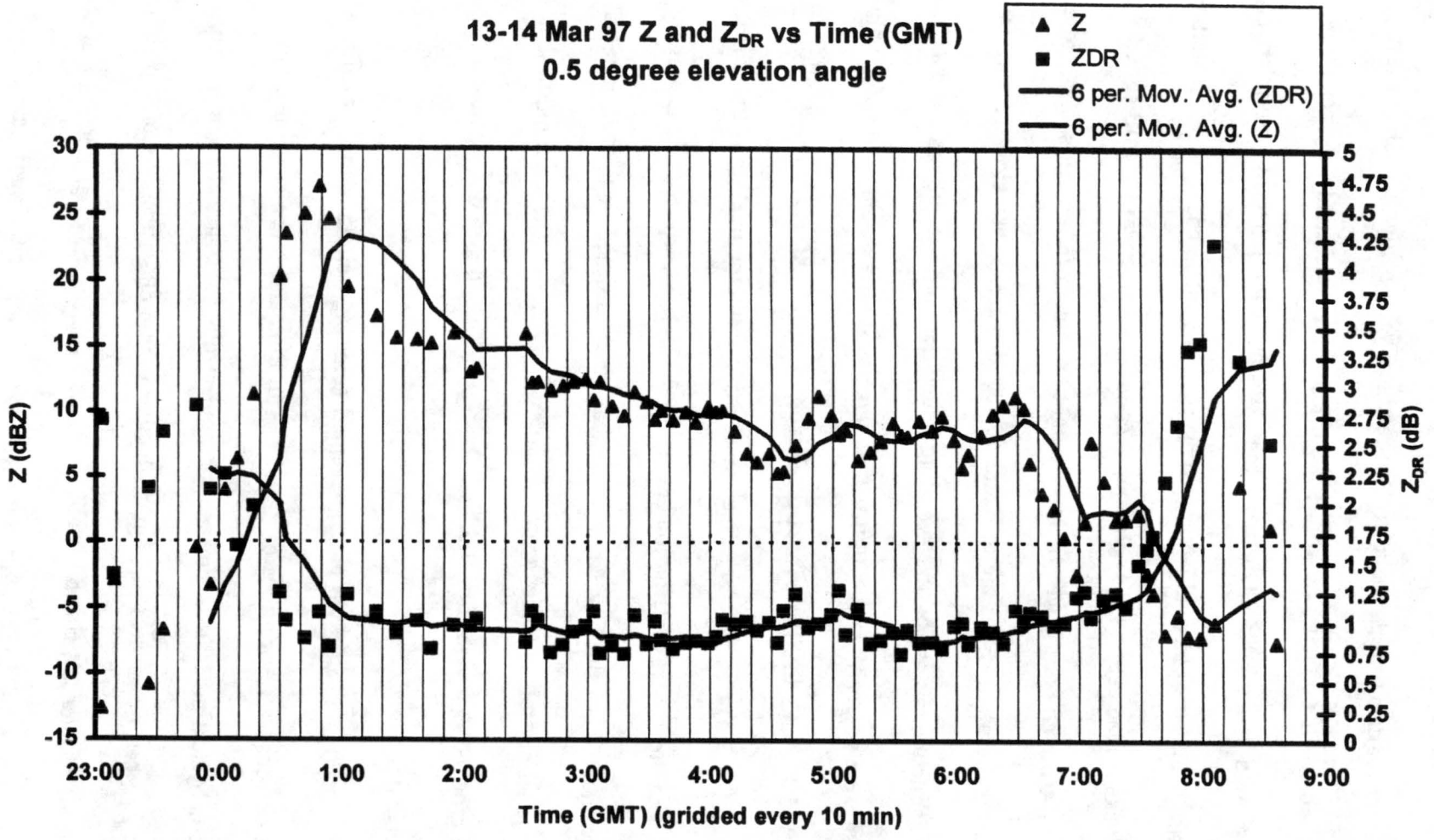

Figure 3.1: Timelines of Z and Z_{DR} from 0.5 degree scans of 13-14 March 1997 event. (Lines show 6 point moving average.)

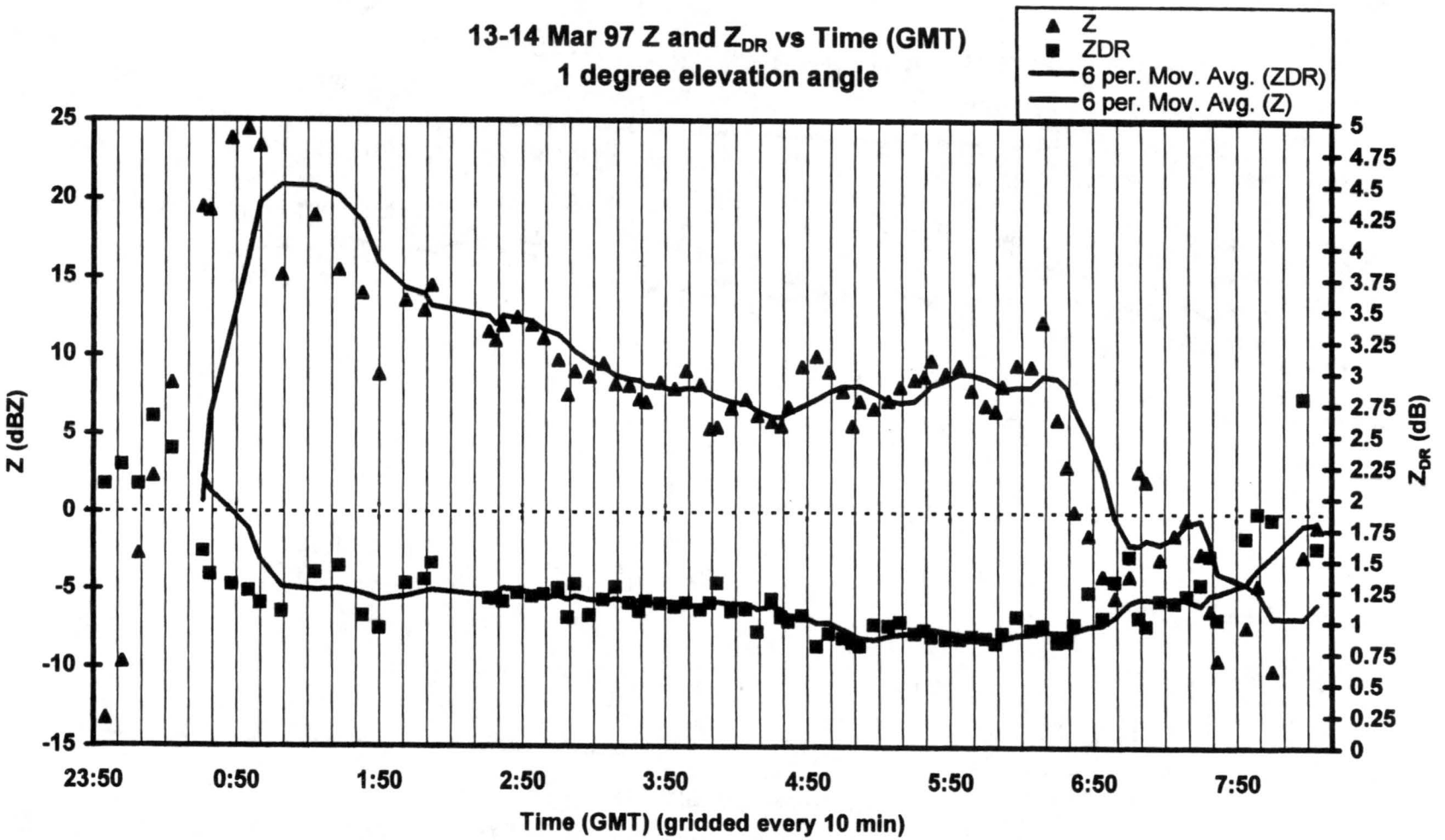

Figure 3.2: Timelines of Z and Z_{DR} from 1 degree scans of 13-14 March 1997 event. (Lines show 6 point moving average.)

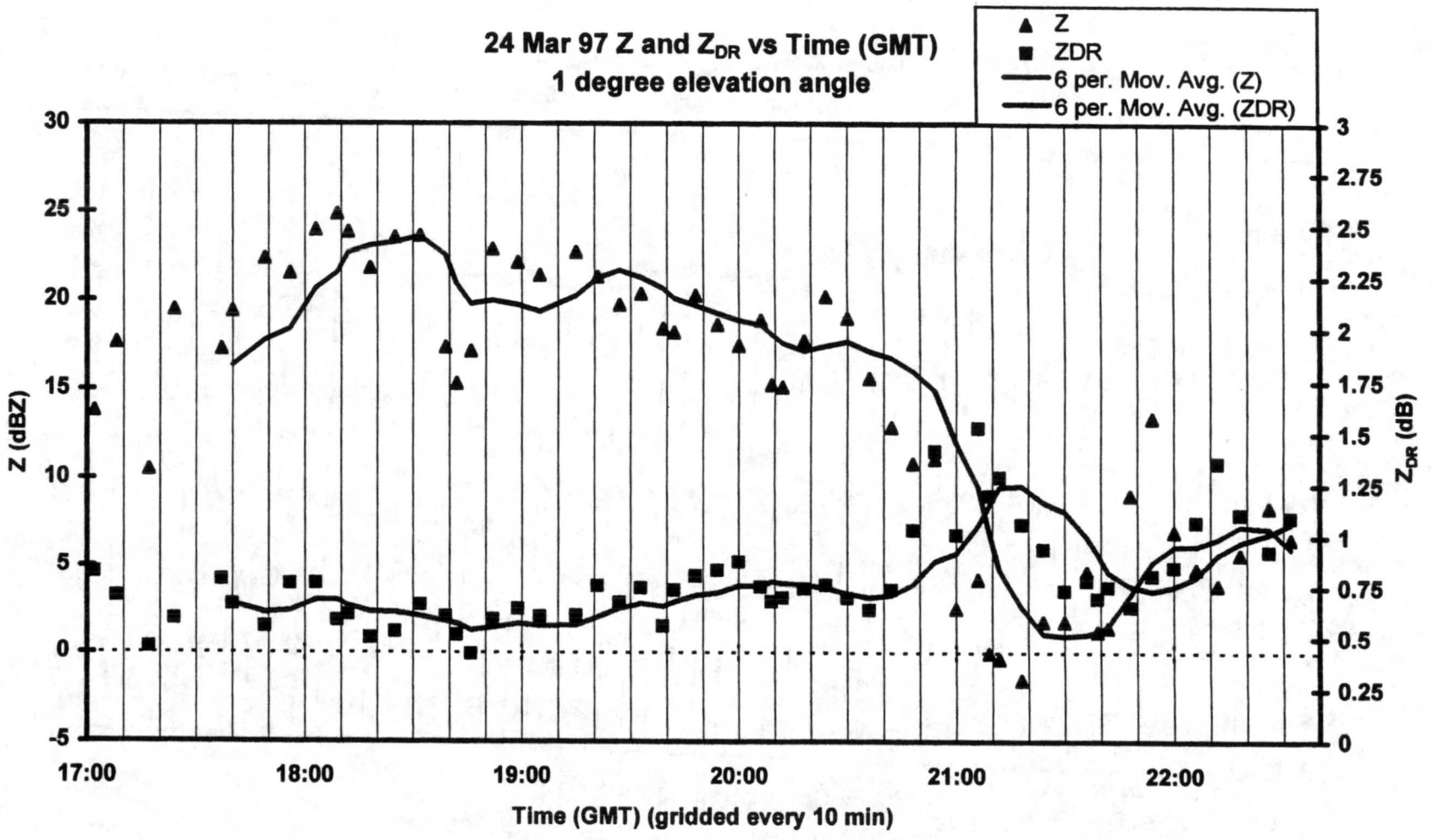

Figure 3.3: Timelines of Z and Z_{DR} from 1 degree scans of 24 March 1997 event. (Lines show 6 point moving average.)

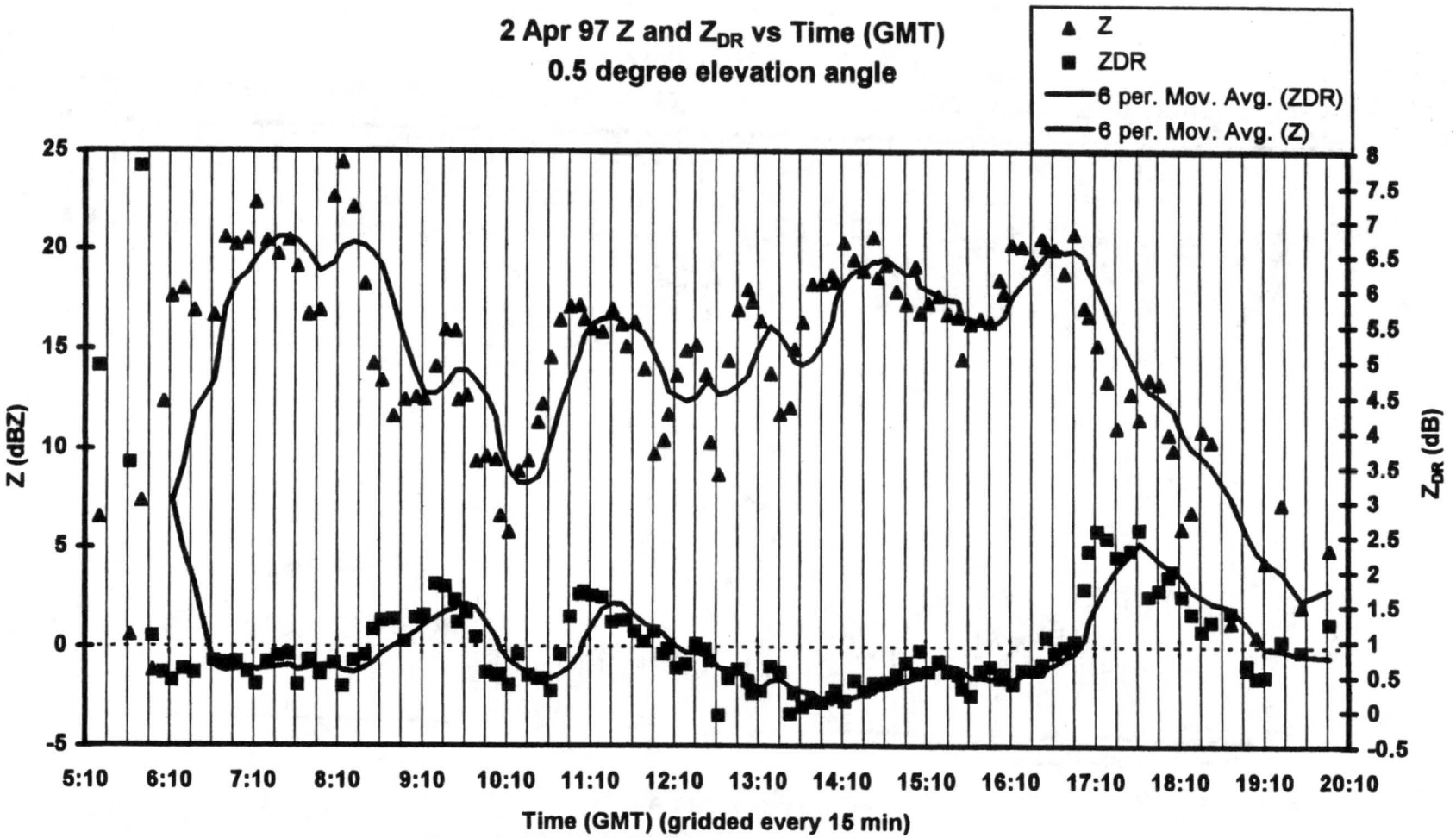

Figure 3.4: Timelines of Z and Z_{DR} from 0.5 degree scans of 2 April 1997 event. (Lines show 6 point moving average.)

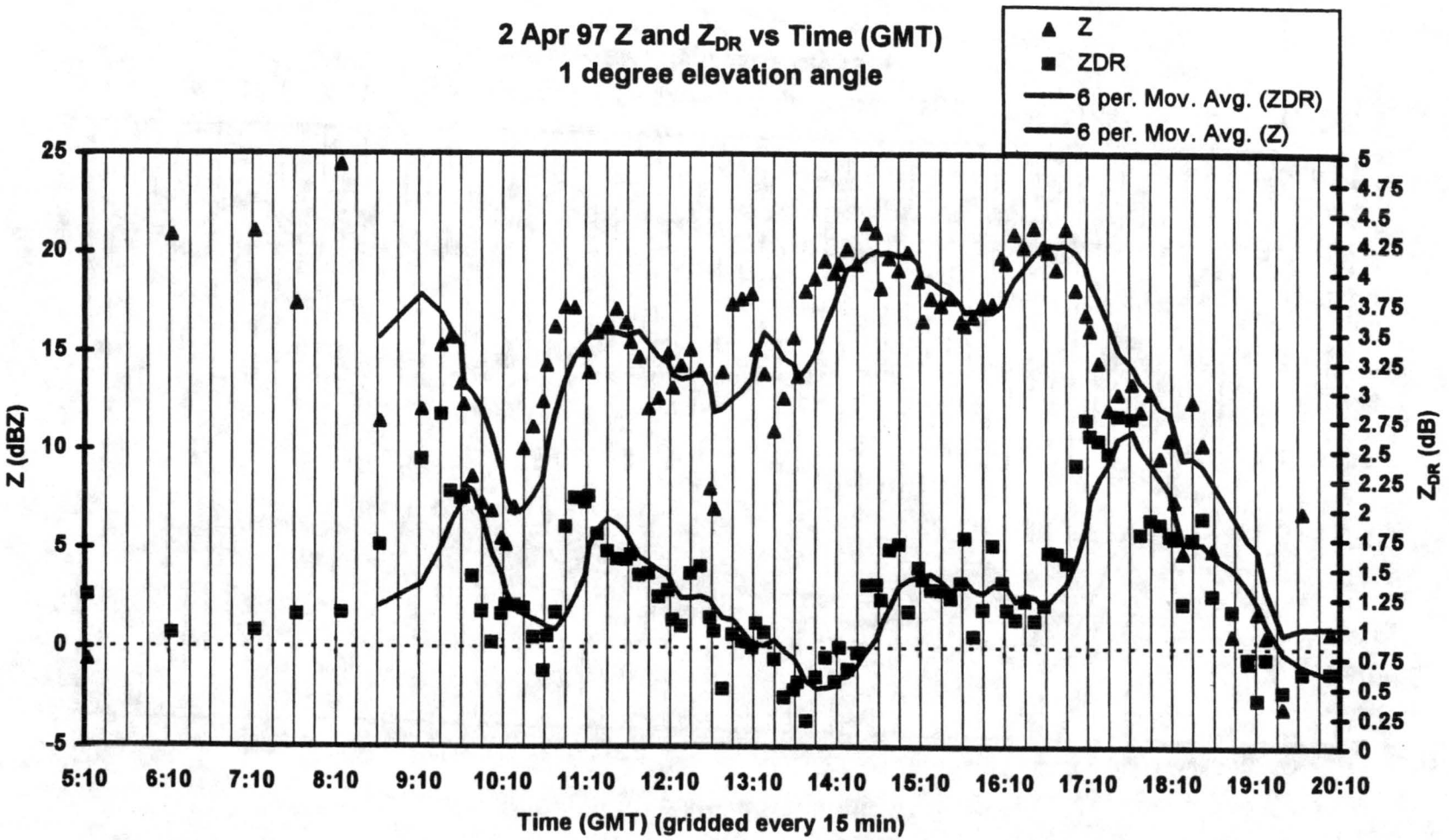

Figure 3.5: Timelines of Z and Z_{DR} from 1 degree elevation scans of 2 April 1997 event. (Lines show 6 point moving average.)

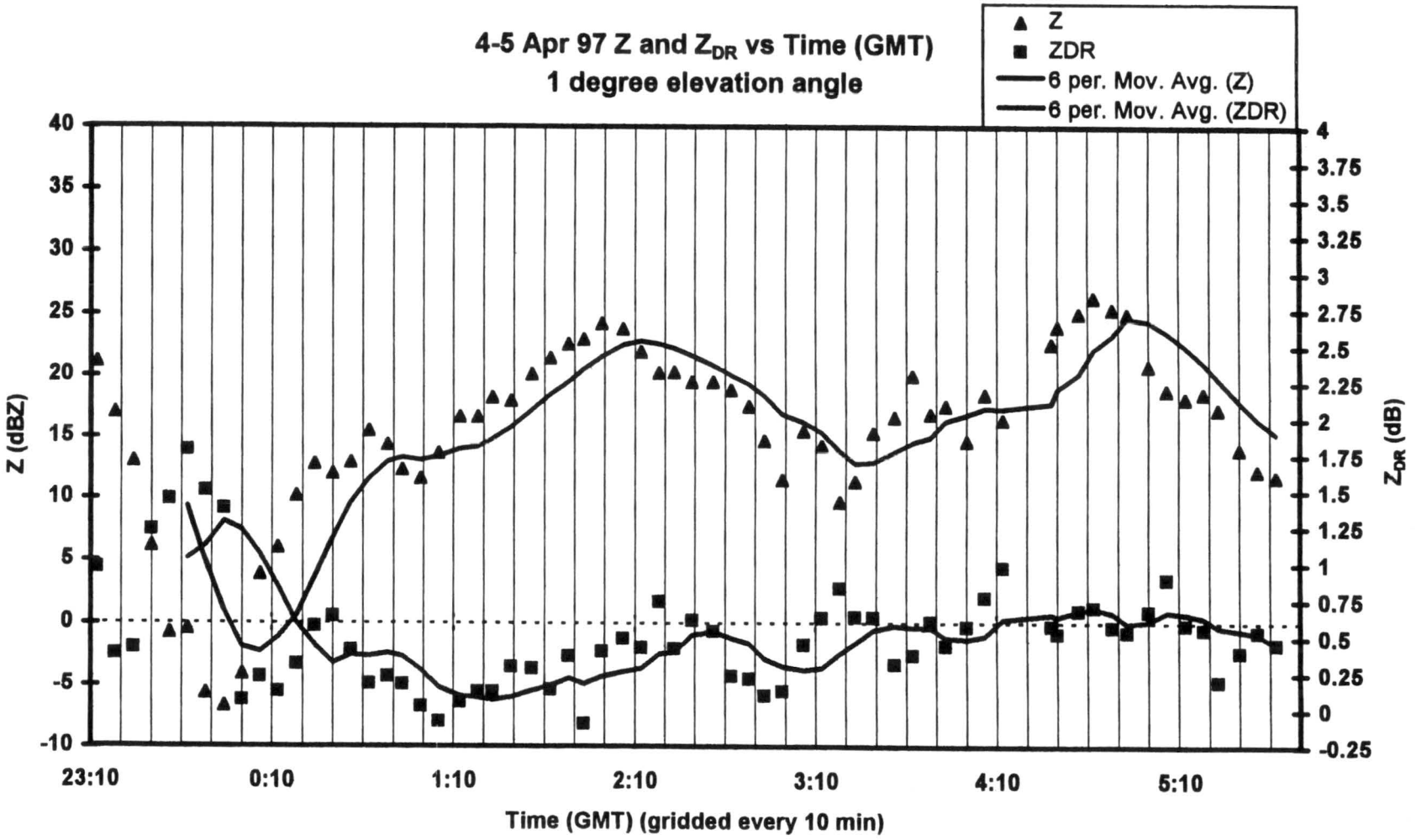

Figure 3.6: Timelines of Z and Z_{DR} from 1 degree scans of 4-5 April 1997 event. (Lines show 6 point moving average.)

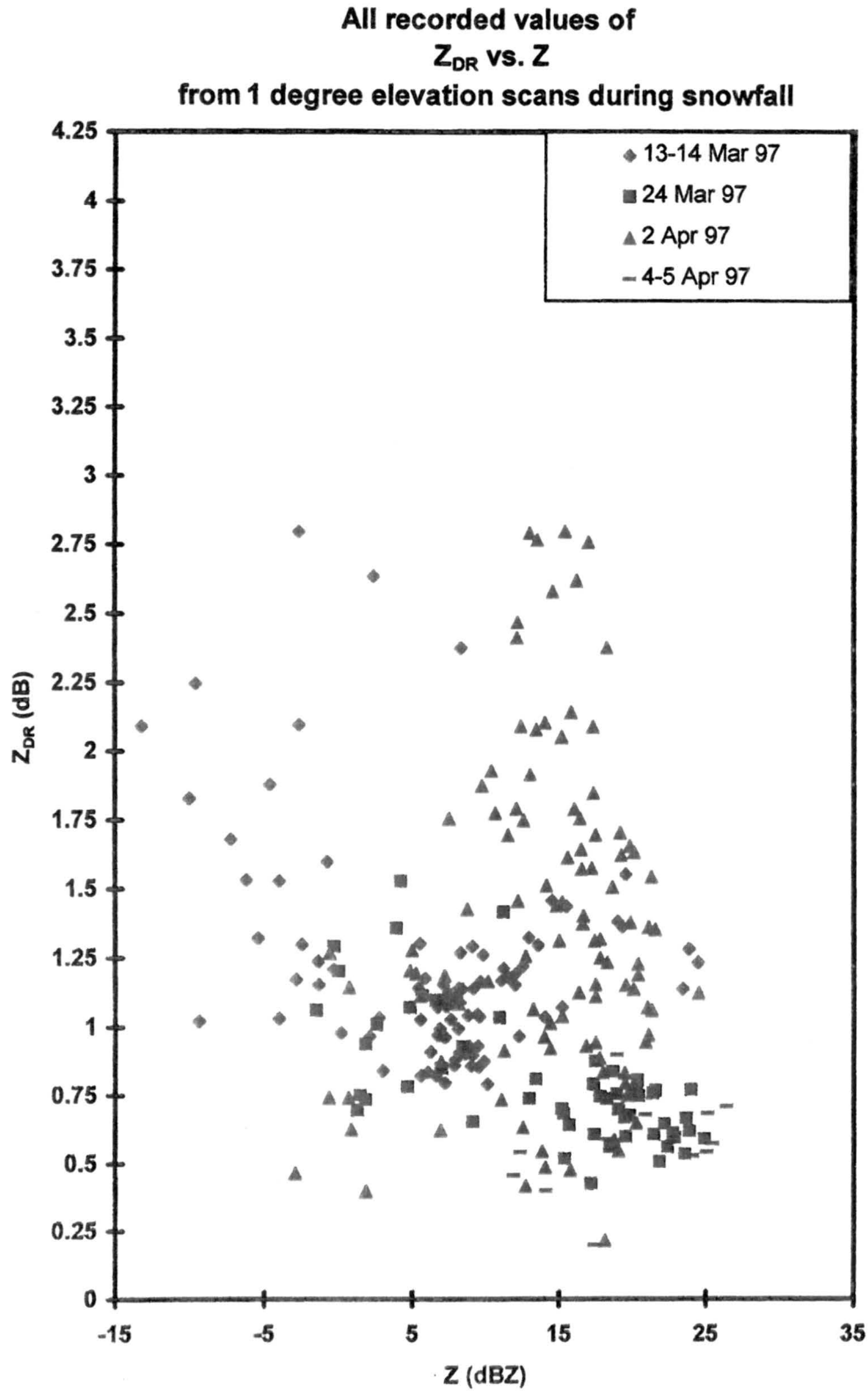

Figure 3.7: Z_{DR} vs. Z from 1 degree scans during all snowfall periods for 4 events.

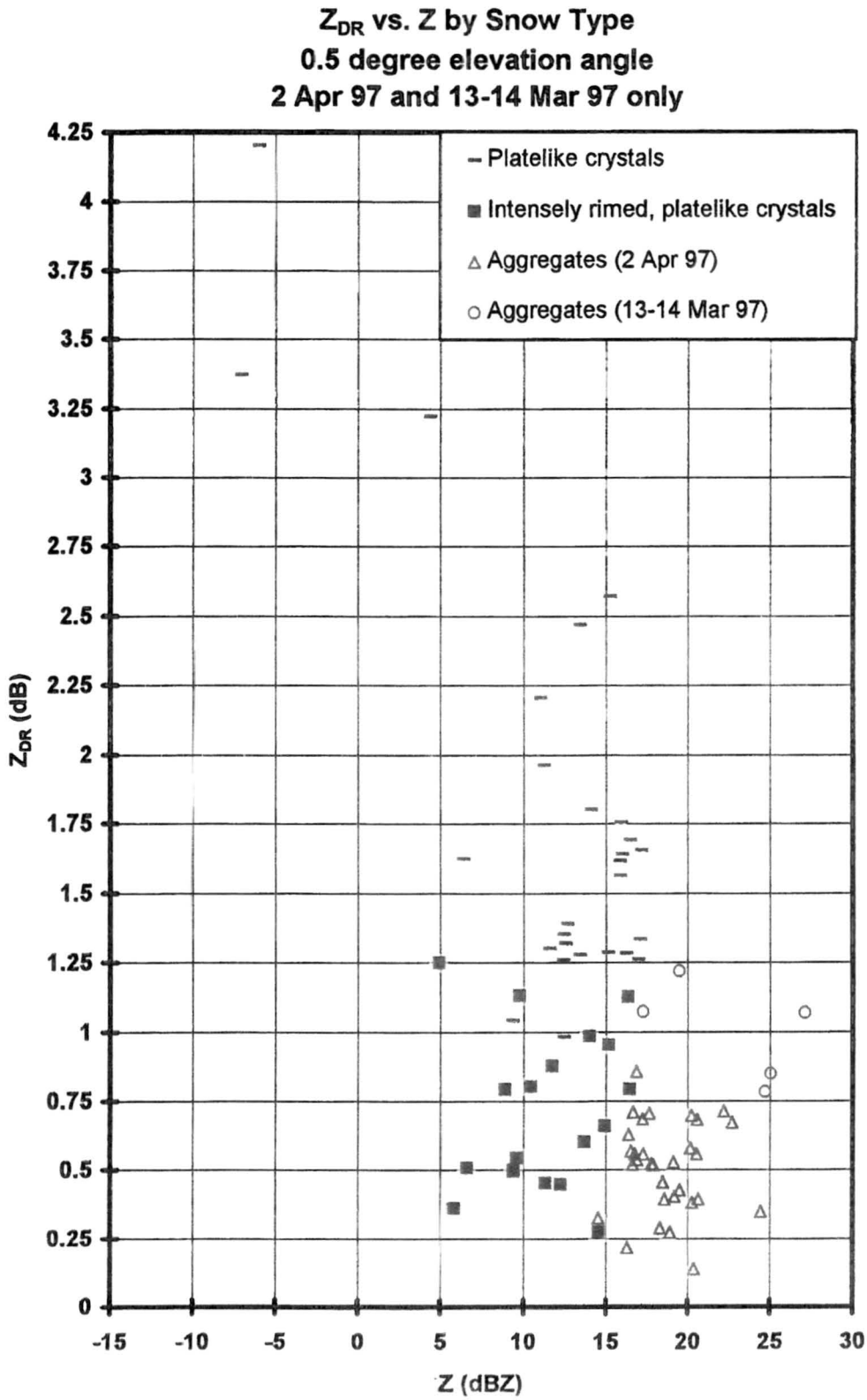

Figure 3.8: Z_{DR} vs. Z from 0.5 degree scans during periods of nearly homogeneous snow type. (only includes 2 April and 13-14 March 1997 events)

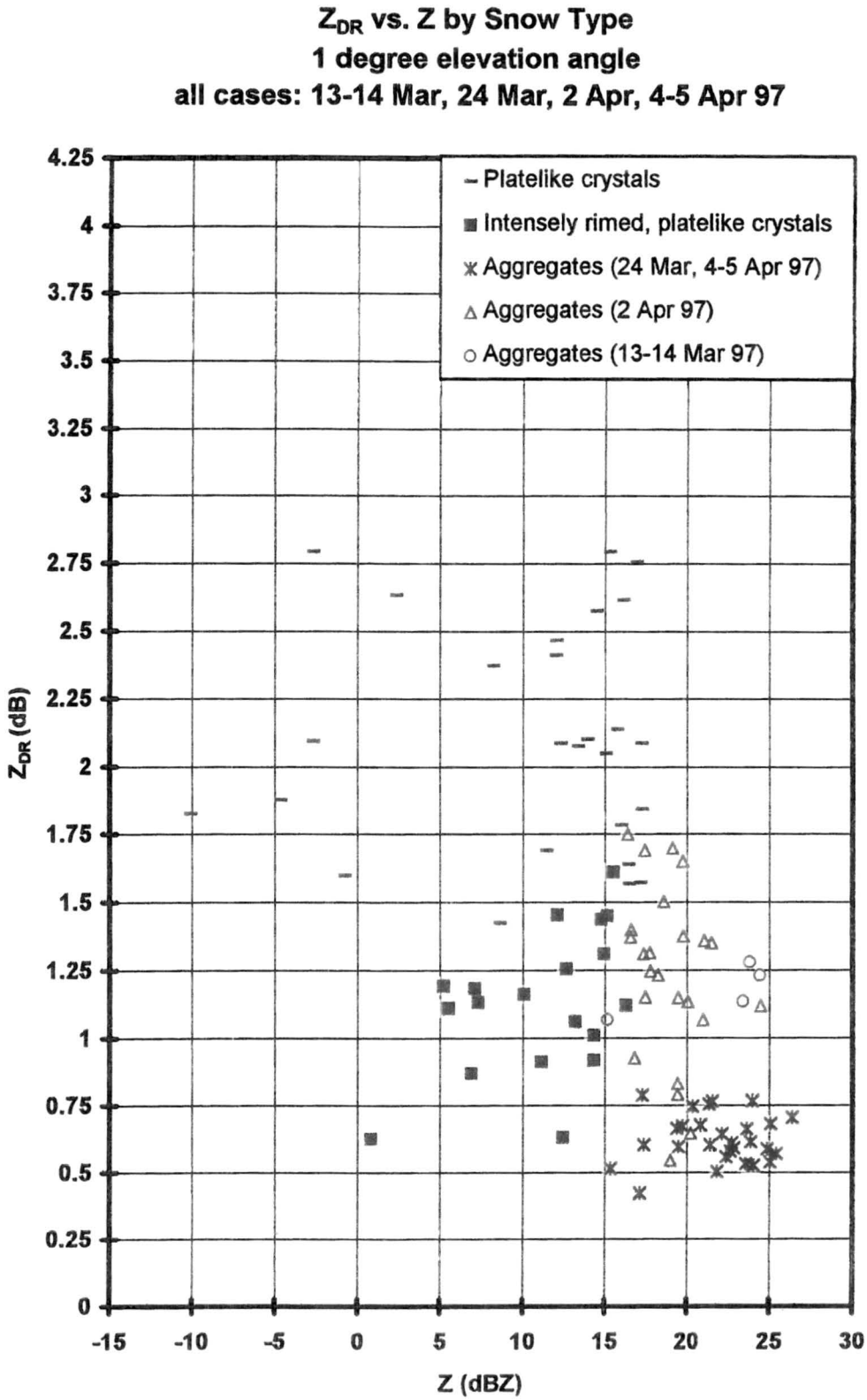

Figure 3.9: Z_{DR} vs. Z from 1 degree scans during periods of nearly homogeneous snow type.

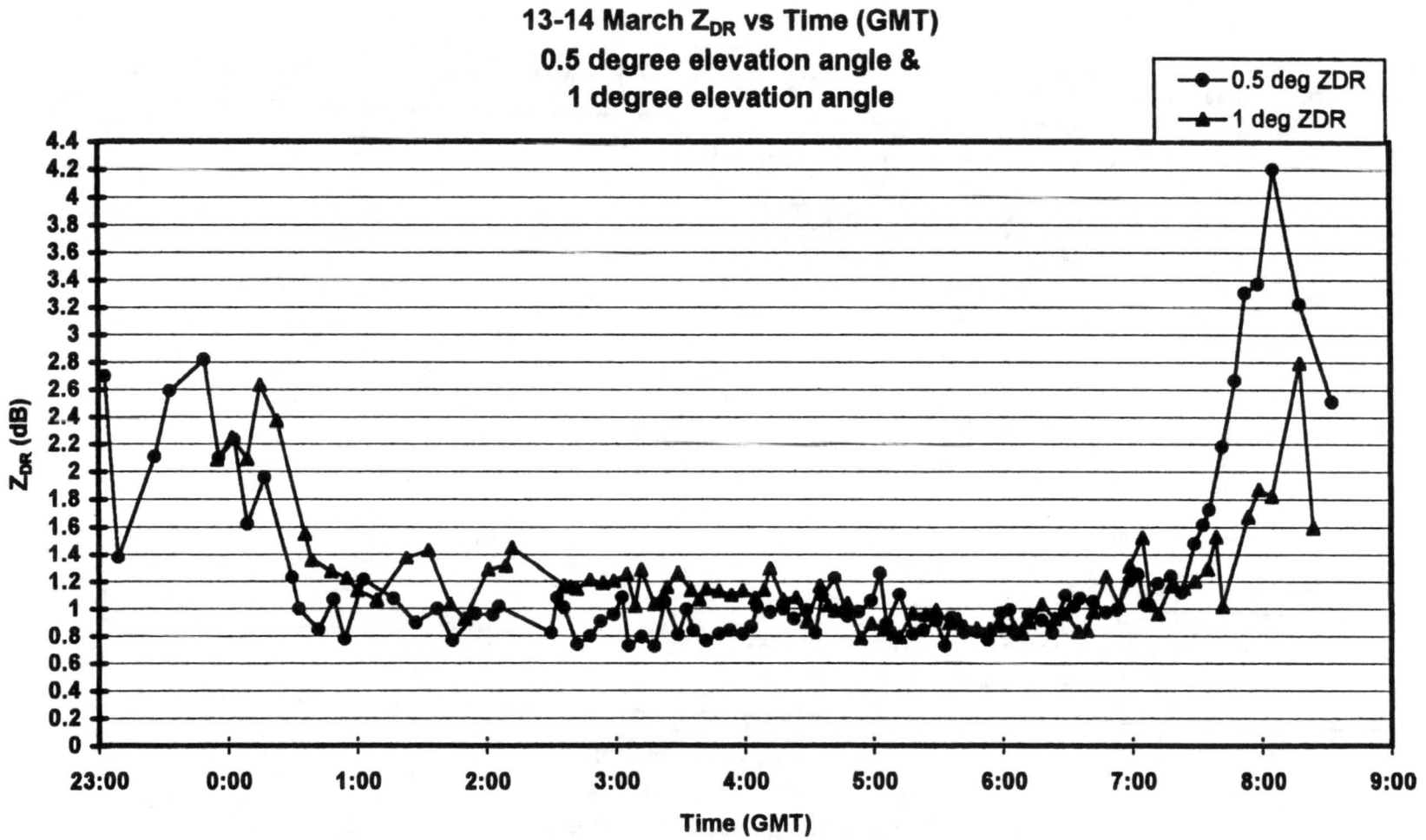

Figure 3.10: Timelines of Z_{DR} -- 0.5 degree scans compared to 1 degree scans for the 13-14 March 1997 event.

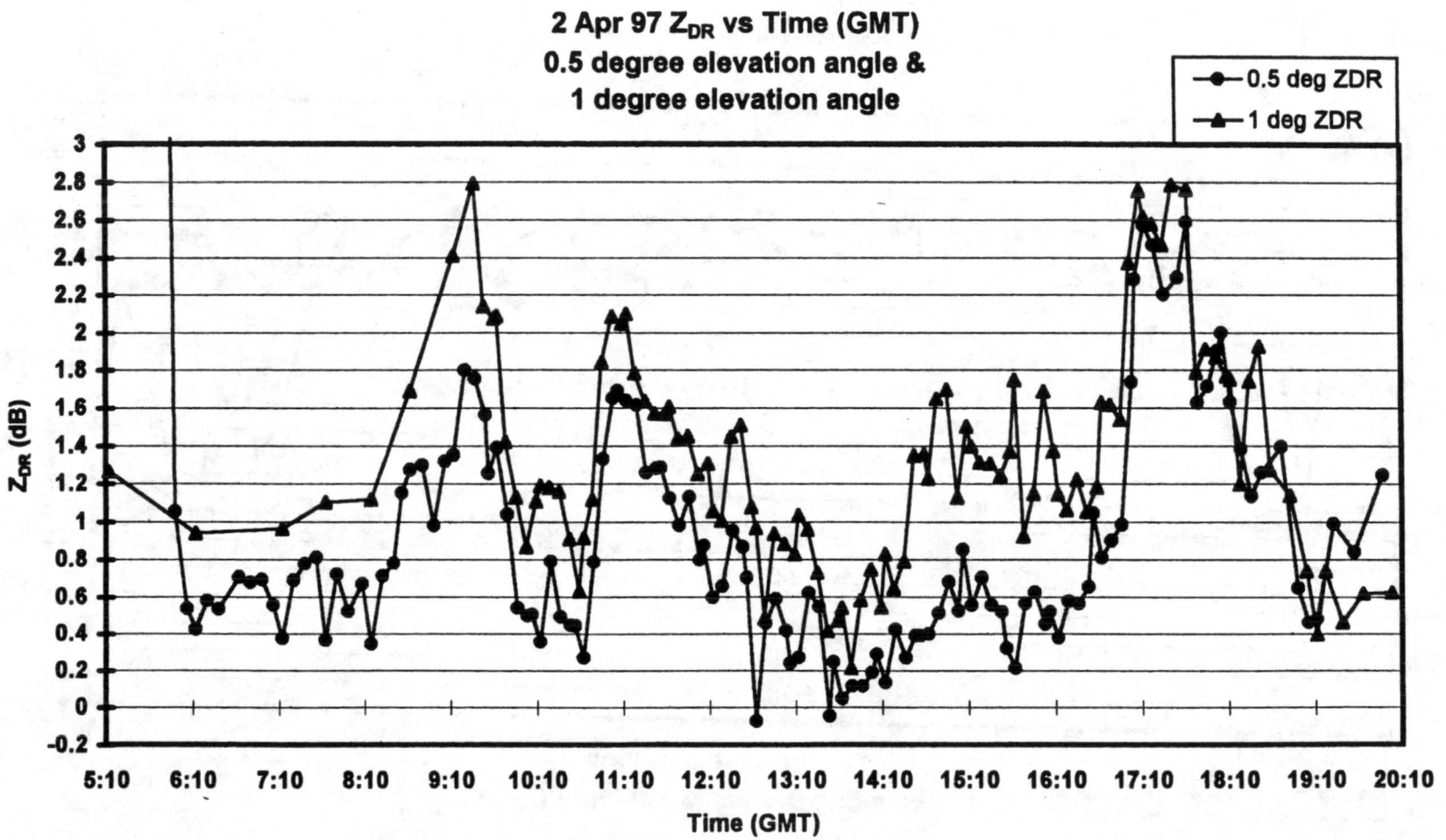

Figure 3.11: Timelines of Z_{DR} – 0.5 degree scans compared to 1 degree scans for the 2 April 1997 event.

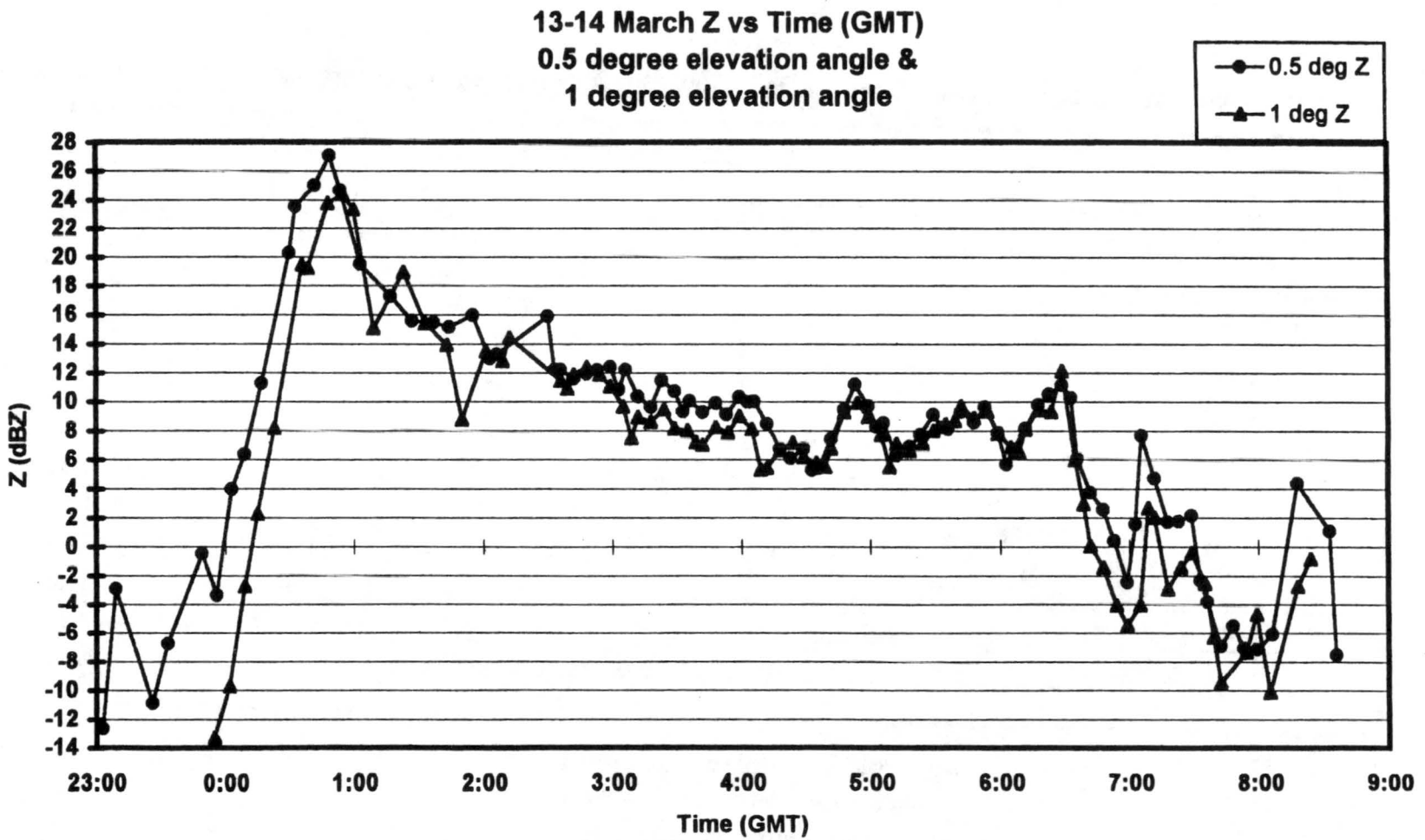

Figure 3.12: Timelines of Z -- 0.5 degree scans compared to 1 degree scans for the 13-14 March 1997 event.

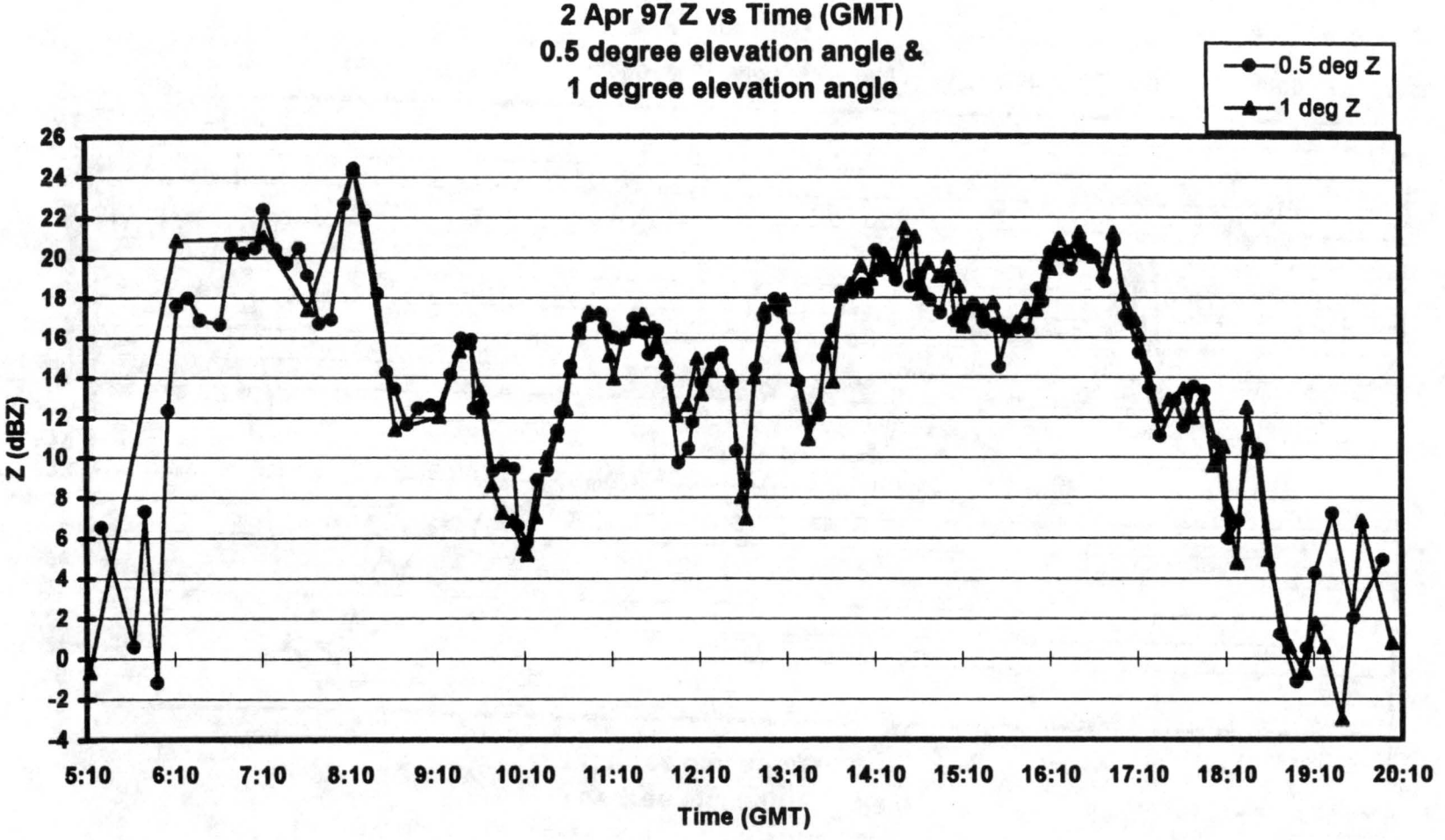

Figure 3.13: Timelines of Z -- 0.5 degree scans compared to 1 degree scans for the 2 April 1997 event.

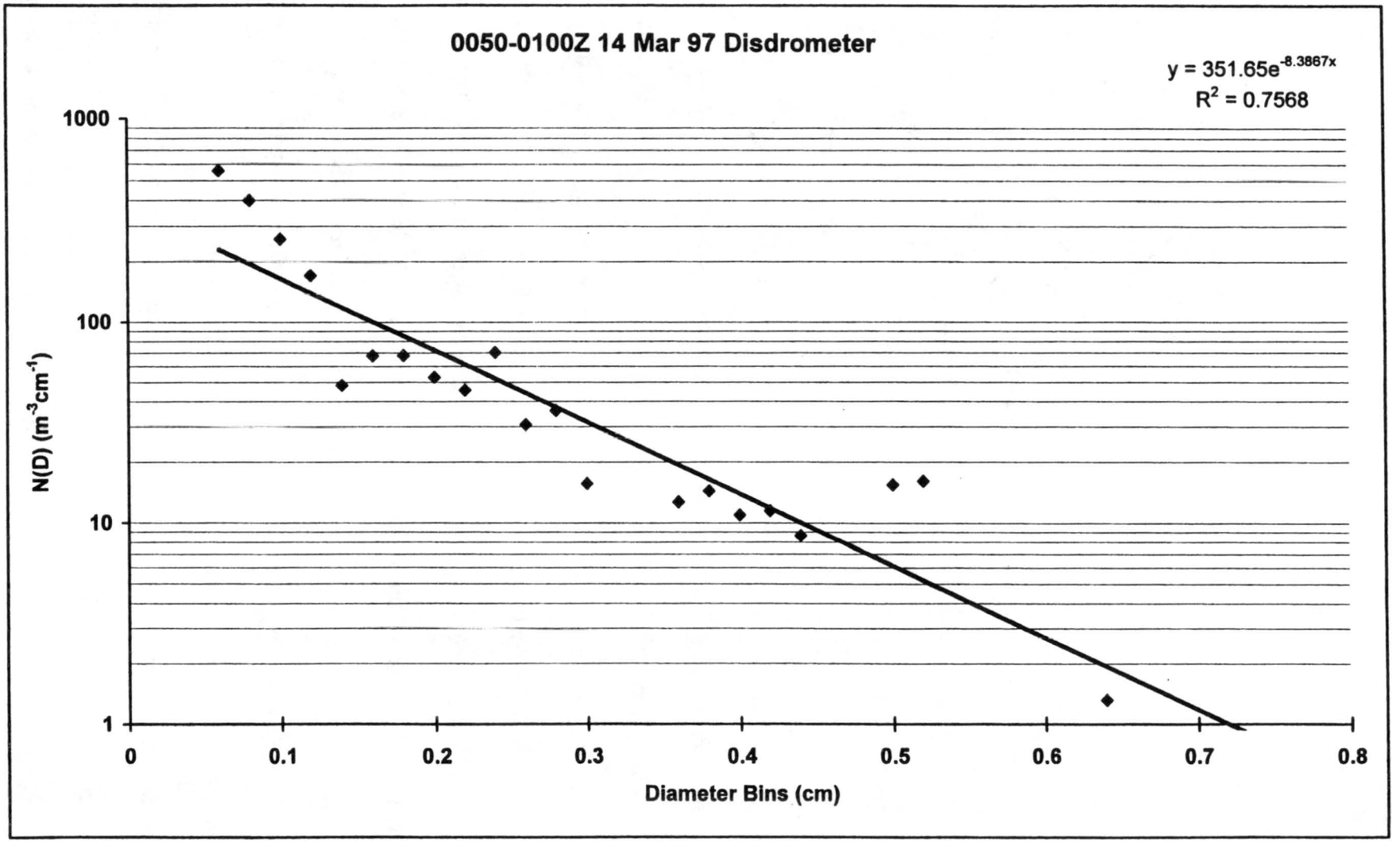

Figure 3.14: Particle size distribution and exponential fit from aggregate period, 0050-0100Z, 14 March 1997.

CHAPTER 4

MODELING

4.1 Introduction

We had a dual purpose for the modeling portion of this research. First, we needed to test the plausibility of the suggestions offered in Chapter 3 to explain the Z_{DR} differences within and between snow type categories. Secondly, we wanted to illustrate that the observed Z_{DR} values were consistent with theory. To fulfill both of these objectives, we chose to emulate three distinct periods of aggregates and two distinct periods of individual crystals from the 2 April 1997 event. These five time periods displayed the contrasting microphysical characteristics and Z_{DR} values discussed in Chapter 3. Most of the model input parameters were designed to represent both the microphysical characteristics noted during the field observations and the characteristics described by our suggested explanations, or hypotheses, in Chapter 3. The remaining model inputs were obtained from previous observational or theoretical studies. The model used code (L. Carey, personal communication) that employed T-matrix theory (Barber and Yeh, 1975; Bringi and Seliga, 1977) and the Mueller matrix method (Vivekanandan et al., 1991). The user-defined input parameters for the model included:

radar wavelength, air temperature, equivolumetric particle size distribution, maximum and minimum equivolumetric diameters, particle axis ratios which can differ according to particle size, the real and imaginary parts of the dielectric constant which can also differ according to particle size, and the fall mode of the hydrometeors defined by the mean and standard deviation of a Gaussian distribution. An equivolumetric diameter (D_{eq}) is the diameter of a theoretical sphere which has the same volume and bulk density as the actual particle.

The radar wavelength was set at 11 cm, the wavelength of the CSU-CHILL radar. Air temperatures were determined from the FCL surface temperature data and the DIA soundings. The particle size distribution was defined by the exponential form:

$$N(D_{eq}) = N_0 \exp(-\lambda D_{eq}) \tag{4.1}$$

where D_{eq} is the equivolumetric diameter in centimeters, $N(D_{eq})$ is the number of particles per cubic meter per centimeter, N_0 is the intercept of the distribution, and λ is the slope of the distribution. The slopes, intercepts, and maximum and minimum equivolumetric diameters for the four examples were derived from the particle size distribution data collected during each period by the 2D video disdrometer operating at FCL. The dielectric constants were calculated from bulk densities using Debye theory as described by Battan (1973) which asserts that:

$$K_{ice}/\rho_{ice} = K_{mix}/\rho_{mix} \tag{4.2}$$

where K is the dielectric function, and ρ is the bulk density. The subscript 'mix' refers to a mixture of ice and air, such as a dendrite or an aggregate, while the subscript 'ice' refers to solid ice. Since K_{ice} and ρ_{ice} are known, defining ρ_{mix} yields a value for $K_{mix,}$ and, subsequently, the dielectric constant for the mixture. The fall mode for all crystal and

aggregate hydrometeors was assumed to be horizontal, meaning that the major axis was oriented parallel to the ground. The research concerning this issue suggests that such an assumption is reasonable (e.g. Sasyo, 1977; Zikmunda and Vali, 1972; Kajikawa 1976, 1982, and 1992) An exception to this assumption was implemented in one case where the purpose was to illustrate the impact of canting particles which is more likely to occur under turbulent conditions. The values for the densities and axis ratios were designed to test our hypotheses from Chapter 3, but they were based on information from literature and specific entries in the field notes.

4.2 Modeling Parameters for Aggregate Periods

The periods chosen to represent the variation among the aggregates were the first three of the four aggregate periods discussed at length in Chapter 3: 0810-0820Z, 1410-1420Z, and 1600-1610Z on 2 April 1997. Table 4.1 summarizes the microphysical descriptions from the field notes and the values of the radar variables in the 0.5° scan.

Table 4.1 Characteristics of three specific aggregate periods

Period	Date/ Time (GMT)	Riming	Particles in Aggregate Composition	Size Range (cm) & Shape	Z_{DR} 0.5° scan	Z 0.5° scan
1	0810-0820 2 Apr 97	not mentioned	snow pellets, dendrites/stellar	majority: 0.8-1 many: 1-1.5; noted 0.4 axis ratios	0.51 dB	23.6 dBZ
2	1410-1420 2 Apr 97	'appears to be less' than earlier	dendrites	majority: 0.5 some: 1	0.28 dB	19.9 dBZ
3	1600-1610 2 Apr 97	heavy	so rimed, hard to tell if was dendritic or stellar origins; some crystals fused together	majority: 0.7 some: 1-1.5; noted elongation	0.45 dB	19.0 dBZ

The first and third periods had more large, elongated aggregates with seemingly denser components, and we suggested in Chapter 3 that for these reasons their Z_{DR} values were higher.

To test our suggestion, we had to design the input parameters for the model. We partitioned the size distributions from the disdrometer data and treated the smallest particles as platelike crystals (i.e. plates, stellar crystals and dendrites), the moderate sized particles as nearly spherical aggregates, and the largest particles as elongated aggregates. We fit an exponential line (distribution) to the size distribution in each of the three size categories. Figures 4.1 to 4.3 display the disdrometer data in 0.02 cm bins and the exponential fits. Table 4.2 summarizes the model input parameters.

Table 4.2 Model input parameters for aggregate periods

	Period	Axis Ratio	Density (g/cm^3)	Size Distrib. Parameters	Fall Mode	D range (cm)
Crystals: $D_{eq} \leq 0.12$cm	1	0.047	0.4	N_0: 15379 $cm^{-1}m^{-3}$ λ: 5.8034 cm^{-1}	horiz	0.22-0.33
	2	0.047	0.4	N_0: 45824 $cm^{-1}m^{-3}$ λ: 36.158 cm^{-1}	horiz	0.22-0.33
	3	0.047	0.4	N_0: 7323 $cm^{-1}m^{-3}$ λ: 26.006 cm^{-1}	horiz	0.22-0.33
Small Aggreg: $0.14 \leq D_{eq} \leq 0.4$cm	1	0.8	0.1	N_0: 21563 $cm^{-1}m^{-3}$ λ: 11.158 cm^{-1}	horiz	0.15-0.43
	2	0.8	0.05	N_0: 388 $cm^{-1}m^{-3}$ λ: 1.0928 cm^{-1}	horiz	0.15-0.43
	3	0.8	0.1	N_0: 65 $cm^{-1}m^{-3}$ λ: -2.308 cm^{-1}	horiz	0.15-0.43
Elongated Aggreg: $D_{eq} \geq 0.42$cm	1	0.4	0.1	N_0: 2753 $cm^{-1}m^{-3}$ λ: 4.8889 cm^{-1}	horiz	0.57-1.4
	2	0.4	0.05	N_0: 7039 $cm^{-1}m^{-3}$ λ: 8.8105 cm^{-1}	horiz	0.57-1.0
	3	0.4	0.1	N_0: 549 $cm^{-1}m^{-3}$ λ: 4.8606 cm^{-1}	horiz	0.57-1.2

The axis ratio assigned to the crystals was calculated for a 2 mm platelike crystal from the widely accepted, size dependent aspect ratio formulas outlined by Matrosov et al. (1996). The value derived from the formula was increased slightly to account for riming. The density for the platelike crystals was also assumed to be that of a 2 mm platelike crystal using the size dependent formulas presented by Matrosov et al. (1996). Sensitivity testing with the model revealed that in periods dominated by aggregates, the contributions from the crystals were so negligible that as long as the values supplied for the axis ratios and densities were within reasonable, documented limits, the radar variables were unaffected. Therefore, it was not necessary to determine more precise values for each crystal size or be concerned about making adjustments for riming.

To gain a better sense of the physical sizes of the hydrometeors in order to partition them, the equivolumetric diameters from the disdrometer size distributions were converted to the major dimension of the particle, D, using the following equation:

$$D = D_{eq}/(r)^{1/3} \tag{4.3}$$

where r is the axis ratio. The ranges of D for each classification of snow are listed in Table 4.2; overlapping and separation of D occurs at the interfaces between different axis ratios. The minimum D_{eq} bin for this portion of the modeling was 0.08 cm, which included values greater than 0.06 cm and less than or equal to 0.08 cm. This cut-off was imposed in order to achieve the best exponential fit to the data, and the sensitivity tests indicated that the impact was negligible.

The axis ratios for the two size categories of aggregates were based upon the subjective observations that smaller aggregates tended to be more spherical and larger aggregates tended to be elongated. Since an observation at 0807Z specifically reported an

axis ratio of 0.4 for the large aggregates at that time, we assigned this value to all large aggregates. The 0.8 axis ratio assigned to the smaller aggregates defined them as nearly spherical, and Vivekanandan et al. (1993) and Vivekanandan et al. (1994) used the same value for that purpose. We did not have any direct density measurements for the aggregates, so we selected density measurements from previous studies. Rogers (1974) explained that the snowflake densities were highly variable and depended upon the degree of riming, the types of component crystals, and the manner in which the crystals were arranged together. He reported densities that ranged from 0.03 g/cm^3 for loosely structured dendritic aggregates to 0.25 g/cm^3 for aggregates containing denser particles like snow pellets and graupel. Herzegh and Jameson (1992) utilized a density range for aggregates between 0.03 g/cm^3 and 0.12 g/cm^3. Passarelli (1978) and Thomason et al. (1995) both tested different density values until they found one that optimized the agreement between the Z values calculated from in situ size distributions, and the Z values observed by radar. Passarelli (1978) found this optimized Z value to be 0.09 g/cm^3. Thomason et al. (1995) found optimized values in the range 0.07-0.1 g/cm^3 to be suitable, except at temperatures above -5 C where densities as high as 0.25 g/cm^3 seemed more applicable. Locatelli and Hobbs (1974) and Rogers (1974) proposed size dependent formulas, but we elected to maintain simplicity by applying reasonable, constant density values to each period. Since our hypothesis in Chapter 3 suggested that the aggregate bulk densities in the first and third periods were higher than the second due to riming and constituent crystals, we assigned a density of 0.1 g/cm^3 to these periods. A density value of 0.05 g/cm^3 was used for the second period.

4.3 Modeling Results for Aggregate Periods

Table 4.3 displays the observed Z and Z_{DR} values, and the values generated by the model using the input parameters described in Table 4.2.

Table 4.3 0.5° elevation scan radar data and model output for aggregate periods

0.5° scan	Z_{DR} (dB)		Z (dB)	
Period	Observed	Modeled	Observed	Modeled
1	0.51	0.45	23.65	41.55
2	0.28	0.23	19.95	25.29
3	0.45	0.44	18.97	32.98

The Z_{DR} values produced by the model are remarkably consistent with the observed values. The agreement strongly suggests that the differences in observed Z_{DR} values between the aggregate periods could indeed be explained by density variations and differing numbers of large, elongated aggregates. In fact, the Z_{DR} values, produced in altered model runs of Period 1 described below in Table 4.4, further demonstrate the important role that both density and elongation assumptions played. When the density was reduced, the Z_{DR} values decreased accordingly, and when the elongation was removed, the Z_{DR} values decreased markedly. Additionally, we tested the idea proposed in Chapter 3 that suggested the lower Z_{DR} values in the 24 March 1997 and 4-5 April 1997 events were a result of significant canting due to more turbulent conditions. In the model, we introduced a Gaussian distribution to describe the canting with a 0° mean and a 45° standard deviation. Table 4.4 displays the resulting, drastic decrease in Z_{DR}. The degree of canting can be adjusted to generate smaller changes in Z_{DR}.

Table 4.4 Additional model output compared to radar data for aggregate periods

0.5° scan	Z_{DR} (dB)		Z (dB)	
Period	Observed	Modeled	Observed	Modeled
1	0.51	0.45	23.65	41.55
with ρ=0.03g/cm^3 for aggreg	0.51	0.28	23.65	31.15
with all aggreg axis ratios=0.8	0.51	0.12	23.65	41.56
with hydrometeors canting up to 45°		0.108		41.51
with N_0 reduced by factor of 10	0.51	0.45	23.65	31.0

The model-generated reflectivity values in Table 4.3, however, deviated significantly from the observed values. We have been unable to identify the source of this problem. Clearly, reflectivities as high as 41 dBZ are not realistic for stratiform snow events, but our efforts to reconcile the Z values without significantly changing the Z_{DR}, to date, have been unsuccessful. Table 4.4 outlines some of the attempted modifications and their results. Since density is one of the most influential parameters on reflectivity, we investigated decreasing the density values assigned to aggregates. The reflectivity produced by the model was reduced, as expected, but the corresponding Z_{DR} became much lower than its observed counterpart. Moreover, the reflectivity modeled for Period 1 was still too high, 31 dBZ, even with such a low density. Upon the recommendation of Dr. V. Chandra, we tested the incorporation into the model of a size dependent, density formula for platelike crystals (Matrosov et al., 1996) and two different versions of an aggregate, size dependent, density formula. One version was for rimed or wet aggregates, and the other was for dry aggregates (Rogers, 1974); however, the first generated little change in either radar variable, and the second caused the same undesirable decrease in Z_{DR} mentioned above. The 0.4 axis ratio was part of the theory we wanted to test, and could be considered questionable. Despite the fact that the axis ratio determines the

major horizontal dimension of the aggregates, the reflectivity remained unchanged when the axis ratio was changed to 0.8. A number of errors could have originated from the defined particle size distribution, another influential factor in the computation of reflectivity. First, the disdrometer-generated size distributions could be in error. The disdrometer was primarily designed to determine drop size distributions in rain events where the shapes and sizes are more similar and predictable. Our field work was likely the first time it had been used in winter precipitation, and the accuracy of the conversion from maximum dimension to equivolumetric diameter for flat platelike crystals is unknown. Secondly, the particle size distribution represented by the exponential fit was not perfect. It was especially misrepresentative for bins where no particles were recorded, but neighboring bins did record a population. In those cases, the exponential distribution artificially included particles from the empty bin that were not a part of the observed population. Lastly, as discussed previously, shifts occur in the particle size distribution as the ice particles fall through the atmosphere, and those shifts have been studied and documented (e.g. Lo and Passarelli, 1982; Passarelli and Srivastava, 1979; and Passarelli, 1978). However, every situation researched was different, and a rigorous attempt to apply an appropriate reverse in the particle size distribution shift was beyond the scope of this thesis. The only simple modification that we knew would reduce Z and leave Z_{DR} untouched was to decrease the value of N_0. Such a decrease could possibly be necessary due to instrument error, or, as in one case seen by Lo and Passarelli (1982), a shift in the population as it fell. We tried an extreme N_0 reduction, an order of magnitude, and even that unjustifiably large reduction was not enough to correct the discontinuity in the reflectivity of Period 1, as shown by the results in Table 4.4. Therefore, this situation

remains unresolved, and although it appears to be possible for the observed Z_{DR} values in the aggregate periods to be reproduced by radar theory and explained by our elongation/density hypothesis, we cannot demonstrate the same for Z.

4.4 Modeling Parameters for Platelike Crystal Periods

The two periods chosen to represent individual ice crystals were 0925-0935Z and 1010-1020Z on 2 April 1997. Table 4.5 highlights the observed characteristics of each time period.

Table 4.5 Observed characteristics of platelike crystal periods

	Time Period	Predominant Size Range	Riming	Observed Z (dBZ)	Observed Z_{DR} (dB)
1	0925-0935Z	2-3 mm	Moderate-Heavy	16	1.7
2	1010-1020Z	$\leq$ 1mm	Heavy-Intense	7.6	.6

The second period appeared to have had more heavily rimed, smaller ice crystals. In Chapter 3 we hypothesized that the combined effects of the riming and the size of the crystals created differences in the axis ratios that were responsible for the differences in the observed Z_{DR} values.

To test this hypothesis, we again designed the input parameters for the model which are outlined in Table 4.6. This time the values assigned to the crystals were more critical. The only disdrometer data that was available to represent the particle size distribution of Period 2 was from 20 minutes earlier, 0949-0959Z. Unfortunately that was the time during which the crystals were transitioning from the 2-3 mm sized crystals of Period 1 to the less than 1 mm sized crystals of Period 2. To compensate, we adjusted the slope of the exponential fit line (it was applied to the whole population, not in partitions) so that instead of indicating 1 particle/m^3 in the 0.4 cm size bin, it indicated 1

particle/m^3 in the 0.2 cm size bin. This adjustment was designed to better represent the ground-based observations that the majority of the particles were less than 1 mm in size.

Table 4.6 Model input parameters for platelike crystal periods

	Period	Rime thickness	Axis Ratio	Density (g/cm^3)	Size Distrib. Parameters	D range
Crystals: $0.06 \leq D_{eq} \leq 0.12$ cm	1	0.5 mm	0.27	0.5	N_0: 11444 $m^{-3}cm^{-1}$ λ: 13.535 cm^{-1}	$\leq$ 0.19cm
$D_{eq} \leq 0.14$ cm		0.5 mm	0.21	0.5	" "	$\leq$ 0.24cm
$D_{eq} \leq 0.16$ cm		0.5 mm	0.17	0.5	" "	$\leq$ 0.29cm
$D_{eq} \leq 0.18$ cm		0.5 mm	0.15	0.5	" "	$\leq$ 0.34cm
$D_{eq} \leq 0.12$ cm	2	1.0 mm	0.9	0.65	N_0: 75274 $m^{-3}cm^{-1}$ λ: 56.14 cm^{-1}	$\leq$ 0.12cm
$D_{eq} \leq 0.14$ cm		1.0 mm	0.6	0.65	" "	$\leq$ 0.17cm
Small Aggreg: $D_{eq} \geq 0.20$cm	1		0.8	0.1	N_0: 75274 $m^{-3}cm^{-1}$ λ: 56.14 cm^{-1}	$\geq$ 0.22cm
$D_{eq} \geq 0.16$ cm	2		0.8	0.1		$\geq$ 0.17cm

It was imperative to make an adjustment in light of our projection that the size of the crystals was one of the major determining factors for Z_{DR}. We also made a minor adjustment to the disdrometer data from Period 1. There was a small population of aggregates with a D_{eq} larger than 0.4 cm that was skewing the model results. We set the maximum D_{eq} to 0.4 cm because it was reasonable to assume that those few, larger aggregates would not have been as large 6 minutes prior, 350 m aloft in the radar beam. Both distributions included minimum D_{eq} values of 0.06 cm. Figures 4.4 and 4.5 depict the adjusted particle size distributions. We also theorized that the degree of riming was a key factor; therefore, we could not depend upon the size dependent formulas previously used to produce representative axis ratios. Instead, we chose a constant thickness of rime for all of the crystals in a period. Using the selected thickness as the minor dimension in

equation (4.4), which was derived from equation (4.3), we calculated the axis ratio for 0.02 cm bins of equivolumetric diameters. The equation was:

$$r = (2a/D_{eq})^{3/2} \tag{4.4}$$

where r is the axis ratio, and 2a is the minor dimension, or rime thickness. We assigned a rime thickness of 1 mm to represent the heavy to intense riming of Period 2 which corresponded to the rime thickness on a representative, intensely rimed crystal that was successfully preserved on a slide. The moderate to heavy rime of Period 1 was estimated to have a 0.5 mm thickness. The densities were calculated for the range of crystal sizes in each period using the same formulas as before from Matrosov et al. (1996), but we increased the calculated values to account for riming and assigned a representative constant to all of the crystals. In these cases where the crystals were not dominated by aggregates, sensitivity tests showed that variations in the assigned, constant density values made minor, but noticeable, differences in the radar parameters generated by the model. Without any actual density measurements, we were unable to analytically determine which values were the most appropriate for each period. However, the model produced reasonable Z and Z_{DR} values with the densities we had chosen; thus, it appeared empirically that our values were appropriate. The disdrometer data indicated that some small aggregates were also present during these periods of individual platelike crystals. Their model input parameters were defined much the same as they were during the aggregate periods. The point of division between crystals and aggregates in the size distribution was established according to the crystal sizes reported in the field notes.

4.5 Modeling Results for Platelike Crystal Periods

Table 4.3 displays the values of Z and Z_{DR} observed by the radar in addition to the model output that was produced using the input parameters described in Table 4.2.

Table 4.7 0.5° scan radar data and model output for platelike crystal periods

0.5° scan	Z_{DR} (dB)		Z (dB)	
Period	Observed	Modeled	Observed	Modeled
1	1.7	2.0	16.0	22.5
2	0.6	0.5	7.6	4.9

The modeled Z_{DR} values are very representative of the observed values, and they successfully reproduce the differences observed between the crystals that were intensely rimed and those that were not. These results strongly suggests that the Z_{DR} differences could indeed be explained by the axis ratios which resulted from the crystal size and degree of riming. The modeled reflectivities were not identical to the observed values, but they were certainly more representative than the aggregate reflectivities were. The slightly low modeled reflectivity for Period 2 could easily be due to a compilation of small inaccuracies in the input parameters such as the adjustment we made to the particle size distribution and to the calculated density. The overestimated reflectivity for Period 1 may also be a compilation of small inaccuracies in the input parameters. These might include the density values assigned to the crystals and small aggregates or the unknown differences between the size distribution of the hydrometeors between ground level and the beam height level. Overall, the model results for the individual platelike crystal periods were consistent enough to conclude that the observed Z_{DR} values could be replicated using radar theory and explained by our size/riming/axis ratio hypothesis described in Chapter 3.

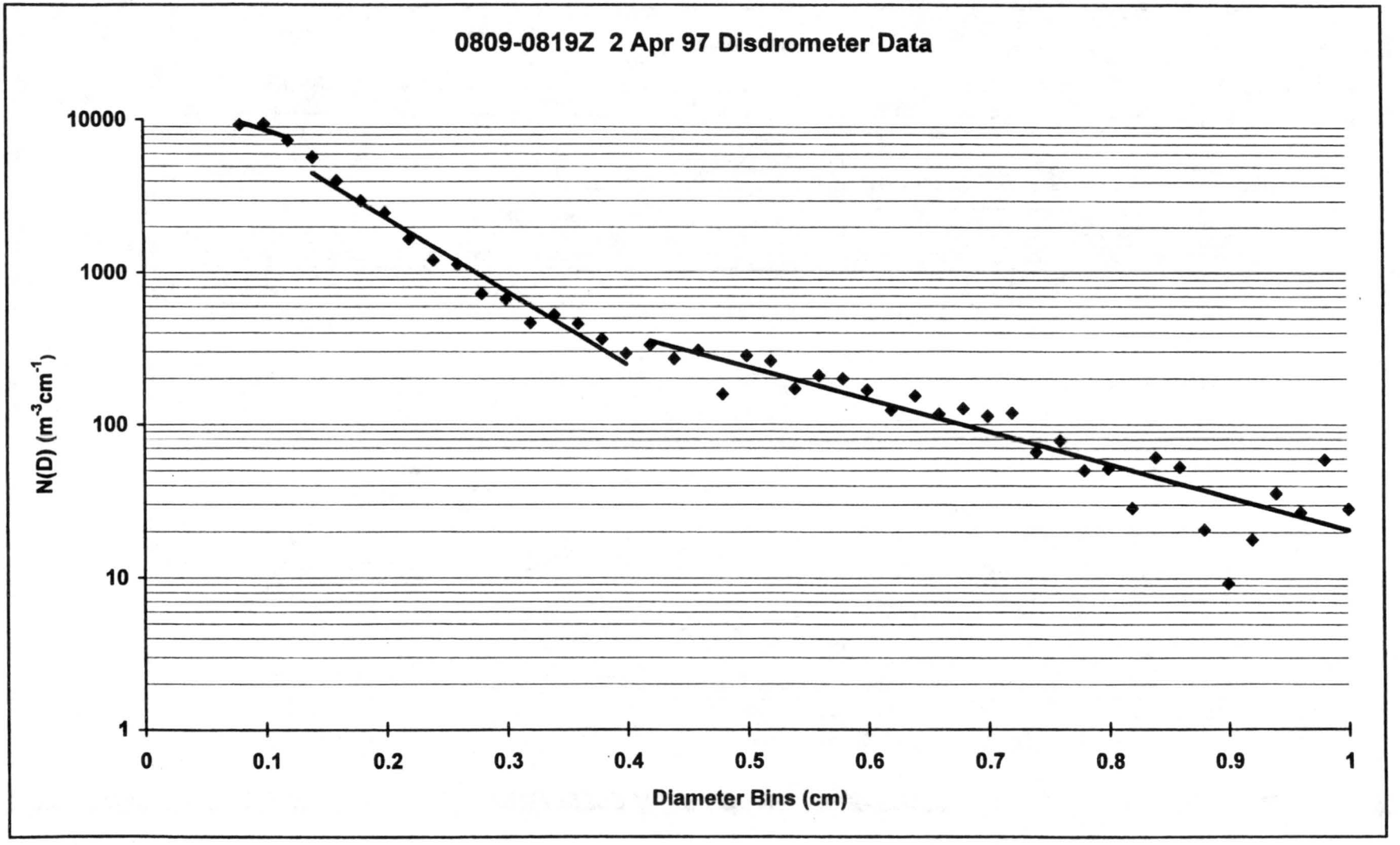

Figure 4.1: Particle size distribution and exponential fit lines used for aggregate period 1, 0810-0820Z 2 April 1997.

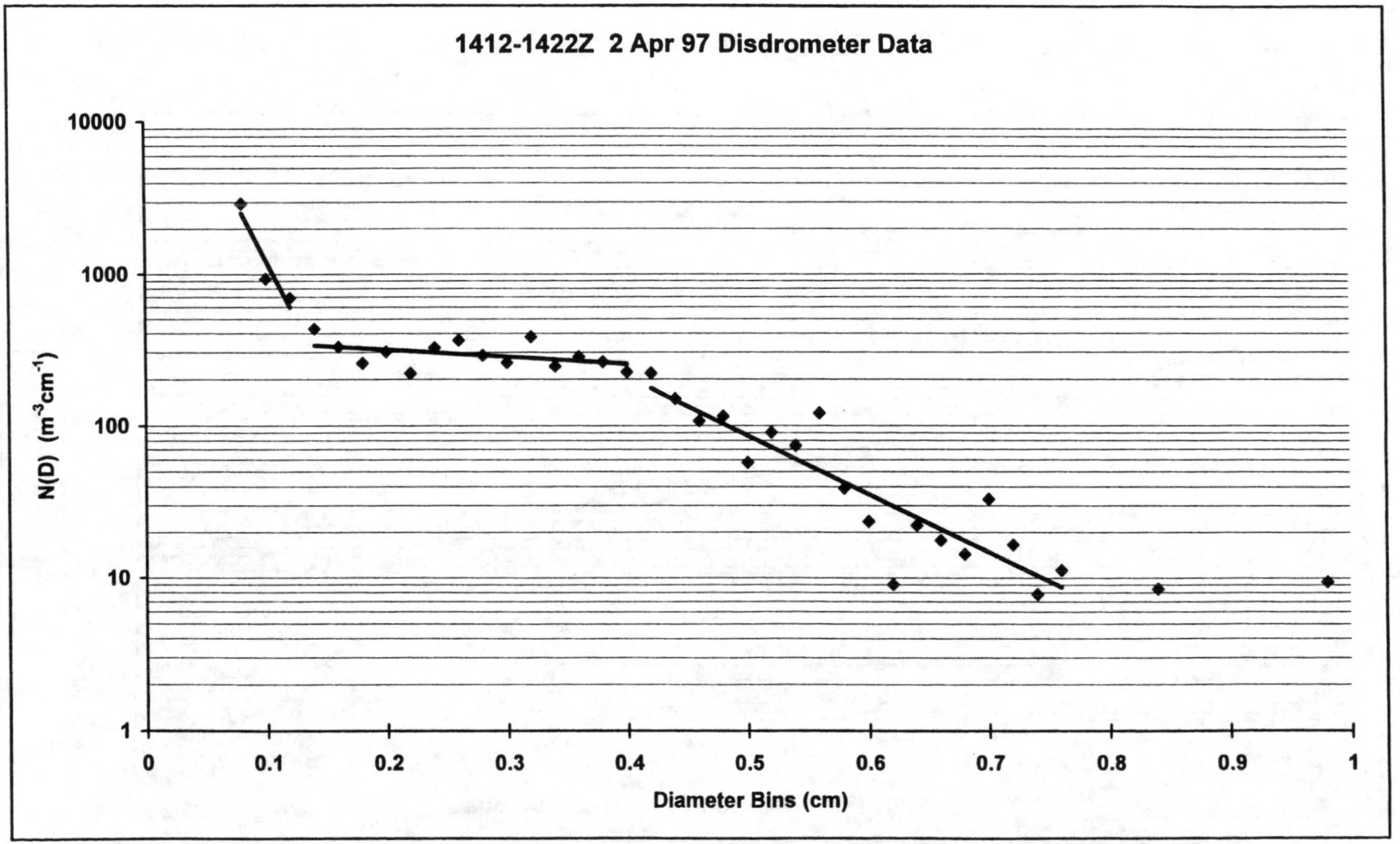

Figure 4.2: Particle size distribution and exponential fit lines used for aggregate period 2, 1410-1420Z 2 April 1997. (Bins greater than 0.76 cm were excluded)

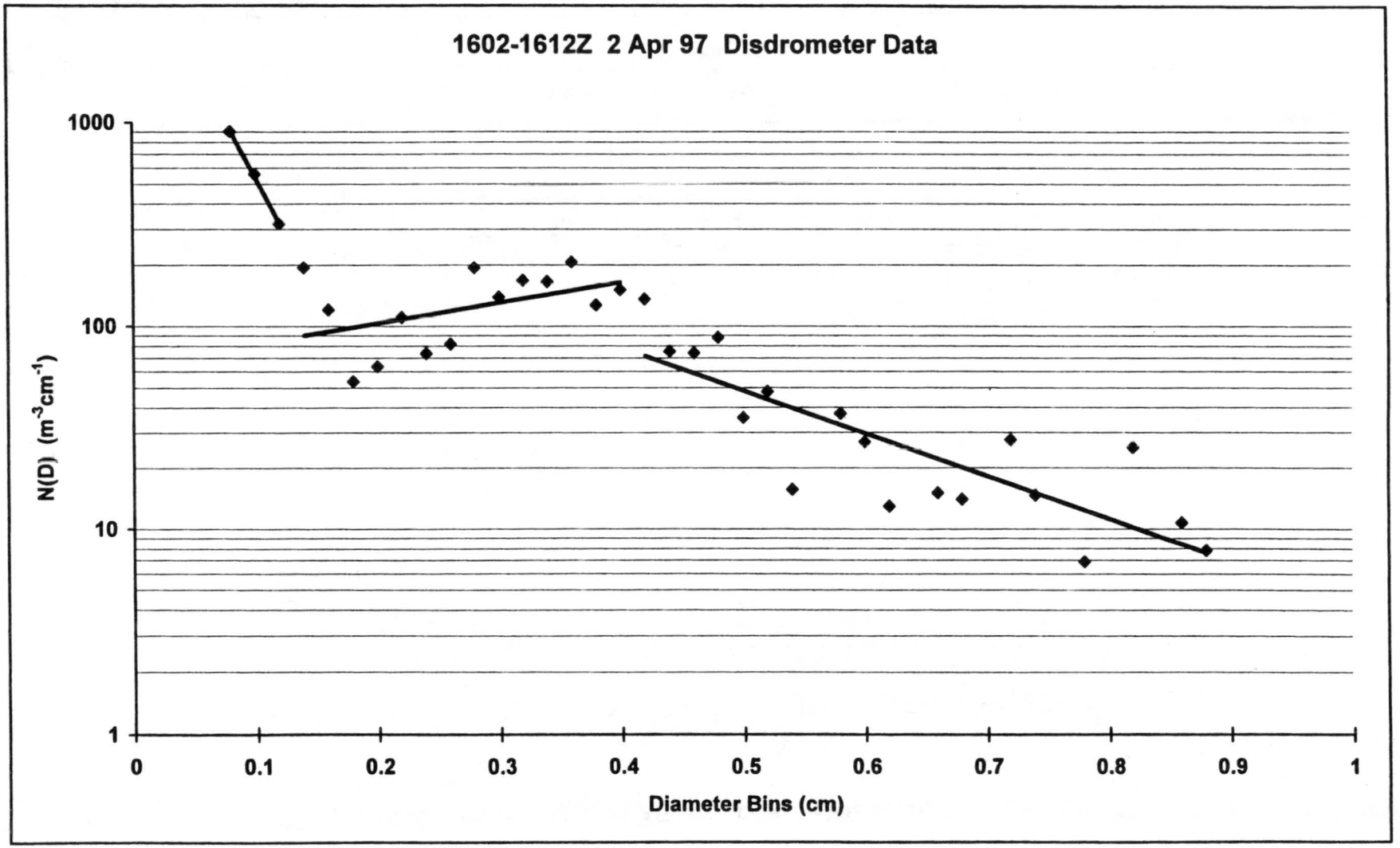

Figure 4.3: Particle size distribution and exponential fit lines used for aggregate period 3, 1600-1610Z 2 April 1997.

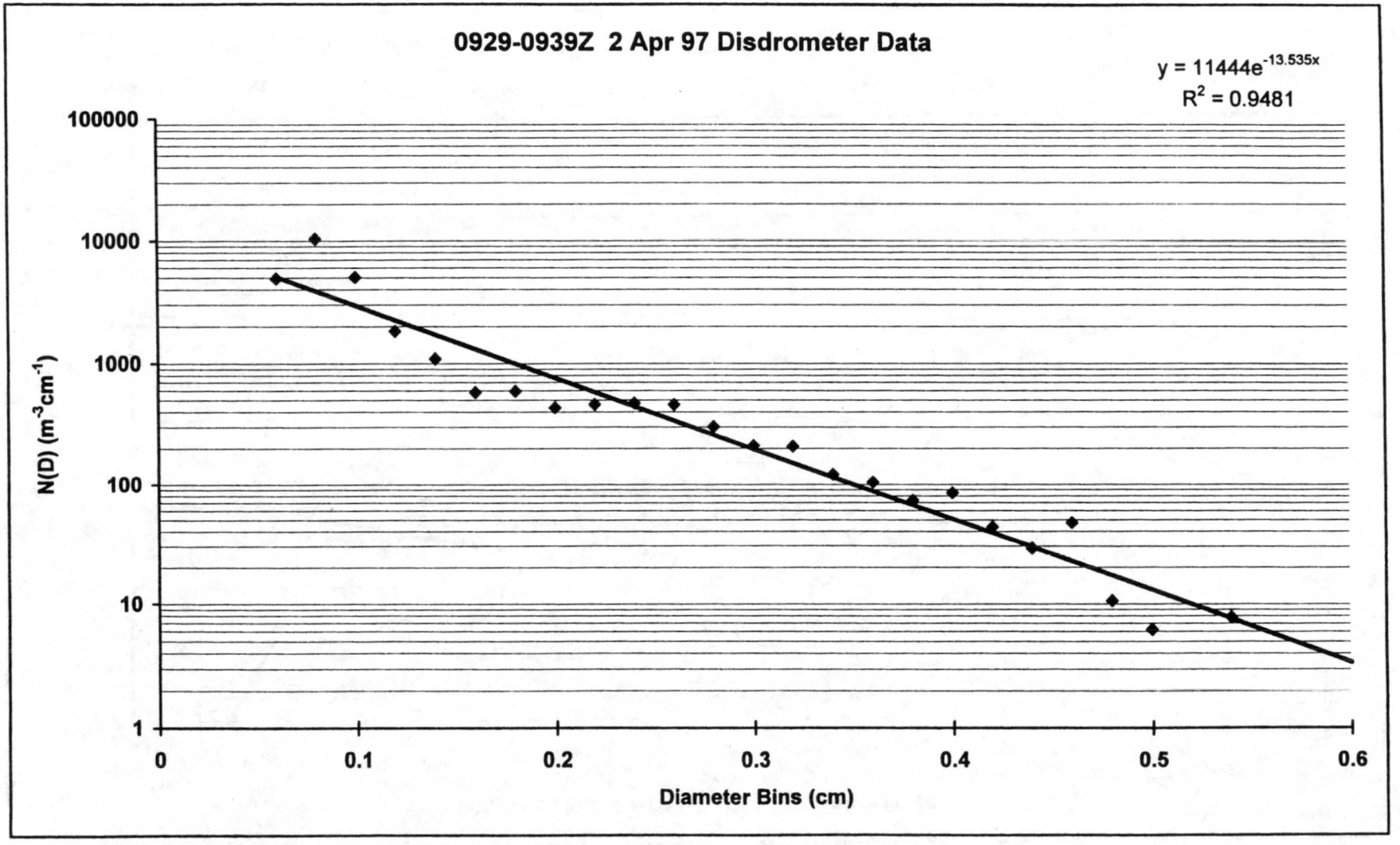

Figure 4.4: Particle size distribution and exponential fit used for crystal period 1, 0925-0935Z 2 April 1997. (Bins greater than 0.4 cm were excluded)

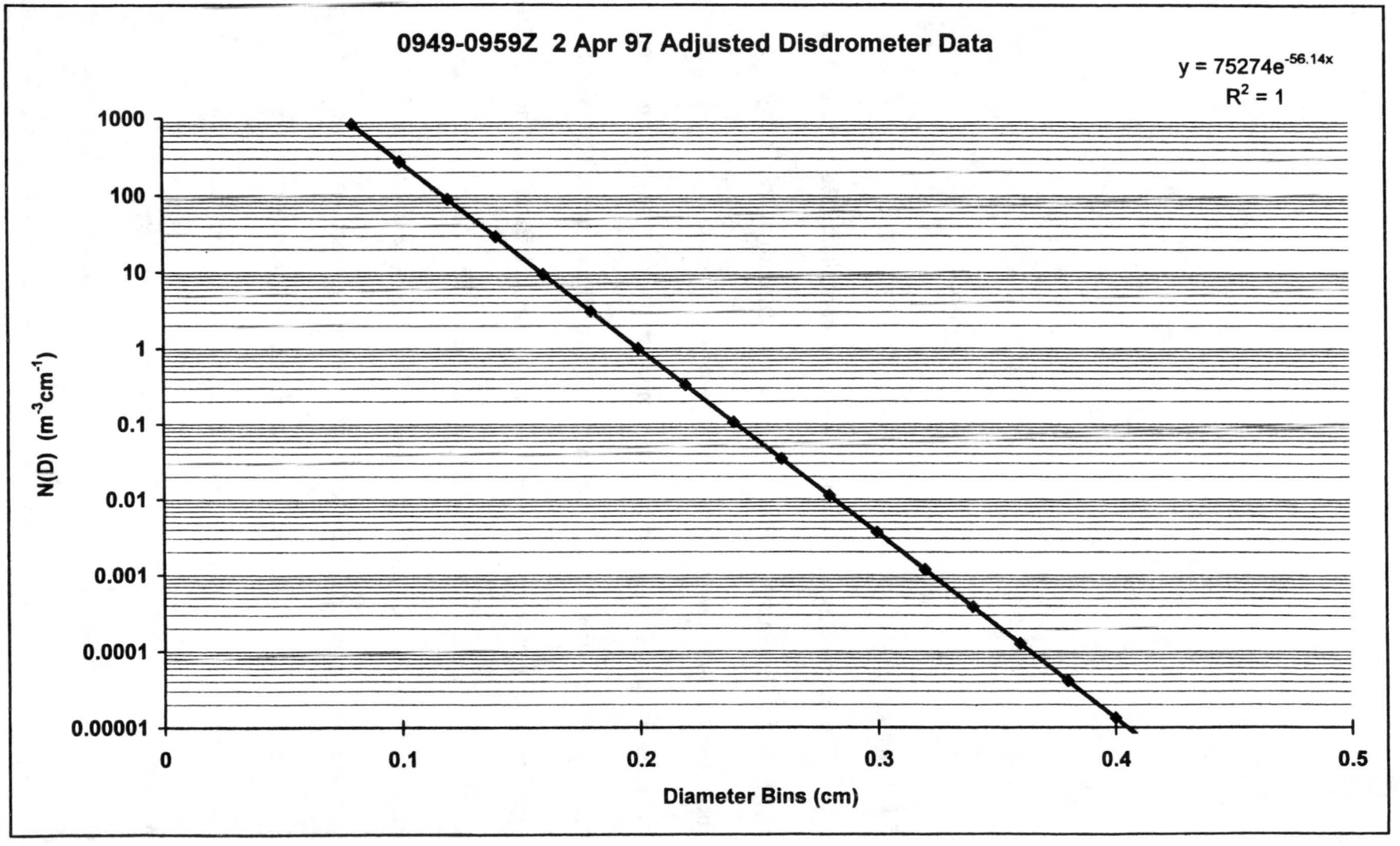

Figure 4.5: Particle size distribution and exponential fit used for crystal period 2, 1010-1020Z 2 April 1997.

CHAPTER 5

CONCLUSIONS

5.1 Summary of Research, Results, and Conclusions

The microphysical characteristics of ice crystals and snowflakes as revealed by co-polar and differential reflectivity were investigated in this study. This research encompassed both observational and theoretical aspects of these polarimetric radar variables in the less explored, yet important winter season precipitation. The observational portion was conducted with the multiparameter, CSU-CHILL radar and supplemented by observers who recorded microphysical features of the snowfall such as snow type, composition, size, and degree of riming. The observer was located at the Fort Collins Weather Station on the Campus of Colorado State University (FCL). In order to compare the appropriate radar data with the ground observations, we computed the approximate trajectory the snow had taken from the height it was interrogated by the radar to the ground. Applying the trajectory in reverse from the location of the observer, we were able to estimate the snow's source region in the 0.5° and 1° elevation scans of the radar. The trajectory calculation was accomplished using dual-Doppler techniques that combined wind velocity data from the CHILL radar with either the NCAR S-pol

radar near Erie, CO, or the NWS NEXRAD WSR-88D Doppler radar in Cheyenne, WY. The trajectory analysis is not a common practice among other winter precipitation researchers, but we found the horizontal distances traveled by the snow during the approximate 700 m (1° scan) and 350 m (0.5° scan) vertical fall to be quite significant. The horizontal distance between FCL and the trajectory-identified source regions in the 0.5° elevation scan of the radar ranged from 0.8 to 5.4 km. The horizontal distance to the source region in the 1° elevation scan ranged from 1.2 to 13.7 km. These distances were large enough for significant variations to occur in the microphysical characteristics of the snow.

We discovered another important factor during the data analysis phase. The calibrations performed at the radar for the differential reflectivity were critical. A histogram of the Z_{DR} values from all of the vertically pointing scans should be centered around 0 dB. If this was not the case, we applied a bias correction to the data from that entire event. These calibration corrections ranged from 0 dB (for an event where vertically pointing scans were not available, but the radar had been calibrated by technicians on that day) to 1.05 dB. This experience highlighted the importance of radar calibration and the incorporation of vertically pointing scans into the scanning strategies, especially in winter precipitation events where small changes in Z_{DR} can have microphysical significance.

We evaluated observational data for four events: 13-14 March, 24 March, 2 April, and 4-5 April 1997. To examine the radar variables associated with specific classifications of snow, we identified periods within each snow event (using the field notes) that were dominated by a particular snow type, either aggregates or individual

platelike crystals (i.e. dendrites, stellar crystals, and plates). Within the platelike crystal category we also separated out periods of intensely rimed platelike crystals. The intense riming was easily characterized by an unmistakable three-dimensional appearance of the crystal. In these circumstances, the axis of the crystal orthogonal to its face had attained a dimension near 1 mm, yet its original shape was not yet obscured like a snow pellet or graupel particle. We compared the Z_{DR} values within each snow classification group and between them. Differential reflectivity values were distinctly lower for aggregated snowflakes (0.12 to 0.8 dB from the 0.5° scan) compared to individual platelike crystals (generally 1.25 to 4.25 dB from the 0.5° scan), with the exception of the intensely rimed platelike crystals (0.25 to 1.25 dB from the 0.5° scan). The intensely rimed platelike crystals generated many Z_{DR} values in the same range as the aggregates, and also some values that were greater than the aggregates, but still less than the other platelike crystals. Reflectivity values provided further distinction between the categories because the intensely rimed crystals produced lower Z values than the aggregates. Thus, our observational results suggest that nearly homogeneous populations of platelike crystals, aggregates, or intensely rimed platelike crystals may be remotely distinguishable using a combination of the Z and Z_{DR} radar observations. Additionally, our observational results challenge the validity of the common assumption that aggregates produce a 0 dB Z_{DR} value.

Within the aggregate category, we noticed that certain microphysical characteristics seemed to be associated with whether the Z_{DR} value of the aggregate period was on the high end or the low end of the observed range of values. Based on observations recorded in the field notes, we speculated that the aggregate populations

producing Z_{DR} values on the high end of the range had relatively higher densities (due to riming and component crystals types), and they were larger in size. The larger size seemed to be associated with an elongated rather than spherical shape, and we theorized that the lower axis ratio of the elongated aggregates together with the higher densities generated the higher Z_{DR} values. To test our theory, we designed model input parameters that were based on three periods of actual observations documented in the field notes, the particle size distributions recorded by the 2-D disdrometer for those periods, and microphysical characteristics outlined by our theory. Two of the three time periods exhibited Z_{DR} values on the high end of the observed range, and those aggregates were assigned higher density values in accordance with the field observations. The other period exhibited Z_{DR} values on the low end of the range, and those aggregates were assigned a lower density as justified by the field observations. The model code we used was based on T-matrix theory and the Mueller matrix method. The Z_{DR} values we generated with the model were nearly identical to the radar observed values for each of the three time periods. Furthermore, when the densities were reduced or the elongation removed from the model input parameters, the Z_{DR} values became significantly different compared to observed values. Additional model runs simulating large degrees of hydrometeor canting produced low Z_{DR} values. This supported our other theory that the likely turbulent conditions during aggregate periods of two of the events may have caused canting that was responsible for their lower observed Z_{DR} values, independent of the microphysical characteristics of the aggregates. In conclusion, although we were unable to achieve the same agreement between the modeled and observed reflectivity values as

we did with the Z_{DR} values, the Z_{DR} correlation strongly suggested that our theories had merit.

Our results have several implications. First, the aggregate shapes are more relevant and have more impact on Z_{DR} than generally expected; therefore, the widely accepted modeling assumption that all aggregates are nearly spherical can produce erroneously low Z_{DR} values. Secondly, the size-dependent density formulas for aggregates which predict that bulk densities decrease with size may not always be applicable and should be used with caution. The Z_{DR} variable is highly sensitive to the density of the aggregates, and inaccurate assumptions will lead to significant modeling errors. Lastly, the background turbulence should be considered when attempting to reproduce observed Z_{DR} values with a model. Our results suggest that significant hydrometeor canting can be the overwhelming factor in determining the Z_{DR} value during turbulent events and should be incorporated into the model. On the other hand, in calmer situations, microphysical characteristics seem to dictate the Z_{DR} values. If a strong canting assumption is included when modeling snowfall in light wind regimes, the model will generate Z_{DR} results that are too low.

We also speculated that the Z_{DR} distinction between the intensely rimed platelike crystals and the other platelike crystal regimes was due to the higher axis ratio of the former caused by a combination of smaller size and thick riming. To test this idea, we ran another simulation of the model. This time we chose two periods from the field notes. The first one was from the individual platelike crystal classification, and the second one was from the intensely rime platelike crystal classification. We assigned rime thicknesses of 0.5 mm and 1 mm to the two periods, respectively, and calculated the axis

ratios of the various sized crystals accordingly. The intensely rimed crystals were closer to spherical in shape, especially the small ones, and subsequently had higher axis ratios. The densities assigned to the two periods were averages from size-dependent formulas, but were adjusted to account for riming. The results of the model runs verified the validity of our theory. These results strengthened our previous conclusion that periods when the individual platelike crystals are intensely rimed (low Z_{DR}) can be distinguished from periods of lesser degrees of riming (high Z_{DR}). Additionally, they highlight the problems that can be encountered if modelers depend upon size-dependent axis ratio formulas without considering the effects of riming.

5.2 Recommendations for Further Research

This research was especially geared toward laying the groundwork for improvements in the Z-S relationships used to estimate snowfall amount. Our distinction of three snow classifications using Z and Z_{DR} is the first step toward identifying the appropriate bulk density to apply to a hydrometeor population. However, more in-situ data needs to be collected to identify typical particle size distributions near the ground, to measure the bulk density of the hydrometeors and quantify its relationship with the associated polarimetric radar variables, and to establish better particle axis ratio distributions for aggregates. Further exploring the use of the 2-D video disdrometer to study and quantify the shapes and axis ratios of the snow particles would be beneficial. Eventually, perhaps optimized Z-S relationships or new polarimetric variable-based snowfall algorithms could be derived for the three snow classification groups we identified.

Further exploration of hydrometeor and particle microphysical characteristics should be pursued using additional polarimetric variables in both rain/snow transition events and pure snow events. Such work would be especially pertinent for the field of aviation where icing and freezing rain conditions are extremely treacherous. Additionally, low visibilities during snow events can be hazardous and wreak havoc on airfield operations. Our field work included visibility observations; thus, it would be possible and worthwhile to analyze our data set for factors contributing to reduced visibilities and search for any related, detectable signatures in the polarimetric radar variables.

Overall, a great deal of study is left to be done in order to fully harness the potential that is contained within the polarimetric radar observations for winter storm applications.

CHAPTER 6

REFERENCES

Atlas, D., M. Kerker, and W. Hitschfeld, 1953: Scattering and attenuation by non-spherical atmospheric particles. *Journal of Atmospheric and Terrestrial Physics*, **3**, 108-119.

Bader, M. J., S.A. Clough, and G. P. Cox, 1987: Aircraft and dual polarization radar observations of hydrometeors in light stratiform precipitation. *Quarterly Journal Royal Meteorological Society*, **113**, 491-515.

Balakrishnan, N., and D. S. Zrnic, 1990: Estimation of rain and hail rates in mixed-phase precipitation. *Journal of the Atmospheric Sciences*, **47**, 565-583.

Barber, P., and C. Yeh, 1975: Scattering of electromagnetic waves by arbitrarily shaped dielectric bodies. *Applied Optics*, **14**, 2864-2872.

Battan, L. J., 1973: *Radar Observation of the Atmosphere*. University of Chicago Press, 324 pp.

Bringi, V. N., and T. A. Seliga, 1977: Scattering from axisymmetric dielectrics or perfect conductors imbedded in an axisymmetric dielectric. *IEEE Transactions on Antenna and Propagation*, **25**, 575-580.

Cressman, G. P., 1959: An operational objective analysis system. *Monthly Weather Review*, **87**, 367-374.

Doviak, R. J., and D. S. Zrnic, 1993: *Doppler Radar and Weather Observations*, 2nd Edition, Academic Press, San Diego, California, 562 pp.

Evans, K. F., and J. Vivekanandan, 1990: Multiparameter radar and microwave radiative transfer modeling of nonspherical atmospheric ice particles. *IEEE Transactions on Geoscience and Remote Sensing*, **28**, 423-437.

Herzegh, P. H., and A. R. Jameson, 1992: Observing precipitation through dual-polarization radar measurements. *Bulletin American Meteorological Society*, **9**, 1365-1374.

Herzegh, P. H., and R. E. Carbone, 1984: The influence of antenna illumination function characteristics on differential reflectivity measurements. *Preprints, 22d Radar Meteorology Conference*, Zurich, Switzerland, American Meteorological Society, 281-286.

Hobbs, P. V., 1974: *Ice Physics*, Clarendon Press, Oxford, England, 837 pp.

Kajikawa, M., 1976: Observation of falling motion of columnar snow crystals. *Journal of the Meteorological Society of Japan*, **54**, 276-283.

Kajikawa, M., 1982: Observation of the falling motino of early snow flakes. Part I: Relationship between the free-fall pattern and the number and shape of component snow crystals. *Journal of the Meteorological Society of Japan*, **60**, 797-803.

Kajikawa, M., 1992: Observations of the falling motion of plate-like snow crystals. Part I: The free-fall patterns and velocity variations of unrimed crystals. *Journal of the Meteorological Society of Japan*, **70**, 1-9.

Locatelli, J. D., and P. V. Hobbs, 1974: Fall speeds and masses of solid precipitation particles. *Journal of Geophysical Research*, **79**, 2185-2197.

Lo, K. K., and R. E. Passarelli, 1982: The growth of snow in winter storms: An airborne observational study. *Journal of the Atmospheric Sciences*, **39**, 697-706.

MacCready, P. B., and C. J. Todd, 1964: Continuous particle sampler. *Journal of Applied Meteorology*, **3**, 450-460.

Magono, C., and C. Lee, 1966: Meteorological classification of natural snow crystals. *Journal of the Faculty of Science, Hokkaido University*, Ser. VII, **2**, 321-335.

Matrosov, S. Y., R. F. Reinking, R. A. Kropfli, and B. W. Bartram, 1996: Estimation of ice hydrometeor types and shapes from radar polarization measurements. *Journal of Atmospheric and Oceanic Technology*, **13**, 85-96.

Oye, R., and R. E. Carbone, 1981: Interactive Doppler editing software. *Preprints, 20th Conference Radar Meteorology*, Boston, Massachusetts, American Meteorological Society, 683-689.

Passarelli, R. E., 1978: Theoretical and observational study of snow-size spectra and snowflake aggregation efficiencies. *Journal of the Atmospheric Sciences*, **35**, 882-889.

Passarelli, R. E., and R. C. Srivastava, 1979: A new aspect of snowflake aggregation theory. *Journal of the Atmospheric Sciences*, **36**, 484-493.

Pruppacher, H. R., and J. D. Klett, 1997: *Microphysics of Clouds and Precipitation*, 2nd Edition, Kluwer Academic Publishers, Dordrecht, The Netherlands, 954 pp.

Rogers, D. C., 1974: *The Aggregation of Natural Ice Crystals*. Rep. No. AR110, Dept. Atmos. Resources, University of Wyoming, 35 pp.

Ryzhkov, A. V., and D. S. Zrnic, 1997: Polarimetric radar discrimination between snow and rain. *Preprints, 20th Conference Radar Meteorology*, Austin, Texas, American Meteorological Society, 19-20.

Ryzhkov, A. V., D. S. Zrnic, and B. A. Gordon, 1998: Polarimetric method for ice water content determination. *Journal of Applied Meteorology*, **37**, 125-134.

Sassen, K., 1980: Remote sensing of planar ice crystal fall attitudes. *Journal of the Meteorological Society of Japan*, **58**, 422-429.

Sasyo, Y., 1977: The collection efficiency of simulated snow particles for water droplets (II)—On the oscillatory angular motion of the snowflake. *Papers in Meteorology and Geophysics*, **28**, 159-168.

Schonhuber, M., H. E. Urban, J. P. V. Polares Baptista, W. L. Randeu, and W. Riedler, 1995: *Measurements of Precipitation Characteristics by a New Distrometer*. Applied Systems Technology report, Joanneum Research, Graz, Austria, 5 pp.

Seliga, T. A. and V. N. Bringi, 1976: Potential use of radar differential reflectivity measurements at orthogonal polarizations for measuring precipitation. *Journal of Applied Meteorology*, **15**, 69-76.

Smith, P., 1984: Equivalent radar reflectivity factors for snow and ice particles. *Journal of Climate and Applied Meteorology*, **23**, 1258-1260.

Stephens, G. L., 1994: *Remote Sensing of the Lower Atmosphere: An Introduction*, Oxford University Press, New York, New York, 523 pp.

Super, A. B., and E. W. Holroyd, 1996: *Snow Accumulation Algorithm for the WSR-88D Radar*. Rep. No. R-96-04, Bureau of Reclamation, U.S. Department of the Interior, 133 pp.

Takahashi, T., and N. Fukuta, 1988: Ice crystal replication with common plastic solutions. *Journal of Atmospheric and Oceanic Technology*, **5**, 129-135.

Thomason, J. W. G., A. J. Illingworth, and V. Marecal, 1995: Density and size distribution of aggregating snow particles inferred from coincident aircraft and radar observations. Preprints, *27th Conference on Radar Meteorology*, Vail, CO, American Meteorological Society, 127-129.

Vivekanandan, J., W. M. Adams, and V. N. Bringi, 1991: Rigorous approach to polarimetric radar modeling of hydrometeor orientation distributions. *Journal of Applied Meteorology*, **30**, 1053-1063.

Vivekanandan, J., R. Raghavan, and V. N. Bringi, 1993: Polarimetric radar modeling of mixtures of precipitation particles. *IEEE Transactions on Geoscience and Remote Sensing*, **31**, 1017-1030.

Vivekanandan, J., V. N. Bringi, M. Hagen, and P. Meischner, 1994: Polarimetric radar studies of atmospheric ice particles. *IEEE Transactions on Geoscience and Remote Sensing*, **32**, 1-10.

Zikmunda, J., and G. Vali, 1972: Fall patterns and fall velocities of rimed ice crystals. *Journal of the Atmospheric Sciences*, **29**, 1334-1347.